Investigation on Fault-Tolerant Converter Topologies for Three Phase Induction Motor Drive System

Submitted in partial fulfilment of requirement
for the award of the degree of

Doctor of Philosophy

By

Y Bhaskar S S Gupta

(Roll No: 716113)

Under the supervision of

Dr. S. Srinivasa Rao

Professor

DEPARTMENT OF ELECTRICAL ENGINEERING
NATIONAL INSTITUTE OF TECHNOLOGY
(An Institution of National Importance, Ministry of Education, Govt. of India)
Warangal-506 004, India

December–2020

Approval Sheet

This Thesis entitled "**Investigation on Fault-Tolerant Converter Topologies for Three Phase Induction Motor Drive System**" by **Y. Bhaskar S S Gupta, Roll No: 716113** is approved for the degree of Doctor of Philosophy

Examiners

_____

_____

Supervisor

Dr. S. Srinivasa Rao
Professor

Chairman

Dr. M Sailaja Kumari
Professor & Head
Department of Electrical Engineering
NIT Warangal

Date: _____

DEPARTMENT OF ELECTRICAL ENGINEERING
NATIONAL INSTITUTE OF TECHNOLOGY
(An Institution of National Importance, Ministry of Education, Govt. of India)
Warangal – 506 004, India

Certificate

This is to certify that the thesis entitled **"Investigation on Fault-Tolerant Converter Topologies for Three Phase Induction Motor Drive System**", submitted by Mr. **Y. Bhaskar S S Gupta,** Roll No: 716113, to the Department of Electrical Engineering, National Institute of Technology, Warangal in partial fulfilment of the requirements for the award of the degree of **Doctor of Philosophy** in Electrical Engineering is a record of bonafide research work carried out by him under my supervision and guidance. The contents of this thesis, in full or in parts have not been submitted simultaneously to any other institute or university for the award of any degree or diploma.

Station :
Date :

Dr. S. Srinivasa Rao
(Thesis Supervisor)
Professor
Department of Electrical Engineering
National Institute of Technology
Warangal – 506004

Declaration

This is to certify that the work presented in the thesis entitled "**Investigation on Fault-Tolerant Converter Topologies for Three Phase Induction Motor Drive System"** is a bonafide work done by me under the supervision of **Dr. S. Srinivasa Rao, Professor**, Department of Electrical Engineering, National Institute of Technology, Warangal, India and was not submitted elsewhere for the award of any degree.

I declare that this written submission represents my ideas in my own words and where others ideas or words have been included, I have adequately cited and referenced the original sources. I also declare that I have adhered to all principles of academic honesty and integrity and have not misrepresented or fabricated or falsified any idea/data/fact/source in my submission. I understand that any violation of the above will be a cause for disciplinary action by the institute and can also evoke penal action from the sources which have thus not been properly cited or from whom proper permission has not been taken when needed.

Y. Bhaskar S S Gupta
(Roll No: 716113)

Date:
Place: NIT Warangal

Acknowledgements

First and foremost, I would like to express my deep sense of gratitude to my thesis supervisor **Dr. S. Srinivasa Rao**, Professor in the Department of Electrical Engineering for his continuous monitoring, moral support, patience, encouragement and timely inputs throughout my research work. His commitment towards research work is always been a source of inspiration for rest of my life.

I would like to extend my gratitude to my Doctoral Scrutiny Committee: Chairman **Dr. M.Sailaja Kumari**, Professor and Head, Department of Electrical Engineering and members **Dr. Bhagwan K Murthy**, Professor, Department of Electrical Engineering, **Dr. B. L. Narasimha Raju**, Associate Professor, Department of Electrical Engineering and **Dr. S Ravi Chandra**, Associate Professor, Department of Computer Science & Engineering for their continuous monitoring, keen interest, insightful comments and encouragement.

My Sincere thanks to **Prof. N V Ramana Rao**, Director NIT Warangal for providing all the necessary facilities to carry out my research work.

I thank all the faculty members in the Department of Electrical Engineering for their support, encouragement and valuable suggestions during various stages of my work. I thank all the supporting staff in the Department of Electrical Engineering for their help, support and co-operation during my research work in the laboratory.

I thank my fellow scholar **Mr. B. Anil Kumar** for his constant support throughout this work and also I would like to thank all my fellow scholars especially, **Mr. M. Vishnu Prasad**, **Mr. K Hema Sundar Rao**, **Mrs. P Mounika, Mr. Satish Reddy D** and **Mr. Ramesh D** from Department of Electrical Engineering who are always ready to share their ideas and extend their support in tough times. I would like to thank all the members who are directly or indirectly involved and supported me in successful completion of this work.

Last but not the least, I would like to thank my parents, **Y Sundara Rao** and **Jyothi**, my sister **Srikanya** and brother in-law **N. Sasidar** and my wife **Pranavi**, sister in-law **K Niveditha** and her parents **K. Narayana Murthy** and **Vara Lakshmi** for their understanding, support and patience which are helped me in the successful completion of work.

Y. Bhaskar S S Gupta

List of Figures

List of Tables

List of Symbols

S_a, S_b and S_c	Inverter control signals
u	Inverter output voltage vector
u_a , u_b and u_c	Inverter output voltages
u_α , u_β and u_γ	Inverter output voltages in stationary reference frame
V_{DC}	DC link voltage
$u_{s\alpha}$ and $u_{s\beta}$	Stator voltages of induction motor in stationary reference frame
$i_{s\alpha}$ and $i_{s\beta}$	Stator currents of induction motor in stationary reference frame
$\psi_{s\alpha}$ and $\psi_{s\beta}$	Stator flux of induction motor in stationary reference frame
R_s and L_s	Stator resistance and stator inductance of induction motor
$i_{r\alpha}$ and $i_{r\beta}$	Rotor currents of induction motor in stationary reference frame
$\psi_{r\alpha}$ and $\psi_{r\beta}$	Rotor flux of induction motor in stationary reference frame
R_r and L_r	Rotor resistance and rotor inductance of induction motor
L_m	Mutual inductance of induction motor
T_e	Electromagnetic torque of induction motor
T_l	Load torque of induction motor
p	Induction motor pole pairs
J	Moment of inertia of induction motor
ω_r	Rotor mechanical speed of induction motor
k	Sampling instant
T_s	Sampling period
T_e^{ref}	Electromagnetic torque reference
$\lvert\psi_s^{ref}\rvert$	Stator flux reference
c	Objective-function
λ_ψ	Weighting factor for stator flux
S_{opt}	Optimal switching state
T_e^{nom}	Nominal electromagnetic torque
ψ_s^{nom}	Nominal stator flux

List of Abbreviations

AC	Alternating Current
CCS-MPC	Continuous Control Set Model Predictive Control
DC	Direct Current
TLBC	Three-Level Boost Converter
CCM	Continuous Conduction Mode
BC	Boost Converter
DTC	Direct Torque Control
FCS-MPC	Finite Control Set Model Predictive Control
FOC	Field Oriented Control
IGBT	Insulated Gate Bipolar Transistor
MPC	Model Predictive Control
PCC	Predictive Current Control
PTC	Predictive Torque Control
PWM	Pulse Width Modulation
VSI	Voltage Source Inverter
PI	Proportional Integrator
IM	Induction Motor
B6	Conventional/Healthy Converter
B4	Conventional Fault-Tolerant Converter
FDI	Fault Detection and Identification

Abstract

Induction motors are popularly used in most of the industrial applications due to their simple speed control, less cost, more efficient and high power to weight ratio etc. Starting and speed control has become more efficient due to invention of power semiconductor device, development of power electronic converter topologies and their control strategies. Since the power semiconductor devices in power electronic converter are prone to failure due to sudden variations in supply or load or both or mal-function of control and protection circuit/s. An extensive research was done by various researchers on the fault-tolerant converter topologies for ac drives for three-phase induction motor drives. Some of these converter topologies require more components and also uses complex control algorithms to implement. Further, operation of the drive in post-fault condition is restricted to speed, torque and also their fluctuations and drive cannot operate in full rated operation during post-fault condition. Therefore it required to design and develop a converter topology with control strategy to resolve some of the issues related to operation of the drive during post-fault condition such as reduction of torque and flux ripple, sinusoidal and balance stator currents and also achieve full rated operation for the drive during post-fault operation. In this research work fault-tolerant converter topologies and control techniques for three-phase two-level inverter fed squirrel cage induction motor drive is explored.

In this research work two fault-tolerant converter topologies such as a three-level boost converter fed two-level voltage source inverter and a boost converter fed two-level voltage source inverter for maintaining continuity of operation during open-circuit and short-circuit fault operation of power electronic device in the inverter leg/s. For control of these two proposed converter combinations, four control schemes such as scalar control (v/f), field oriented control (FOC), direct torque control (DTC) and predictive torque control (PTC) techniques are implemented for three-phase induction motor drive. These control techniques are implemented for reduction of torque and flux ripple, sinusoidal and balance stator currents and also to achieve full rated operation for the drive during post-fault operation. Further the control technique proposed also balance the DC-link voltage at the converter combination. Analysis, design and simulink models for various apparatus used to implement these fault-tolerant converter fed drives such as two-level voltage source inverter, boost converter, three-level boost converter and three-phase induction motor are developed.

Experiments are conducted on the lab-scale prototype for all possible operating conditions and results are obtained for healthy operation of the converter and post-fault operation for load changes as well as speed changes. Simulation results are validated with the experimental results for conventional converter (B6), conventional fault-tolerant converter (B4) and proposed fault-tolerant converter topologies. Based on the results obtained from both simulations and experiments, it is observed that the proposed fault-tolerant converter topologies attains a reduction in torque ripple and flux ripple and also obtain sinusoidal and balance stator currents, achieved full rated operation for the drive during post-fault operation. Further voltage at the DC-link is balanced and improvement in the dynamic response is observed. Detailed analysis of the induction motor drive with the simulations and experimental results when compared with B6 converter, B4 converter are presented in various chapters of the thesis.

Keyword: Fault-tolerant converter, three-level boost converter, scalar control, field oriented control, direct torque control, predictive torque control, three-phase induction motor.

CONTENTS

Chapter-1
Introduction

1.1. Background

Electric motors are widely used operate with a power rating of few kW to MW based on their applications in industry. Decoupled nature of the magnetic flux and electromagnetic torque of dc motors and simple control techniques made the dc motors popular in various applications in industry. However, armature reaction and commutation process restrict the operation of these machines to use in all environmental conditions and also demand frequent maintenance. On the other hand due to rugged construction, maintenance free, low cost, high power to weight ratio, ac motors particularly three-phase squirrel cage induction motors are widely used in various environmental conditions in industry for variable speed applications. Further speed control of this motor is simple due to invention of power semiconductor devices and development of various converter topologies and control techniques to obtain closed loop control with good dynamic response. Therefore three-phase induction motor has become a workhorse for many industries [1]-[2].

Fig. 1.1 represents the general block diagram of the induction motor drive. Three-phase supply is given to the diode bridge rectifier through isolation transformer. The output of the rectifier is given to two-level voltage source inverter (VSI) to feed three-phase induction motor. The voltage, current and speed are sensed to generate the control signals for the inverter to drive the induction motor to obtain the different speed ranges.

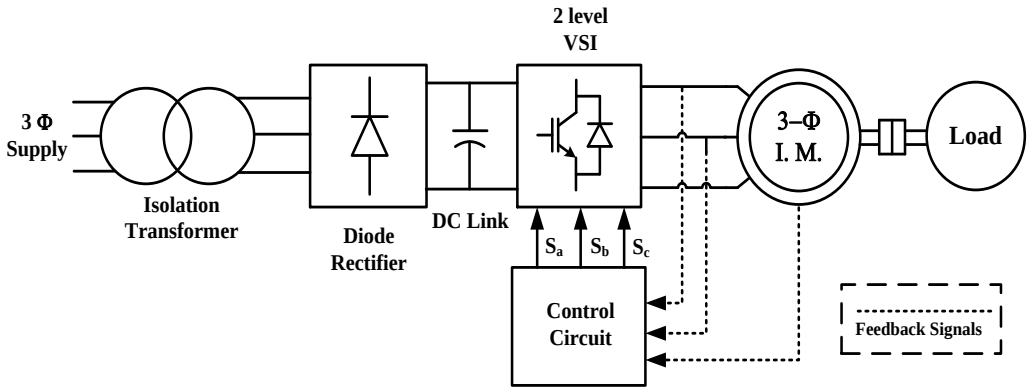

Fig. 1.1 Block diagram of an induction motor drive

In addition to the development of power semiconductor devices in the fast few decades and technology associated with the electric power processing; the induction machines operate in dynamic condition to execute in real-time with control algorithms for adjustable/variable speed drives. However, the power electronic devices used in the power modulator (converter) are prone to failure of devices due to ordeal operating conditions. The failures

may be due to stator winding faults, bearing faults, rotor faults and mechanical speed sensor faults from the motor side and supply fluctuations, overheating of power devices and aging/minor problems associated with control and isolation circuits associated with power converters. According to the Electronic Power Research Institute (EPRI) survey [3]-[4], the stator winding faults are estimated as 36% of motor faults, which include phase-to-ground faults, phase-to-phase short-circuits fault, open-coil faults or inter-turn short-circuit faults. Bearing faults are about 41% of motor faults which occur because of improper maintenance, fast switching occurrence in PWM techniques etc. Rotor faults are about 9% of motor faults which occur because of ageing effect/manufacturing defects, frequent starting operations, thermal and mechanical stress etc.

Another survey on the possibility of the faults in the power converter and auxiliary devices used in the induction motor drives are given in [5], [6]. From this survey is observed that 60% of failures are in capacitors used in the power converters, 34% of failures related to the power devices used in the inverter and 6% are related to the other components like sensors failures etc. Therefore it is identified that fault tolerant converters are required for trouble free operation to operate the drive in variable speeds with variations in loads for all the possible environmental conditions particularly in continuous process industry.

An extensive research was done by various researchers in the field of fault-tolerant converter topologies for ac drives particularly for three-phase induction motor drives. A parallel redundancy and conservative design techniques have been widely adopted to improve their immunity as a straight forward solution. Multiphase (more than three-phases) PWM drives are also reported in the literature to provide fault-tolerant capability. The trade-off lies in the increased system cost and size of such systems [7]-[15]. In order to minimize the cost as a consequence of system redundancy, a lot of attention has been cantered on developing intelligent fault mitigation control methods, along with the appropriate hardware modifications to the conventional three-phase adjustable-speed PWM drives [7], [15]-[30], [57-64]. To further explore the possibility of cost reduction, various reduced switch-count converter topologies for three-phase AC motor-drive systems have been developed with high reliability due to the reduced number of power switching components [31]-[41]. Other converter topologies such as matrix converters [42]-[44] or multilevel PWM inverters [45], [46] for three-phase AC motor-drive systems have also been introduced with fault-tolerant

capability for transistor/switch faults. Survey on fault-tolerance techniques for three-phase voltage source inverter and power electronic converters are explained in [73]-[76]. Delta connected induction motor drive for fault-tolerant converter is explained in [77], but majority of studies consider wye –connected induction motors with two-level inverters. The fault-tolerant converters using multi-phase drives, multi-level converters and open-ended-winding induction motor drives are proposed in [78]–[80].

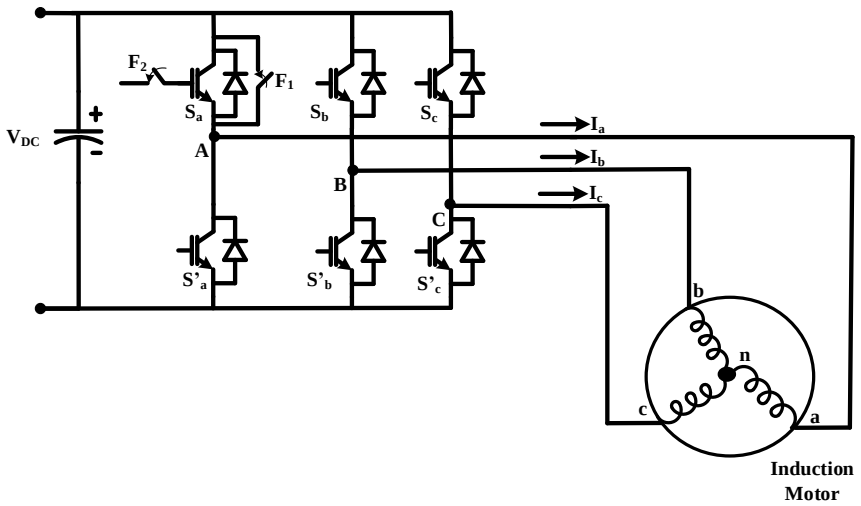

Fig. 1.2 Type of inverter switch faults identification

Two common types of faults investigated in power electronic drives [7], [9]-[30], [54], [57-64] are power electronic device short-circuit faults in the inverter (F_1), gate-drive open-circuit fault in inverter, power electronic device open-circuit fault (F_2) as depicted in Figure 1.2. Short-circuit fault of inverter switch (F_1) can lead to failure of the drive, if the power devices of the same leg of inverter is turned-on, resulting in a direct short-circuit or shoot-through of the dc-bus link [54]. Conversely, open-circuit faults in inverter switch (F_2) may still operate the drive but much inferior performance due to the resulting significant torque pulsations introduced by the consequent asymmetry in the circuit of the motor drive system and the resulting unipolar nature of one of the motor phase currents [54]. Therefore, a drive fault diagnostic approach is a crucial step in determining the type of fault for appropriate remedial action to mitigate the fault in the inverter. This is due to the fact that various efficient and reliable diagnostic methods have already been conceived by various investigators in the literature [47]-[53]. A prior knowledge of the nature of the fault is studied and proposed suitable measures immediately upon the occurrence of such a fault. Some of the fault-tolerant converter topologies and control techniques presented in [7], [9]-[30], [57-

64] offer the motor performance w.r.t rated torque and power. However further scope in this area is identified after a detailed and this research work is carried out.

1.2. Literature review

Three-phase induction motors controlled with power electronic converters are classified as shown in Fig. 1.3.

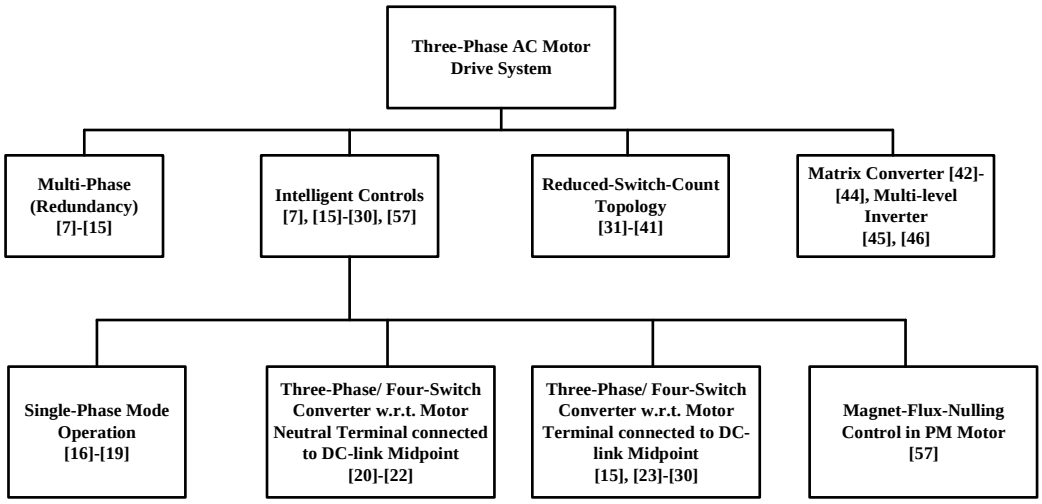

Fig. 1.3 Classification of fault-tolerant strategies for three-phase ac motor-drives

The first fault-tolerant converter topology for two-level voltage source inverter fed induction motor drive was proposed by Liu et al. [20] as shown in Fig. 1.4. If any one of the power devices in any one of the inverter legs fails, the topology is modified in post-fault operation by connecting the motor neutral terminal to the midpoint of the dc-link capacitors by trigging the TRAIC tr_n. This topology mitigates both the faults i.e., open-circuit and short-circuit of any power devices in any one of the inverter legs. In the pre-fault operation, all TRAICS are turned-off and the motor-drive system functions in its normal condition. During the post-fault operation, the faulty inverter leg is first isolated using a fault isolation scheme described in [22]. Therefore in post-fault operation the motor operates in two phase mode with neutral terminal connected to midpoint of the dc-link capacitors. The need for the motor neutral point connection is to allow the individual control of the amplitude and phase of the currents in the remaining two healthy phases. In order to maintain the rated motor performance and development of electromagnetic torque, the currents in the remaining two healthy phases need to be regulated to a magnitude of $\sqrt{3}$ times their original value and phase-shifted by 60^0 electrical with respect to each other. It has been shown that this post-fault control method allows the motor to maintain its normal three-phase performance. Three TRAICS, namely,

tr_a, tr_b, and tr_c, as well as the three fuses, f_a, f_b, and f_c are used for fault isolation [22]. A similar topology capable of mitigating only power devices open-circuit faults was proposed by Elch-Heb et al. [21], without the incorporation of the three fuses and the three TRAICs. A similar topology capable of mitigating only open-phase faults was proposed by Mohammad jannati [60], [62]. In these, a modified and indirect rotor flux filed oriented control technique are proposed for obtaining the normal operation of the drive.

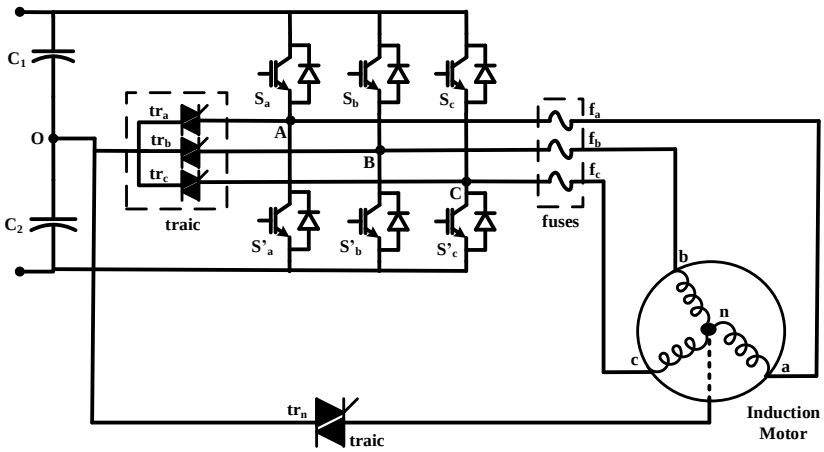

Fig. 1.4 Fault-tolerant topology proposed by Liu et al. [20]

Despite the fact that this fault-tolerant topology ensures the same rated motor performance, still many demerits are associated with it such as; no accessibility to the motor neutral in case of Y-connected stator winding, which is normally not provided by many motor manufacturers and also not suitable for delta-connected stator winding of induction motors. Second drawback is, increase in the fundamental rms motor phase current magnitude in the healthy phases under faulty conditions. This implies that the drive and the motor have to be overrated to withstand this higher level of current for at least a significant period of time. Third drawback is, the neutral current is no longer zero. It is comprise of sum of the currents in the remaining two healthy phases, which results in three times the value of the original phase current during the healthy operation. It causes a circulating current to flow through dc- link capacitors. This circulating neutral current may cause severe voltage fluctuations that may degrade the performance of the drive in the form of increased winding ohmic losses and motor torque ripples/pulsations. Hence, a larger size dc capacitor is required to sustain the desired voltage level and minimize the dc voltage ripples.

Fault-tolerant inverter topology called “B4 converter” proposed by Van Der Broeck et al. [23] to operate the three-phase induction motor using a component-minimized voltage-fed inverter bridge with only four switching devices. This idea was later adopted by Ribeiro et al. [15] for fault-tolerant purposes in a standard six-switch three-phase inverter in Fig. 1.5. This fault-tolerant topology is based on connecting the terminals of the motor to the mid-point of the split dc- link capacitor through a set of TRAICs. This topology is capable of mitigating both open-circuit and short-circuit switch faults. Other investigators, such as Covic et al. [24], [25], Blaabjerg et al. [26], [27], Sobanski P [61] and Dehong Zhou [62] and had also utilized this “B4 converter” topology with various PWM control schemes to compensate dc-link voltage ripples.

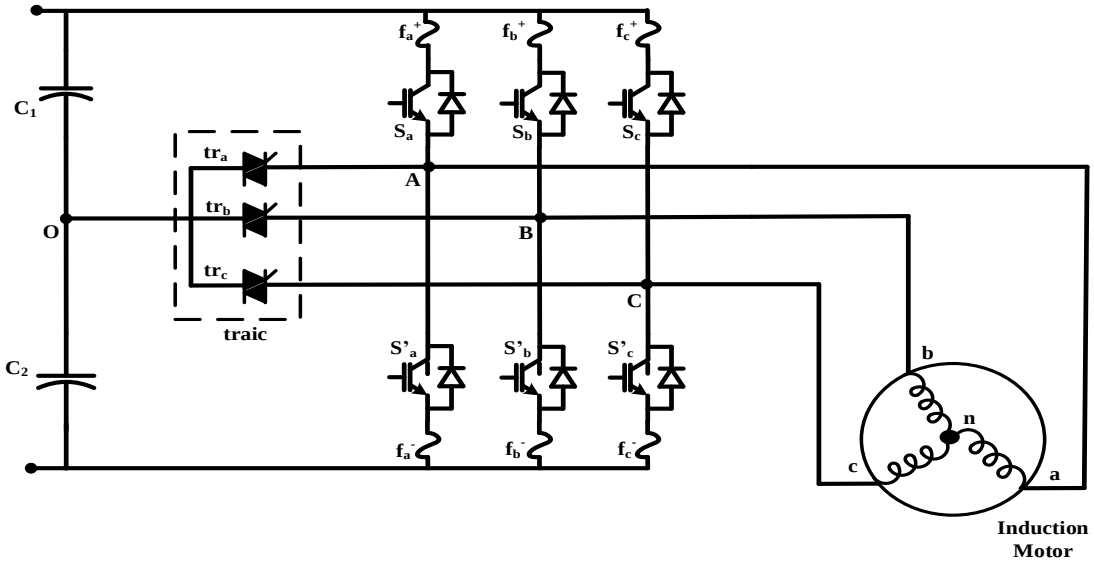

Fig. 1.5 Fault-tolerant topology proposed by Van Der Broeck et al. [23] and Ribeiro et al. [15]

In the healthy operation of the system in Fig. 1.5, the TRAICs, namely, t_{ra}, t_{rb}, and t_{rc}, are turned-off and the motor-drive system operates in its normal condition. During the post-fault operation, the faulty inverter leg is first isolated by means of fast-acting fuses, namely f_a, f_b, or f_c [15]. Thereafter, the terminal of the motor corresponding to the faulty leg is connected to the midpoint of the split dc-bus capacitor link by turning-on the TRAIC of the associated faulty leg of the inverter. It has been reported in [23] and [15] that in order to maintain the rated three-phase motor performance, the dc-bus voltage should be doubled which can be realized by using a controlled rectifier at the drive front-end or a dc-dc boost converter. Along with this, the motor phase voltages in the two phases, which are not connected to the centre of the split dc-link, should be phase-shifted by 60^0 electrical with respect to each

other. Another potential problem associated with this topology is the single-phase circulating current through the dc-bus capacitor may cause severe voltage variations and hence affect the system performance. Hence, an oversized dc capacitor is needed to absorb this single-phase circulating current. Despite the reasonable performance exhibited by the fault-tolerant topologies of Fig. 1.4 and Fig. 1.5, the above drawbacks may appear to be intolerable in some motor-drive applications.

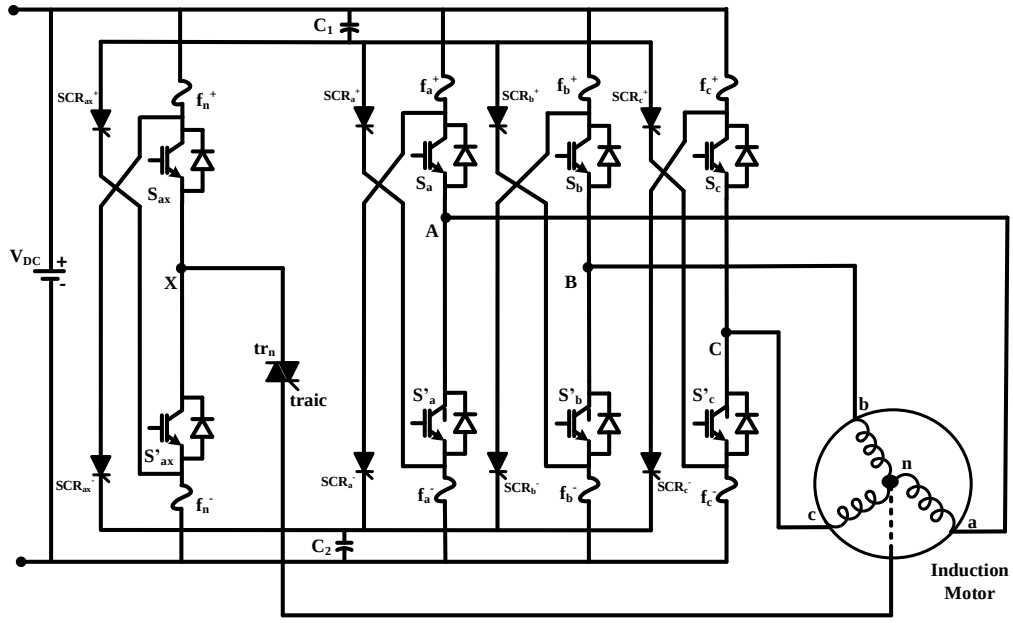

Fig. 1.6 Scheme-I of fault-tolerant converter topology proposed by Bolognani et al. [11]

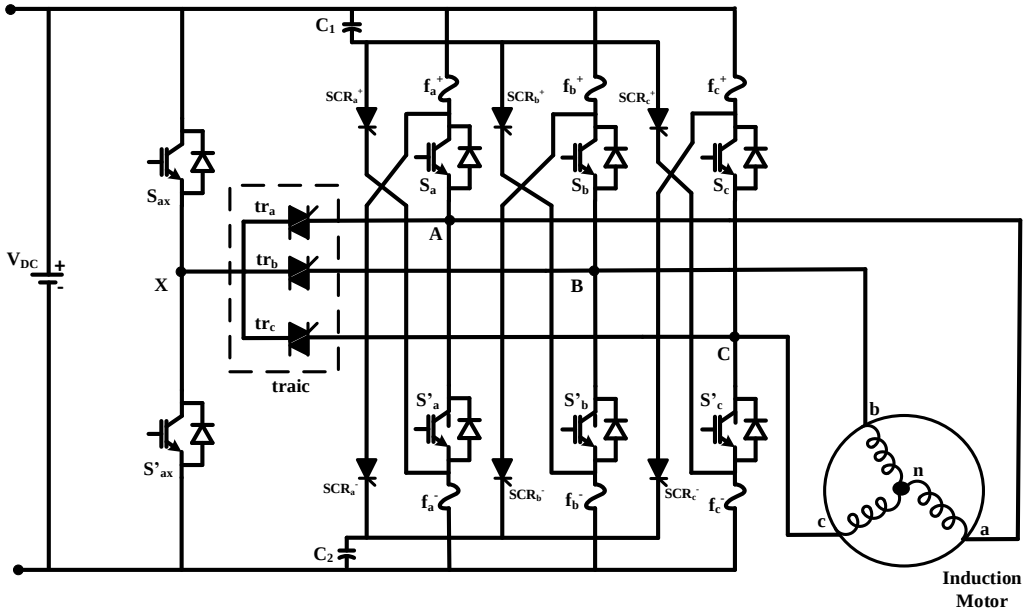

Fig. 1.7 Scheme –II of fault-tolerant converter topology proposed by Bolognani et al. [11]

Fault-tolerant inverter topology based on redundancy concept are reported in the literature proposed by Bolognani et al. [11], Corrêa et al. in [13] and Ribeiro et al. in [15]. The fault-tolerant inverter topology schemes proposed by Bolognani et al. [11] are depicted in Fig. 1.6 and Fig. 1.7 for open-circuit or short-circuit fault in power devices. The difference in fault-tolerant converter fed drives configurations proposed by Corrêa et al. [13] and Ribeiro et al. [15], is w.r.t., fault isolation scheme. Scheme proposed by Corrêa et al. [13] do not have any fault isolation capability, it is only intended for mitigating a power device open-circuit fault, while Ribeiro et al. [15] proposed scheme has two fast-acting fuses for each inverter leg that is equivalent to the fault isolation scheme as depicted in Fig. 1.5. When either a power device open-circuit or short-circuit fault has been detected, the faulty power device will be first isolated, and the fourth inverter leg will be activated by turning-on the associated TRAIC. In the case of the topology of Fig. 1.7, all three-phases of the motor are connected to the inverter during the pre- and post-fault operations, the current amplitude in each of the phases remains the same in order to ensure a smooth torque production. In [58] a fault-tolerant topology for PMSM drives was proposed with similar concept as shown in Fig. 1.7. In this topology they are using thyristors for isolation mitigating open-circuit fault or short-circuit faults.

Fault-tolerant inverter topology proposed by Bekheira Tabbache in [59] has an improved fault-tolerant control scheme for induction motor drive for EV's is shown in Fig. 1.8. In this scheme no fault isolation is provided instead of it, a 3D space vector control algorithm for the fault-tolerance. A similar topology capable of mitigating only open-circuit faults was proposed by Rebah Maamouri in [64]. In this, an effective fault detection and identification (FDI) process for a robust IGBT open-switch faults diagnosis in sensor less speed-controlled induction motor drive is proposed. For the topology shown in Fig. 1.6 only two motor phases and the motor neutral are connected to the inverter, the fundamental rms current amplitudes in the motor phases are increased by a factor of $\sqrt{3}$ in order to maintain the same rated motor performance. This is equivalent to the post-fault operating condition of the topology given in Fig. 1.4. Furthermore, the fault-tolerant inverter topologies of Fig. 1.6 and Fig. 1.7 involve too many circuit components for the fault isolation scheme, which presents a drawback or these methods.

Meanwhile, other investigators, such as Elch-Heb et al. [16] and Kastha et al. [17]-[19], had proposed schemes to operate the three-phase induction motor-drive system in a single-phase mode, in the event of an inverter switch fault. Due to the single-phase motor operation, a pulsating torque at the line frequency is generated. In order to minimize the torque pulsation, Kastha et al. [17]-[19] proposed a scheme to inject odd harmonic voltages at the appropriate phase angles into the motor terminal voltages to neutralize the lower-order harmonic pulsating torques by shifting these pulsating torque frequencies to the higher range. Therefore the machine's inertia can filter them substantially and permit satisfactory operation. However, the drawback of this method is its complexity in implementation, which requires exact computation of the phase angles of the injected harmonic voltages. Any error in the computation process will result in severe torque pulsation.

In [57] Welchko et. al. proposed another method which will nullify the magnet flux in the short-circuited phase of an interior permanent-magnet motor following short-circuit faults in either in the inverter or the motor stator windings. In this scheme a zero-sequence current is introduced to suppress the current induced in the faulty/short-circuited phase. However, the downside of the proposed method is the need to increase the currents in the remaining healthy phases by a factor $\sqrt{3}$. This scheme requires that each phase of the motor three-phase winding is to be driven by an H-bridge inverter or alternatively employing a six-leg inverter. However this method will increase the cost of the overall motor-drive system.

The influence and compensation of inverter voltage drop in direct torque controlled four switch inverter topology for three-phase permanent magnet brushless AC drives was presented in [65]. In this, voltage based stator flux estimation and current based stator flux estimation techniques are used to compensate the voltage drops in the B4 configuration to correct the predicted stator flux to obtain the improved current waveforms with balanced magnitudes. In [66] Bassem El badsi proposed a DTC scheme for the four-switch inverter fed induction motor by emulating the six-switch inverter operation. Normally four-switch inverter having four sectors to generate the switching states but in this, the four sectors are modified to generate six sectors for the B4 inverter. Mohamed kamel metwally [67], Dehong Zhou [68] and Chong Zhu [69] proposed different control algorithms for the B4 inverter fed induction motor. In these sensor less speed estimator based on MARS algorithm, predictive torque control algorithm with DC-link voltage offset suppression and space vector pulse

width modulation techniques are implemented respectively to obtain the operation of the drive. From all these techniques for the B4 converter the drive performance is increased in terms of stator flux, reduction in torque ripple, obtaining sinusoidal currents, reduces the oscillations in the speed and balance the dc-link voltage across the capacitors. These techniques are more complex because of adding extra control parameter for the each component in the algorithm. However with these techniques the drive cannot operate in full rated capacity.

In [70] Masoud Farhadi proposed a DC-AC converter fed induction motor drive with fault-tolerant capability under open-circuit and short-circuit of switches as shown in Fig. 1.8. This topology mitigates the faults in DC-DC converter and two-level inverter. Parallel redundant switches are connected with relays in the DC-DC converter to mitigate the faults. The fault detection technique used for DC-DC converter switches is based on inductor input current slope. After detection, the faulty switch is replaced by the redundant switch by activating the relays. The open-circuit fault in the inverter switch is detected based on the normalized dc current method. For detection of short-circuit fault in the inverter, comparison of gate voltage with the reference voltage is observed. In post-fault operation by connecting the motor neutral terminal to the midpoint of the dc-link capacitors by trigging the relay. In this, the dc-link voltage across the capacitors is balanced and ensure superior post-fault operation, two third order integral-lead controllers is used to minimize the error between the desired reference outputs and the generated outputs. The need for the motor neutral point connection is to allow the individual control of the amplitude and phase of the currents in the remaining two healthy phases. In order to maintain the rated motor performance and the same torque production, the currents in the remaining two healthy phases need to be regulated to a magnitude of $\sqrt{3}$ times their original value and phase-shifted by 60^0 electrical with respect to each other. Despite the fact that this fault-tolerant topology ensures the same rated motor performance, this scheme suffers with few demerits such as accessibility to the motor neutral, not be applicable to delta-connected motors, increase in the fundamental rms motor phase current magnitude in the healthy phases under faulty conditions. This implies that the drive and the motor have to be overrated to withstand this higher level of current for at least a significant period of time.

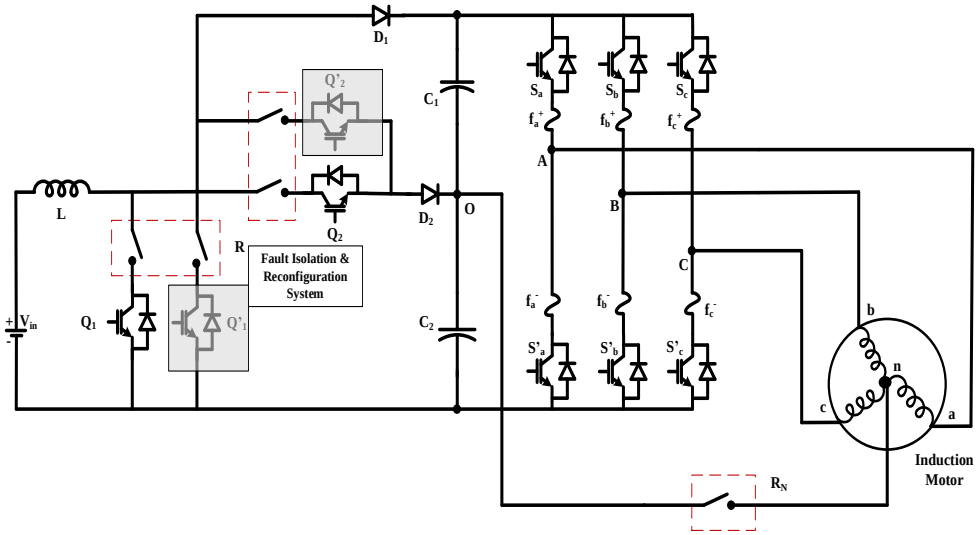

Fig. 1.8 DC-AC fault-tolerant topology was proposed by Masoud Farhadi [70]

Also, the neutral current is three times the value of the original phase current during the healthy operation mode and circulating neutral current through the dc-bus capacitors. This circulating neutral current may cause severe voltage fluctuations which may degrade the performance of the drive in the form of increased winding ohmic losses and motor torque ripples/pulsations. Hence, a larger size dc capacitor is required to sustain the desired voltage level and minimize the dc voltage ripples.

In [71] Mahdi tousizadeh proposed a unified feed-forward method for fault-tolerant filed oriented control of induction motor drive. This control technique is implemented for all fault-tolerant topologies exist in the literature and observe the performance of each topology. For the same topologies Mahdi tousizadeh in [72] observed the performance comparison of fault-tolerant three-phase induction motor drives considering the voltage and current limits. From this, three-leg inverter with phase terminal clamped to midpoint of the DC-link (3L-PCM) is able to give rated torque with reduced speed (less than 50% of its rated capacity) because faulty phase voltage is reduced to $\sqrt{3}$ times of the remaining healthy phase voltages of the drive. Whereas three-leg inverter and four-leg inverter with neutral terminal clamped to midpoint of the capacitor or additional leg (3L-NCM and (3+1)L-NAL) gives lower torque (less than 50% of rated capacity) because healthy phase currents are increased by $\sqrt{3}$ times of the normal phase currents. In 3L-PCM and 3L-NCM, the voltage fluctuations in the DC-link midpoint may degrade the performance and also require large size of the DC-link capacitors. The (3+1)L-NAL do not offer voltage fluctuations in the DC-link midpoint

but drive operates in two-phase mode with control complexity and also more component count with higher volt-ampere ratings.

Detailed study was made on the reported literature related to fault-tolerant converter topologies for three-phase induction motor drives. From the literature, it is identified that even though these methods promise rated motor operation in the event of a power device faults in inverter leg, some of their drawbacks may be intolerable or undesirable in some applications or operating conditions. The issue are related to converter topologies, control techniques, operating power range of drive, components count in the inverter configurations, torque ripples and speed fluctuations in post-fault operation. To address these issues investigations are made to propose few converter topologies and their control techniques.

1.3. Motivation

Fault-tolerant converter topologies proposed in the literature have various configurations with different control algorithms for three-phase induction motor drives. Many of these converter topologies require more components and also uses complex control algorithms to implement. Further, operation of the drive in post-fault condition is restricted to speed, torque and also their fluctuations in dc-link and drive cannot operate in full rated operation during post-fault condition. It gave a motivation to develop a converter topology with control strategies for a two-level inverter to make it fault-tolerant operation for induction motor drive. Since open-circuit and short-circuit faults in the power devices of the inverter are common, for development of control strategies for induction motor drive to perform fault detection, diagnosis, isolation and remedial action it is necessary to measure pole voltage at inverter. Therefore converter topology with control strategy developed should able to solve some of the issues related to operation of the drive during post-fault condition such as capacitor voltage balance, reduction of torque and flux ripple, sinusoidal and balance stator currents and also achieve full rated operation for the drive during post fault operation. Therefore research work is carried out to reduce complexity in control and improve performance of three-phase induction motor drive during inverter switch fault conditions. Simulation and experimental results are carried out to highlight the proposed fault-tolerant converter topologies for three-phase squirrel cage induction motor drive.

1.4. Scope of the Thesis

The scope of this research work is to propose a fault-tolerant topology for induction motor drive to operate the drive in normal operation during post-fault condition with dc-link voltage balance and less ripples in torque and stator flux and also obtain the less fluctuations in the speed with sinusoidal stator currents.

Accordingly, the contributions made in this dissertation are summarized as follows:

1. The induction motor drive should be operated in full rated condition in post-fault operation.
2. The dc-link voltage across the capacitors should be balanced in all operating conditions such as load changes and speed changes.
3. The stator currents should be sinusoidal with minimal ripples in the torque and stator flux and also having less fluctuations in speed.

To obtain these objectives, two fault-tolerant converter topologies are proposed to operate the drive with various control techniques:

In the first proposed topology, a three-level boost converter based fault-tolerant inverter fed induction motor drive is implemented to obtain the above objectives for different control algorithms such as scalar control, field oriented control, direct torque control and predictive torque control.

In the second proposed topology, a boost converter based fault-tolerant inverter fed induction motor drive is implemented to obtain the above objectives for different control algorithms such as scalar control, field oriented control, direct torque control and predictive torque control.

Both the proposed converter topologies with their control algorithms offered reduced torque and stator flux ripple, stator currents are sinusoidal and also dc-link voltage balance across the capacitors is eliminated.

1.5. Organisation of the Thesis

In Chapter-1, background of the topic, literature review on fault-tolerant operation for induction motor drives and motivation for the problem formulation and scope of the thesis are presented.

In chapter-2, Modeling, analysis and design of three-level boost converter, boost converter, two-level VSI and three-phase squirrel cage induction motor are explained in detail.

In chapter-3, experimental results are presented for proposed fault-tolerant converter topologies using speed control algorithm. These topologies are compared with the conventional fault-tolerant topology and healthy inverter topology to show the merits of proposed topologies under various operating conditions.

In chapter-4, simulation and experimental results are presented for proposed fault-tolerant converter topologies using field oriented control algorithm. These topologies are compared with the conventional fault-tolerant topology and healthy inverter topology to show the merits of proposed topologies under various operating conditions.

In chapter-5, simulation and experimental results are presented for the proposed fault-tolerant converter topologies using direct torque control. Results are compared with the conventional fault-tolerant topology and healthy inverter topology to show the merits of proposed topologies under various operating conditions.

In chapter-6, simulation and experimental results are presented for the proposed fault-tolerant converter topologies using predictive torque control. Results are compared with the conventional fault-tolerant topology and healthy inverter topology to show the merits of proposed topologies under various operating conditions.

In chapter-7, overall summary of the results, comparison of torque ripple, flux ripple and stator current THD of healthy, conventional and proposed topologies are presented and future scope for the research work is suggested.

Chapter-2
Design and Modelling of Fault-Tolerant Converters

2.1. Introduction

In this chapter analysis, design and modelling of fault-tolerant converters for three-phase induction motor are explained in detail. The converter topologies considered for study and investigation are derived and developed from the simple boost converter, three-level boost converter and two-level voltage source inverter. Two fault-tolerant converters are developed from the combination of these converters to obtain fault-tolerant operation of induction motor drive for various operating conditions in the scalar control, field oriented control, direct torque control and predictive torque control. Converter topologies developed in this chapter are used to obtain fault-tolerant operation of induction motor are discussed in detail in subsequent chapters.

2.2. Analysis and Modelling of Three-Level Boost Converter (TLBC)

This converter consists of an input inductor L_0, switches S_1 and S_2 and capacitors C_1 and C_2 are connected in such a fashion to obtain three voltage levels at the output voltage are shown in Fig. 2.1. The midpoint of capacitors is connected to middle of switches S_1 and S_2. Operation of this converter in continuous current mode (CCM) is discussed in four modes which are reported in [131]-[133] and are represented in Fig. 2.1.

Mode-I: Switches S_1 and S_2 are turned *ON*; input voltage is equal to the inductor voltage i.e. $V_L = V_{in}$. The current rises in positive direction.

$$\frac{d}{dt} i_L = \frac{V_{in}}{L_0} \tag{2.1}$$

$$\frac{d}{dt} V_{C1} = -\frac{V_{C1}}{R_1 C_1} \tag{2.2}$$

$$\frac{d}{dt} V_{C2} = -\frac{V_{C2}}{R_2 C_2} \tag{2.3}$$

Where V_{in} is input voltage, V_{C1}, V_{C2} are voltages across the capacitors C_1 and C_2, i_L is inductor current and R_1, R_2 are load resistors.

Mode-II: Switch S_1 is turned *ON* and switch S_2 is turned *OFF*. The current rise may be either positive or negative. Therefore, capacitor C_2 is charging and capacitor $C_1$is discharging:

$$\frac{d}{dt} i_L = \frac{V_{in} - V_{C2}}{L_0} \tag{2.4}$$

$$\frac{d}{dt} V_{C1} = -\frac{V_{C1}}{R_1 C_1} \tag{2.5}$$

$$\frac{d}{dt}V_{C2} = \frac{i_L R_2 - V_{C2}}{R_2 C_2} \tag{2.6}$$

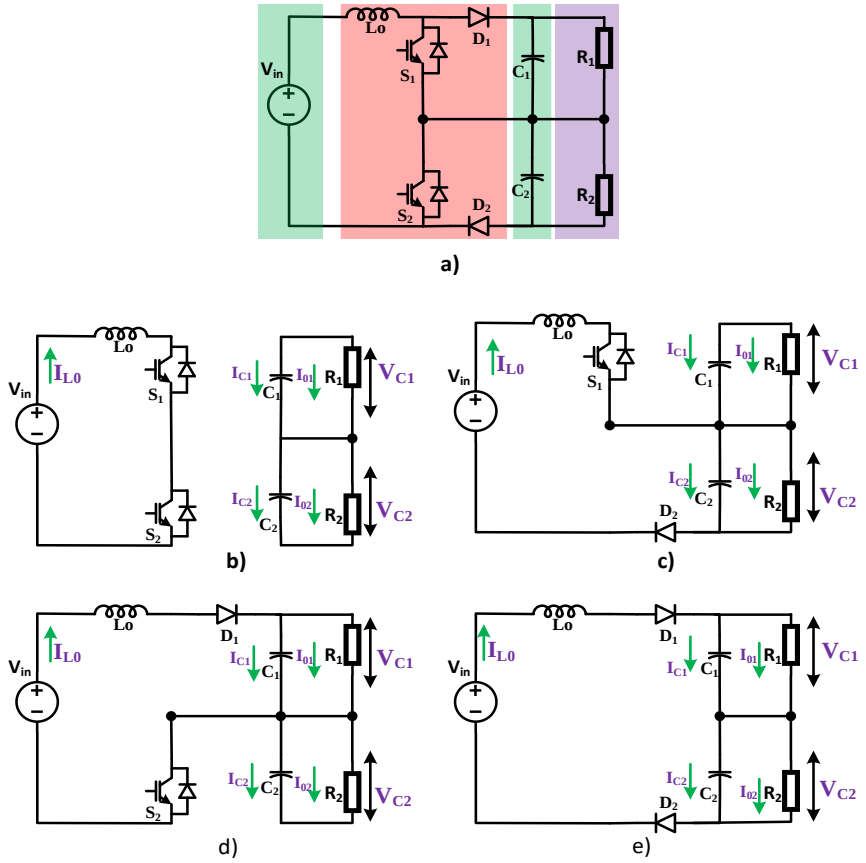

Fig. 2.1 a) Schematic of three-level boost converter
b) Mode-I c) Mode-II d) Mode-III e) Mode-IV

Mode-III: Switch S_1 is turned *OFF*, whereas switch S_2 is turned *ON*. The current rise may be either positive or negative. The capacitor C_1 is charging and the capacitor C_2 is discharging:

$$\frac{d}{dt}i_L = \frac{V_{in} - V_{C1}}{L_0} \tag{2.7}$$

$$\frac{d}{dt}V_{C1} = \frac{i_L R_1 - V_{C1}}{R_1 C_1} \tag{2.8}$$

$$\frac{d}{dt}V_{C2} = -\frac{V_{C2}}{R_2 C_2} \tag{2.9}$$

Mode-IV: Both switches S_1 and S_2 are turned *OFF*; inductor voltage V_L is the difference of input voltage V_{in} and dc-link voltage. i.e. $V_L = V_{in} - (V_{C1} + V_{C2})$.

$$\frac{d}{dt}i_L = \frac{V_{in} - V_{C1} - V_{C2}}{L_0} \tag{2.10}$$

$$\frac{d}{dt}V_{C1} = \frac{i_L R_1 - V_{C1}}{R_1 C_1} \tag{2.11}$$

$$\frac{d}{dt}V_{C2} = \frac{i_L R_2 - V_{C2}}{R_2 C_2} \quad (2.12)$$

This TLBC operates in two different regions, i.e. non-overlapping and overlapping regions. In both regions, current flow in inductor may either increase or decrease based on switching conditions and voltage across capacitor C_1 and C_2. In non-overlapping region of operation of the converter, the average voltages are based on Kirchhoff's law as:

$$-V_{in} + V_L + V_{sw} = 0 \quad (2.13)$$

Where, V_{SW} is average voltage across the switches.

$$V_{sw} = V_{sw1} + V_{sw2} = V_o\,(1 - D)/2 + V_o/2 \quad (2.14)$$

Where, V_{SW1} and V_{SW2} are average voltages across the switches S_1, S_2.

From Eq. (2.13) and (2.14)

$$V_o = 2V_C = 2V_{in}/(2 - D) \quad (2.15)$$

Where, V_C is voltage across each capacitor.

From an overlapping region operation of converter, average voltage across the switch is

$$V_{sw} = V_{sw1} + V_{sw2} = V_o\,(1 - D)/2 + 0 \quad (2.16)$$

From Eq. (2.16) and (2.13)

$$V_o = 2V_C = 2V_{in}/(1 - D) \quad (2.17)$$

Hence, it is observed that TLBC gives more output voltage and efficiency than traditional boost converter. Input inductor L_o is designed in CCM as:

$$\Delta I_1 = \frac{V_o\left(1-\frac{V_{in}}{V_o}\right)\left(\frac{2V_{in}}{V_o}-1\right)}{Lf_{sw}} \quad \text{Non-overlapping region} \quad (2.18)$$

$$\Delta I_2 = \frac{V_o\left(\frac{V_{in}}{V_o}\right)\left(1-\frac{2V_{in}}{V_o}\right)}{Lf_{sw}} \quad \text{Overlapping region} \quad (2.19)$$

From Eq. (2.18) and (2.19), ΔI of inductor is small in both the regions of TLBC when compared with conventional boost converter. DC-link voltage required to drive the induction motor is more than twice the input voltage, which is obtained due to overlapping of gate pulses to switches in the TLBC. Therefore, input inductor (L_o) is designed based on Eq. (2.19).

2.2.1 Modelling of TLBC

For both overlapping and non-overlapping regions of TLBC, modelling of inductor current and dc-link voltages of capacitors are expressed in state in state-space form is $\dot{x} = Ax + Bu$ and $y = Cx + Eu$ from the fundamentals as:

$$\begin{pmatrix} \frac{di_{L0}}{dt} \\ \frac{dV_{C1}}{dt} \\ \frac{dV_{C2}}{dt} \end{pmatrix} = \begin{pmatrix} 0 & -\frac{(1-S_{1t})}{L_0} & -\frac{(1-S_{2t})}{L_0} \\ \frac{(1-S_{1t})}{C_1} & 0 & 0 \\ \frac{(1-S_{2t})}{C_2} & 0 & 0 \end{pmatrix} . \begin{pmatrix} i_{L0} \\ V_{C1} \\ V_{C2} \end{pmatrix} + \begin{pmatrix} \frac{1}{L_0} \\ 0 \\ 0 \end{pmatrix} . (V_{in}) + \begin{pmatrix} 0 & 0 \\ -\frac{1}{C_2} & 0 \\ 0 & -\frac{1}{C_1} \end{pmatrix} . \begin{pmatrix} i_{01} \\ i_{02} \end{pmatrix} \tag{2.20}$$

$$\begin{pmatrix} Y_1 \\ Y_2 \end{pmatrix} = \begin{pmatrix} 0\,1\,0 \\ 0\,0\,1 \end{pmatrix} . \begin{pmatrix} i_{L0} \\ V_{C1} \\ V_{C2} \end{pmatrix} = \begin{pmatrix} V_{C1} \\ V_{C2} \end{pmatrix} \quad \text{or} \quad (Y) = (0 \quad 1 \quad 1) . \begin{pmatrix} i_{L0} \\ V_{C1} \\ V_{C2} \end{pmatrix} = (V_{DC}) \tag{2.21}$$

Where S_{1t} is excitation of S_1 (S_1= *ON* then S_{1t}=1; S_1= *OFF* then S_{1t}= 0) and S_{2t} is excitation of S_2 (S_2= *ON* then S_{2t}=1; S_2= *OFF* then S_{2t}= 0).

The state variable matrix x is chosen as $[i_{L0} \quad V_{C1} \quad V_{C2}]^T$; u is input variable V_{in} and y is output variable V_{DC}. From above equations by state-space averaging technique, state matrix A, B, C and E are represented as

$$A = \begin{pmatrix} 0 & \frac{-(1-S_{1t})}{L_0} & \frac{-(1-S_{2t})}{L_0} \\ \frac{(1-S_{1t})}{C_1} & 0 & 0 \\ \frac{(1-S_{2t})}{C_2} & 0 & 0 \end{pmatrix}; B = \begin{pmatrix} \frac{1}{L_0} \\ 0 \\ 0 \end{pmatrix}; C = (0 \quad 1 \quad 1); E = (0) \tag{2.22}$$

Where, (S_{1t}=d_1) and (S_{2t}=d_2), C_1=C_2=C_0.

2.2.2 Control of TLBC

The proposed current control algorithm is to achieve dc-link capacitors voltage balance and increase in magnitude of dc-link voltage. This control action is required to operate the drive in full rated condition under fault condition of switches of the inverter connected at its output terminals is shown in Fig. 2.2. Control algorithm is executed in two steps, in first step switch S_1 is controlled to obtain desired dc-link voltage and in second step switch S_2 is controlled to maintain dc-link voltage balance for load or speed changes.

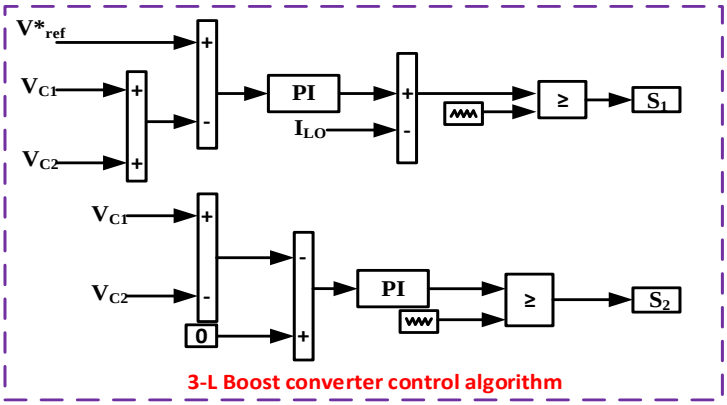

Fig. 2.2 Three-level boost converter control algorithm

First step:

Output voltage across each capacitor is sensed and added as (V_{C1}+V_{C2}). The total voltage across dc-link is compared with reference voltage (V^*_{ref}). The output of the comparator is voltage error (v_e)

$$v_e = V^*_{ref} - (V_{C1} + V_{C2}) \tag{2.23}$$

Voltage error is given to PI controller to generate reference inductor current. The controlled signal as

$$I^*_{ref} = k_p v_e + k_i v_e \tag{2.24}$$

Where, k_p and k_i are proportional and integral controller gains. The output of PI controller is compared with inductor current (I_{LO}). The output of the comparator is current error (i_e)

$$i_e = I^*_{ref} - I_{LO} \tag{2.25}$$

Controlled signal as

$$V_{DC} = k_p i_e + k_i i_e \tag{2.26}$$

This controlled signal is used to generate modulating signal to obtain output voltage V_{DC}. The output of PI controller is compared with carrier signal of frequency 2 kHz and generates PWM pulses to switch S_1 to obtain dc-link voltage V_{DC}.

Second step:

Capacitors voltage difference is compared with set point i.e. zero (0). The output of comparator is an error signal (e)

$$e = 0 - (V_{C1} - V_{C2}) \tag{2.27}$$

Controlled signal as

$$S = k_p e + k_i e \tag{2.28}$$

This controlled signal is used to generate modulating signal. The output of PI controller is compared with 180^0 phase shifted frequency carrier signal of frequency 2 kHz and generates PWM pulses to switch S_2 to obtain balanced dc-link voltage. Due to this capacitor voltages are balanced across the DC-link for any change of load. The total dc-link voltage ($=V_{C1}+V_{C2}$) is regulated by inverter.

2.3 Analysis and Modelling of Boost Converter

Classical boost converter in continuous current mode operates in two modes which are represented in [131] and are shown in Fig. 2.3 (a) – (c).

Mode I: When switch S_1 is turned ON, the current in the boost inductor increases linearly and diode D_1 will turn OFF.

Mode II: When switch S_1 is turned OFF, the energy stored in the inductor is release through the diode D_1 to the dc-link.

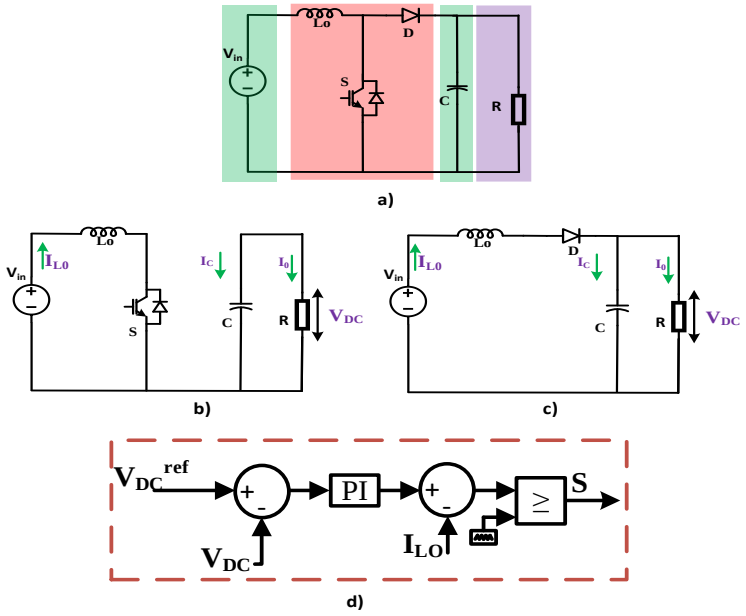

Fig. 2.3 Schematic of boost converter
a) Circuit diagram
b) Mode-I operation
c) Mode-II operation
d) Control algorithm

The voltage gain of the boost converter is given by

$$V_{DC} = \frac{V_{c0}}{(1-D)} \tag{2.29}$$

The boost converter operated in continuous conduction mode (CCM) for the inductor $L_O > L$ is designed as

$$L = \frac{(1-D)^2 DR}{2f} \tag{2.30}$$

Where D is duty cycle and f is switching frequency.

2.3.1 Control of Boost Converter

DC-link capacitor voltage (V_{C1}) is compared with a reference voltage (V_{DC}^{ref}) to obtain error voltage (v_e)

$$v_e = V_{ref}^* - (V_{C1}) \tag{2.31}$$

Which is used to generate reference inductor current (I_{ref}^*) by PI controller as

$$I_{ref}^* = k_p v_e + k_i v_e \tag{2.32}$$

Where, k_p and k_i are PI controller gains.

Current error (i_e) is obtained by comparing (I_{ref}^*) with inductor current (I_{LO}) as

$$i_e = I_{ref}^* - I_{LO} \tag{2.33}$$

Reference signal (V_{DC}) is generated as

$$V_{DC} = k_p i_e + k_i i_e \tag{2.34}$$

This reference signal is compared with carrier signal of frequency 4 kHz to generate PWM pulses for boost converter. Whereas in post-fault condition, the reference dc-link voltage value is shifted to 2 times of the healthy reference dc-link voltage value. According to the modified reference dc-link voltage value, the boost converter control technique is implemented in post-fault condition to operate the drive-in full rated condition. The control algorithm for boost converter is shown in Fig. 2.3 (d).

2.4 Modelling of Two-level VSI

The circuit diagram of three-phase two-level VSI is shown in Fig. 2.4. A DC voltage source of constant voltage is connected at the input and it can be controlled with various control techniques to obtain the three-phase variable voltage variable frequency output to control the speed of three phase induction motor [134]. Each phase of this VSI contains two IGBTs. S_a, S_b and S_c are the control signals given to the VSI in order to obtain the output voltage at desired magnitude and frequency for induction motor drive applications. The following are the switching state (‘ON’ and ‘OFF’) conditions for the above-mentioned control signals [85].

$$S_A = \begin{cases} 1 \text{ if } S_a \text{ ON and } S'_a \text{ OFF} \\ 0 \text{ if } S_a \text{ OFF and } S'_a \text{ ON} \end{cases} \quad (2.35)$$

$$S_B = \begin{cases} 1 \text{ if } S_b \text{ ON and } S'_b \text{ OFF} \\ 0 \text{ if } S_b \text{ OFF and } S'_b \text{ ON} \end{cases} \quad (2.36)$$

$$S_C = \begin{cases} 1 \text{ if } S_c \text{ ON and } S'_c \text{ OFF} \\ 0 \text{ if } S_c \text{ OFF and } S'_c \text{ ON} \end{cases} \quad (2.37)$$

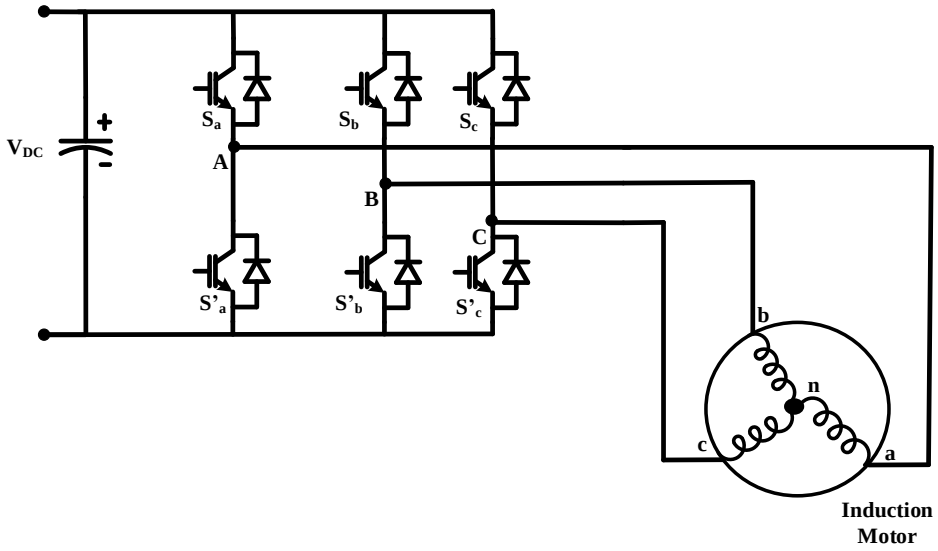

Fig. 2.4 Two-level voltage source inverter fed induction motor

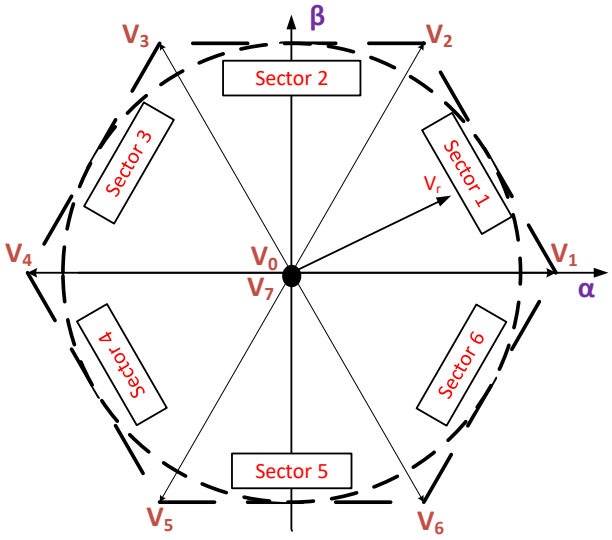

Fig. 2.5 Healthy two-level inverter voltage vectors representation in α-β plane

During the healthy (normal) condition of the inverter, the line-to-line voltages are given as:

$$\begin{bmatrix} V_{AB} \\ V_{BC} \\ V_{CA} \end{bmatrix} = V_{DC} \begin{bmatrix} 1 & -1 & 0 \\ 0 & 1 & -1 \\ -1 & 0 & 1 \end{bmatrix} \begin{bmatrix} S_a \\ S_b \\ S_c \end{bmatrix} \quad (2.38)$$

Where V_{AB}, V_{BC}, V_{CA} are the line-to-line voltages and S_a, S_b, S_c are the switching signals for the inverter. A total of eight switching states are available for a two-level VSI and the output voltage vector in stationary reference frame can be obtained by using the following relation

$$V_s(t) = \frac{2}{3}(V_{AN} + a*V_{BN} + a^2*V_{CN}) \quad (2.39)$$

Where $a = \exp(j2\pi/3)$

In healthy case eight voltage vectors are generated, where six are active vectors and two are null or zero vectors (0,0,0) and (1,1,1). The voltage vectors are presented in Table-2.1 and their representation in α-β plane is shown in Fig. 2.5.

Table-2.1. Voltage vectors of the inverter during normal operation

Voltage vector	State of transition	Vector [V]
V_0	S_a, S_b, S_c= 0	0
V_1	S_a= 1 & S_b, S_c= 0	$\frac{2}{3}V_{DC}$
V_2	S_a, S_b, = 1 &S_c= 0	$(\frac{1}{3} + j.\sqrt{3}\frac{1}{3})V_{DC}$
V_3	S_a, S_c= 0 & S_b= 1	$(-\frac{1}{3} + j.\sqrt{3}\frac{1}{3})V_{DC}$
V_4	S_a= 0 & S_b, S_c= 1	$-\frac{2}{3}V_{DC}$
V_5	S_a, S_b= 0 &S_c= 1	$(-\frac{1}{3} + j.-\sqrt{3}\frac{1}{3})V_{DC}$
V_6	S_a, S_c= 1 & S_b= 0	$(\frac{1}{3} + j.-\sqrt{3}\frac{1}{3})V_{DC}$
V_7	S_a, S_b, S_c= 1	0

2.4.1 Voltage vectors for Inverter during switch failure

The two-level voltage source inverter with TRAIC connected between midpoint of dc-link capacitors and each pole of inverter is shown in Fig. 2.6. Inverter phase voltage significantly reduces due to open-circuit or short-circuit of a switch in the inverter. Inverter voltage vectors during fault in inverter phase A is shown in Fig. 2.7.

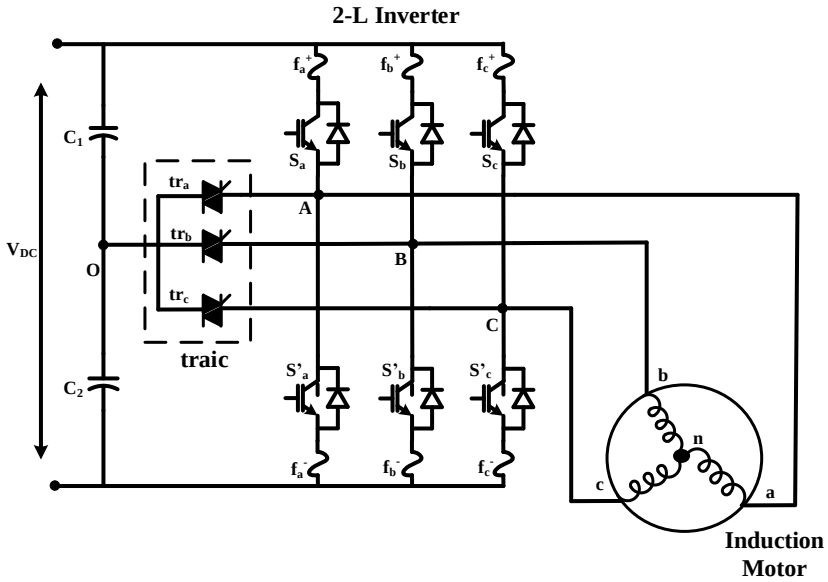

Fig. 2.6 Healthy two-level voltage source inverter fed induction motor

In this, entire leg of phase A is disconnected; as a result the phase voltage V_{AN} is equal to zero. Voltages vectors applied to inverter are obtained using Eq. 2.39 and their magnitudes are shown in Table-2.2. In case inverter upper or lower switch fails, two active voltage vectors become zero and remaining four active voltage vectors are shifted by an angle close to $\frac{\pi}{6}$, in stationary α-β plane co-ordinates, as shown in Fig. 2.8. As a result, asymmetrical voltages are applied to the motor which offer ripples in torque.

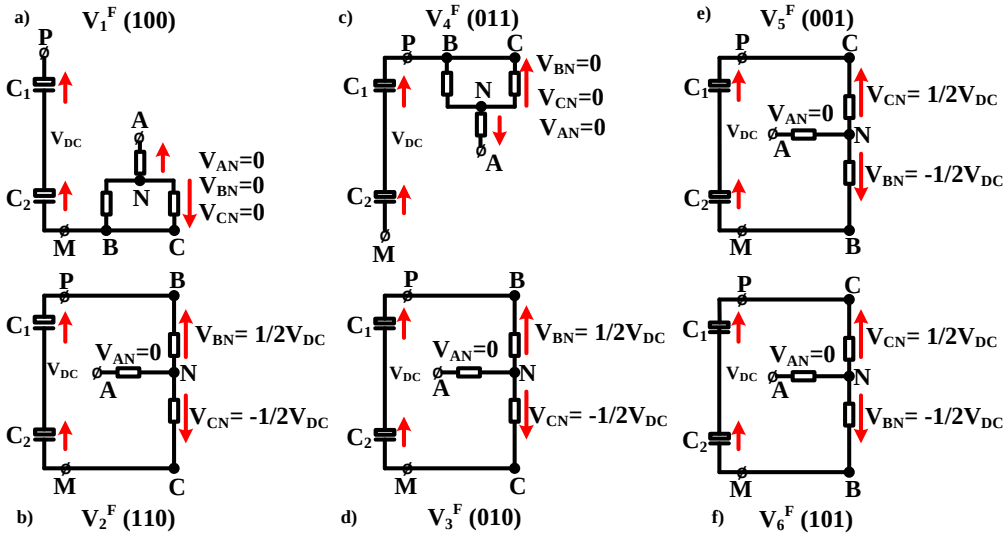

Fig. 2.7 Equivalent inverter configurations for switching states of S_a and S'_a.

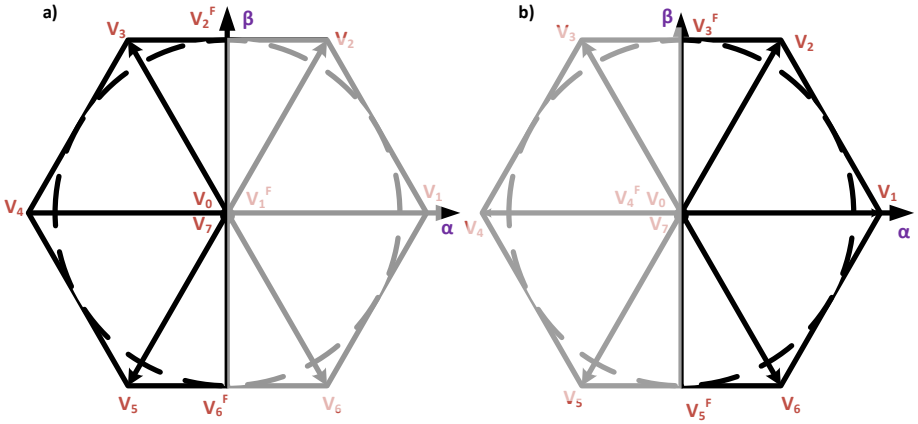

Fig. 2.8 Representation of inverter voltage vectors during fault of a switch
a) S_a b) S'_a

Table-2.2. Inverter voltage vectors during fault in inverter phase A

Faulty Switch	**Voltage Vectors [V]**		
S_a	$V_1^F = 0$	$V_2^F = \frac{V_{DC}}{\sqrt{3}} e^{j\frac{\pi}{2}}$	$V_6^F = \frac{V_{DC}}{\sqrt{3}} e^{j\frac{3\pi}{2}}$
S_a'	$V_4^F = 0$	$V_3^F = \frac{V_{DC}}{\sqrt{3}} e^{j\frac{\pi}{2}}$	$V_5^F = \frac{V_{DC}}{\sqrt{3}} e^{j\frac{3\pi}{2}}$

2.4.2 Fault identification and reconfiguration of inverter

Open-circuit or short-circuit of switch in any leg of the inverter will be identified by change in pole voltages. The difference of inverter pole voltages and reference voltage generates control signal [7]. The analysis of the control signal is used to identify fault in inverter leg, as shown in Fig. 2.9. The voltage error obtained from the comparison of measured pole voltage V_{sj}' and its reference pole voltage V_{sj}* is given by

$$\text{error} = V_{sj}^* - V_{sj}' = \pm \Delta V_{sj} \tag{2.40}$$

Where j = A, B, C.

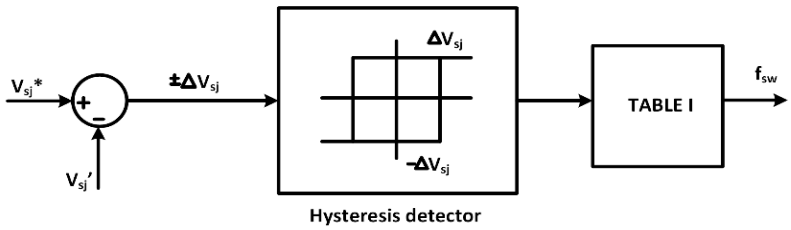

Fig. 2.9 Block diagram for fault identification.

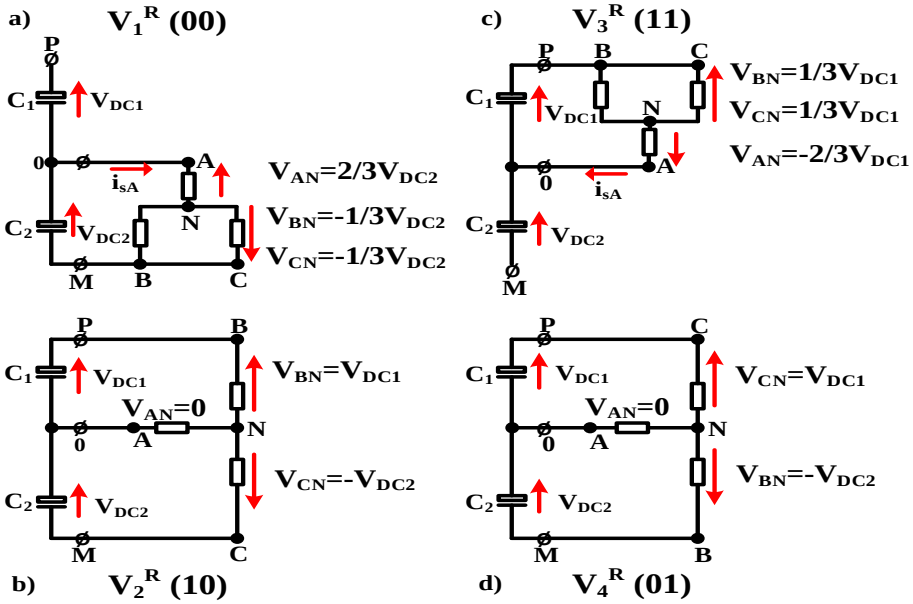

Fig. 2.10 Equivalent post-fault inverter configurations for switching states.

Table-2.3 Voltage vectors related to fault switch detection in the inverter

Fault	ΔV_{s1}	ΔV_{s2}	ΔV_{s3}
S_a	ΔV_{s1}	0	0
S_b	0	ΔV_{s2}	0
S_c	0	0	ΔV_{s3}
S_a'	$-\Delta V_{s1}$	0	0
S_b'	0	$-\Delta V_{s2}$	0
S_c'	0	0	$-\Delta V_{s3}$

Table-2.3 shows voltage errors used to identify faulty switch in the inverter leg. With this fault identification technique, the faulty leg is isolated and switch T_j (where j = A, B, C) is turned *ON*. Due to this, inverter is re-configured as shown in Fig. 2.10.

2.4.3 Voltage vectors for Reconfigured Inverter during post-fault operation

To restore normal operation of the drive due to failure of switch in inverter phase A, the converter topology is modified such that the faulty phase of the motor is connected to mid-point of the DC-link as shown in Fig. 2.10. Four active voltages are calculated as per Eq. 2.39 and are represented in Table-2.4. From Table-2.4 it is observed that, four basic non-zero voltage vectors are generated in post-fault operation. If the dc-link voltages are not equal, amplitude and angle of the voltage vectors changes. Due to this, a ripple in dc-link capacitor voltage occurs, which leads to a deviation of vectors. To overcome this, dc-link

voltage of the two capacitors is maintained constant at $V_{DC}/2$ by TLBC to produce four voltage vectors for four switching combinations.

Table-2.4. Inverter voltage vectors for the post-fault inverter topology

Voltage vector	State of transition	Vector [V]
V_1^R	$S'_bS'_c$ON S_bS_cOFF	$\frac{2}{3}V_{DC2}$
V_2^R	$S_b\,S'_c$ ON S'_bS_c OFF	$\frac{(V_{DC2}-V_{DC1})}{3}+j.\sqrt{3}\frac{(V_{DC1}+V_{DC2})}{3}$
V_3^R	$S_b\,S_c$ ON $S'_bS'_c$ OFF	$-\frac{2}{3}V_{DC1}$
V_4^R	S'_bS_c ON $S_b\,S'_c$OFF	$\frac{(V_{DC2}-V_{DC1})}{3}-j.\sqrt{3}\frac{(V_{DC1}+V_{DC2})}{3}$

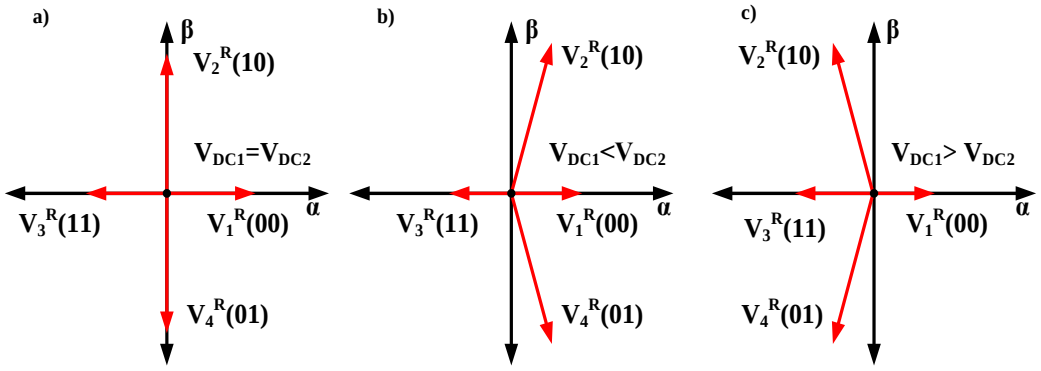

Fig. 2.11 Voltage vectors of the inverter :
a) $V_{DC1} = V_{DC2}$ b) $V_{DC1} < V_{DC2}$ c) $V_{DC1} > V_{DC2}$

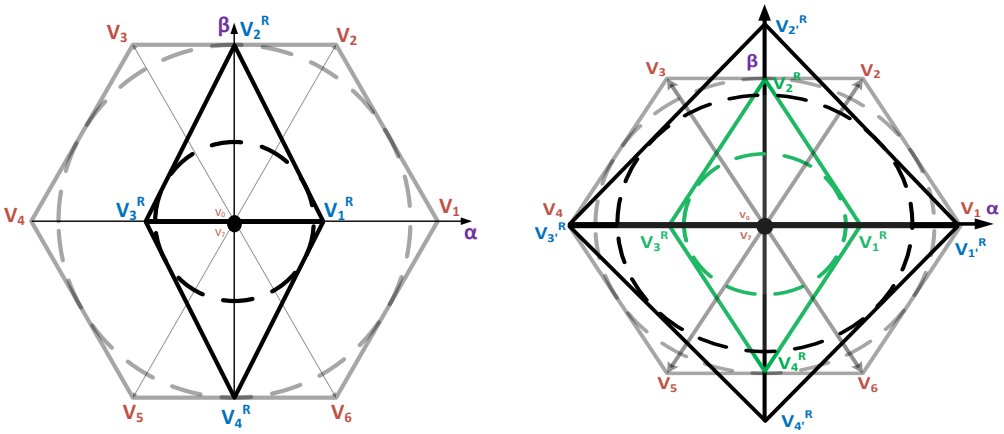

a) b)

Fig. 2.12 Representation of inverter voltage vectors after circuit re-configuration.
a) Voltage vector after inverter re-configuration
b) Voltage vector after inverter re-configuration with and without dc-link voltage boosted.

The vector positions are shown in Fig. 2.11 and voltage vectors during post-fault operation is shown in Fig. 2.12 (a). Due to this, drive cannot operate in full rated condition. To

overcome this, dc-link voltage is boosted with the help of TLBC to operate the drive in full rated condition. Hence the modified voltage vectors during post-fault operation are shown in Fig. 2.12 (b). From Fig. 2.12 (b) V_1^R, V_2^R, V_3^R, V_4^R are voltage vectors before the dc-link voltage boosted. $V_1'^R$, $V_2'^R$, $V_3'^R$, $V_4'^R$ are voltage vectors after the dc-link voltage boosted.

2.4.4. Representation of Inverter (Motor Stator Terminal connected to positive terminal of capacitor C_2)

The proposed healthy (normal) two-level voltage source inverter with TRAICs connected to negative terminal of DC bus with capacitor is shown in Fig. 2.13. It is essential to eliminate the fault at the earliest after detection of fault with the help of a control algorithm, i.e. either short-circuit or open-circuit fault in any device of a particular leg will be disconnected by turning ON of the switch T_j (where j = A, B, C). As a result, the inverter is reconfigured i.e., the entire inverter leg is disconnected and the corresponding phase terminal of the motor is connected to the positive terminal of capacitor C_2.

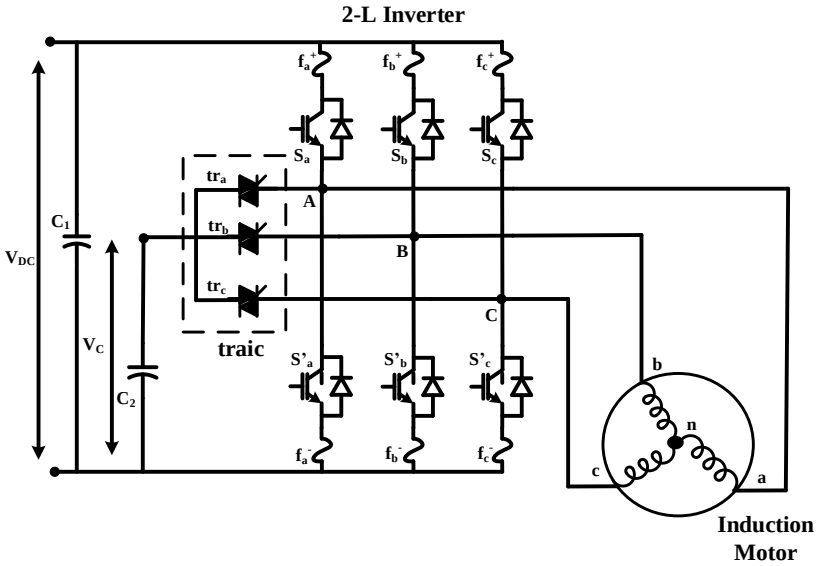

Fig. 2.13 Healthy two-level voltage source inverter fed induction motor

From Eq. 2.39, inverter voltage vectors V_1^R to V_4^R are calculated after the inverter reconfiguration and are shown in Fig. 2.14. Fig. 2.12 (a) shows the post-fault inverter voltage vectors in space vector representation. After reconfiguration of the inverter, the faulty phase voltage of the motor terminal is reduced to $\sqrt{3}$ of healthy value. Due to this, the drive cannot operate its full rated capacity. To overcome this, a combination of the boost converter and

two-level inverter is proposed for induction motor. The boost converter increases the dc-link voltage to a level that can operate the drive under full rated capacity in post-fault operation. Fig. 2.12 (b) represents the modified voltage vectors i.e., $V_1{}^{,R}$ to $V_4{}^{,R}$ and corresponding motor phase voltages are shown in Table-2.5.

Table-2.5 Switching states of inverter and phase voltages of motor during post fault

States	V_{AO}	V_{BO}	V_{CO}	V_{AN}	V_{BN}	V_{CN}	V
00	$\frac{V_{DC}}{2}$	0	0	$\frac{V_{DC}}{3}$	$-\frac{V_{DC}}{6}$	$-\frac{V_{DC}}{6}$	$V_1{}^{,R}= \frac{V_{DC}}{3} e^{j0}$
10	$\frac{V_{DC}}{2}$	V_{DC}	0	0	$\frac{V_{DC}}{2}$	$-\frac{V_{DC}}{2}$	$V_2{}^{,R}= \frac{V_{DC}}{\sqrt{3}} e^{j\frac{\pi}{2}}$
11	$\frac{V_{DC}}{2}$	V_{DC}	V_{DC}	$-\frac{V_{DC}}{3}$	$\frac{V_{DC}}{6}$	$\frac{V_{DC}}{6}$	$V_3{}^{,R}= \frac{V_{Dc}}{3} e^{j\pi}$
01	$\frac{V_{DC}}{2}$	0	V_{DC}	0	$-\frac{V_{DC}}{2}$	$\frac{V_{DC}}{2}$	$V_4{}^{,R}= \frac{V_{DC}}{\sqrt{3}} e^{j\frac{3\pi}{2}}$

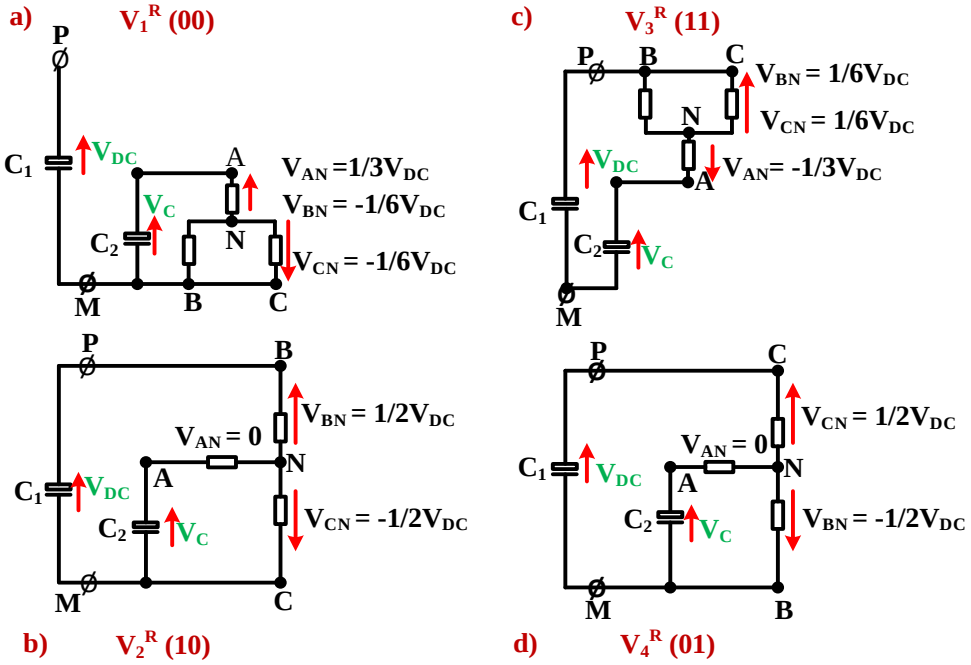

Fig. 2.14 Post-fault condition inverter switching states

2.4.5. Design of Capacitors C_1 & C_2

The design of the dc-link capacitor (C_1) and the Capacitor connected to faulty phase terminal in post-fault operation (C_2) is calculated from

$$\frac{1}{2}C(V_{DC}^2 - V_{DC1}^2) = 3 * a * V_{ph} * I * t \qquad (2.41)$$

Where 'V_{DC}' is the reference dc-link voltage, 'V_{DC1}' is the minimum level of dc-link voltage, 'a' is overloading factor, 'V_{ph}' is the phase voltage, 'I' is the maximum phase current and 't' is the time for recovery of dc-link voltage.

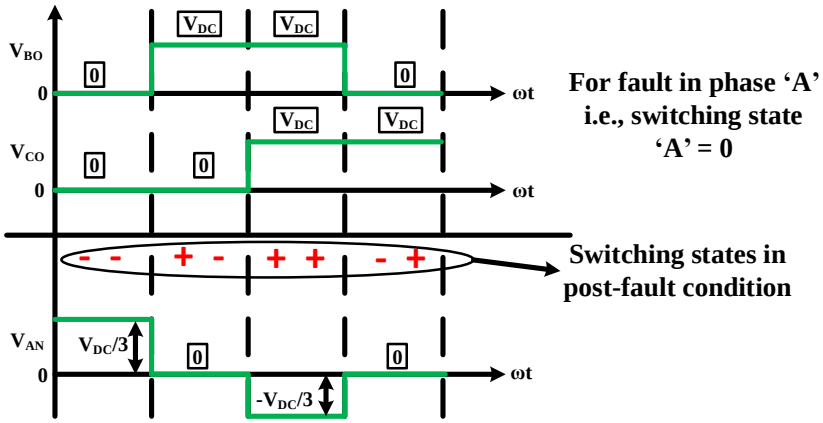

Fig. 2.15 Waveforms to calculate pole voltage of inverter

Calculation for C_1 & C_2:

V_{DC} = 1200 V, V_{DC1} = 1% of V_{DC} = 1188 V, a = 1.2, V_{ph} = 240 V.

By assuming maximum current, I = 1.25 X Rated current = 5.75 A, t = 0.005 sec.

$$C_1 = (2*3*1.2*240*5.75*0.005)/((1200)^2-(1188)^2)$$

$$C_1 = 1733.6684\ \mu F.$$

V_{DC} = 600 V, V_{DC1} = 2% of V_{DC} = 588 V, a = 1.2, V_{ph} = 240 V.

$$C_2 = (2*3*1.2*240*5.75*0.005)/((600)^2-(588)^2)$$

$$C_2 = 3484.8484\ \mu F.$$

Let voltage across the capacitor C_2 as V_{A0} and is calculated for each switching state using

$$V_{AN} = V_{A0} - V_{N0} \tag{2.42}$$

Where $V_{N0} = \frac{1}{3}(V_{A0} + V_{B0} + V_{C0})$, therefore

$$V_{AN} = V_{A0} - \left(\frac{1}{3}(V_{A0} + V_{B0} + V_{C0})\right) \tag{2.43}$$

$$V_{AN} = \frac{2}{3}V_{A0} - \frac{1}{3}V_{B0} - \frac{1}{3}V_{C0} \tag{2.44}$$

From Fig. 3.5; For switching state 0 0, $V_{AN} = \frac{1}{3}V_{DC}$, $V_{B0} = V_{C0} = 0$ then

$$V_{AN} = \frac{2}{3}V_{A0} - \frac{1}{3}V_{B0} - \frac{1}{3}V_{C0}$$

$$\frac{1}{3}V_{DC} = \frac{2}{3}V_{A0} - 0 - 0$$
$$V_{A0} = \frac{1}{2}V_{DC}$$

For switching state 1 0, $V_{AN} = 0$, $V_{B0} = V_{DC}, V_{C0} = 0$ then

$$V_{AN} = \frac{2}{3}V_{A0} - \frac{1}{3}V_{B0} - \frac{1}{3}V_{C0}$$
$$0 = \frac{2}{3}V_{A0} - \frac{1}{3}V_{DC} - 0$$
$$V_{A0} = \frac{1}{2}V_{DC}$$

For switching state 1 1, $V_{AN} = -\frac{1}{3}V_{DC}$, $V_{B0} = V_{C0} = V_{DC}$ then

$$V_{AN} = \frac{2}{3}V_{A0} - \frac{1}{3}V_{B0} - \frac{1}{3}V_{C0}$$
$$-\frac{1}{3}V_{DC} = \frac{2}{3}V_{A0} - \frac{1}{3}V_{DC} - \frac{1}{3}V_{DC}$$
$$V_{A0} = \frac{1}{2}V_{DC}$$

Similarly for switching state 0 1, $V_{AN} = 0$, $V_{B0} = 0, V_{C0} = V_{DC}$, then

$$V_{AN} = \frac{2}{3}V_{A0} - \frac{1}{3}V_{B0} - \frac{1}{3}V_{C0}$$
$$0 = \frac{2}{3}V_{A0} - 0 - \frac{1}{3}V_{DC}$$
$$V_{A0} = \frac{1}{2}V_{DC}$$

From the above calculations, it is observed that voltage across the capacitor C_2 for each switching state is constant and its magnitude is $\frac{V_{DC}}{2}$.

2.5. Schematics of the Proposed Topologies

In this, the proposed fault-tolerant converter topologies for open-circuit or short-circuit of inverter switch in any one of the legs are presented. The proposed fault-tolerant converter topologies for induction motor drive are shown in Fig. 2.16. Fig. 2.16 (a) consists of three-level boost converter, two-level inverter fed induction motor with fault-tolerant capability. If any inverter switch fails in any one of the inverter leg; the corresponding motor terminal connected to the faulty inverter leg is isolated and connected to the midpoint of the dc-link capacitors with help of TRAIC. The TLBC boost the voltage across the dc-link of

the inverter to operate the drive in full rated condition during pre-fault and post-fault condition. Fig. 2.16 (b) consists of boost converter, two-level inverter fed induction motor with fault-tolerant capability. If any inverter switch fails in any one of the inverter leg; the corresponding motor terminal connected to the faulty inverter leg is isolated and connected to the auxiliary capacitor with help of TRAIC. The boost converter boosts the voltage across the dc-link of the inverter to operate the drive in full rated condition during pre-fault and post-fault condition.

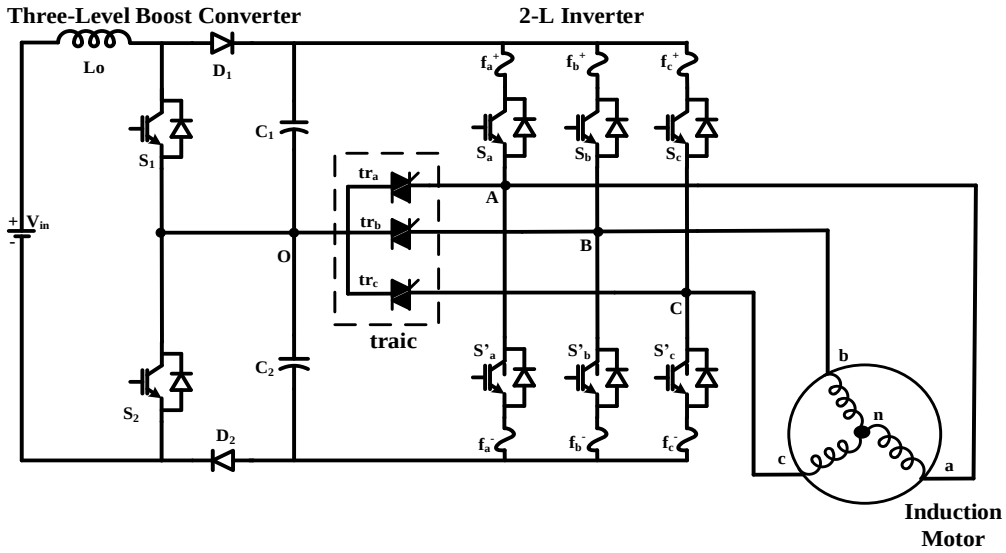

a)

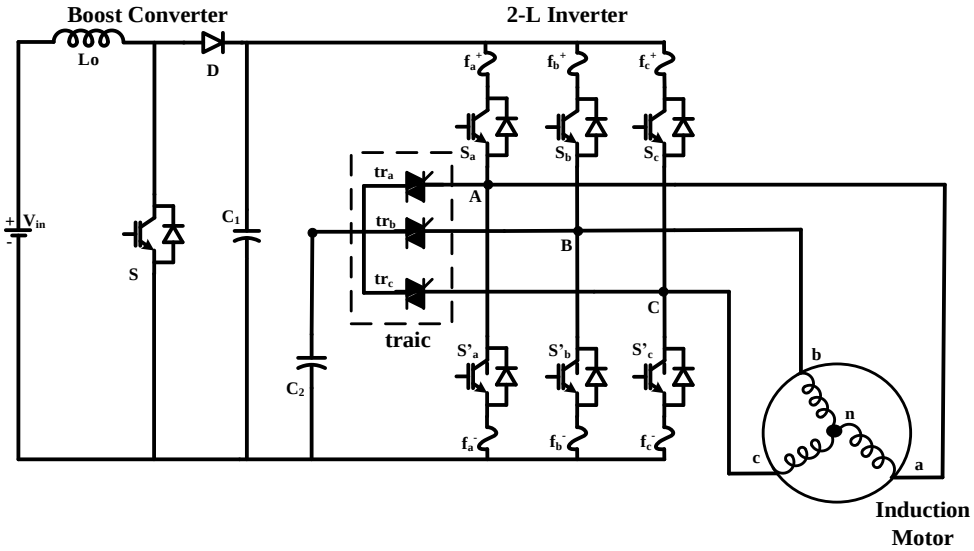

b)

Fig. 2.16 Schematics of the proposed fault-tolerant converter topologies

a) TLBC based fault-tolerant two-level inverter fed induction motor (Topology-A)
b) BC based fault-tolerant two-level inverter fed induction motor (Topology-B)

2.6. Modeling of Induction Motor

The popular representation of three-phase squirrel-cage induction motor in a stationary reference frame is given as follows [135], [136]

$$V_{s\alpha} = R_s i_{s\alpha} + \frac{d\varphi_{s\alpha}}{dt} \tag{2.45}$$

$$V_{s\beta} = R_s i_{s\beta} + \frac{d\varphi_{s\beta}}{dt} \tag{2.46}$$

$$0 = R_r i_{r\alpha} + \frac{d\varphi_{r\alpha}}{dt} + \omega_r \varphi_{r\beta} \tag{2.47}$$

$$0 = R_r i_{r\beta} + \frac{d\varphi_{r\beta}}{dt} - \omega_r \varphi_{r\alpha} \tag{2.48}$$

$$\varphi_{s\alpha} = L_s i_{s\alpha} + L_m i_{r\alpha} \tag{2.49}$$

$$\varphi_{s\beta} = L_s i_{s\beta} + L_m i_{r\beta} \tag{2.50}$$

$$\varphi_{r\alpha} = L_r i_{r\alpha} + L_m i_{s\alpha} \tag{2.51}$$

$$\varphi_{r\beta} = L_r i_{r\beta} + L_m i_{s\beta} \tag{2.52}$$

$$T_e = \frac{3}{2} p\left(\varphi_{s\alpha} i_{s\beta} - \varphi_{s\beta} i_{s\alpha}\right) \tag{2.53}$$

$$J\frac{d\omega_r}{dt} = T_e - T_l \tag{2.54}$$

In the above representation, subscripts *s* and *r* represent the stator and rotor respectively. *u*, *I* and φ represent voltage vector, current vector and flux vector respectively. *R* and *L* represent resistance and inductance respectively. L_m represents the mutual inductance and w*r* is the rotor angular velocity. T_e and T_l represent electromagnetic torque and load torque respectively. *J* and *p* represent moment of inertia and number of pole pairs respectively. The electromagnetic system of induction motor is represented by Eq. 2.45 to Eq. 2.52 and the mechanical system is represented by Eq. 2.53 and Eq. 2.54.

The continuous-time model of electromagnetic system of the induction motor by considering stator flux and stator current as state variables can be obtained by using the following relations [137], [138].

$$\dot{X(t)} = A(t)X(t) + B(t)U(t) \tag{2.55}$$

$$Y(t) = C(t)X(t) + D(t)U(t) \tag{2.56}$$

Where *X* represents the matrix for state variables, *U* represents the matrix for input variables, Y represents matrix for output variables and A, B, C and D represent state matrices respectively and they are given as follows

$$X = \begin{bmatrix} \varphi_{s\alpha} & \varphi_{s\beta} i_{s\alpha} & i_{s\beta} \end{bmatrix}^T \tag{2.57}$$

$$U = \begin{bmatrix} V_{s\alpha} & V_{s\beta} & 0 & 0 \end{bmatrix}^T \tag{2.58}$$

$$Y = \begin{bmatrix} i_{s\alpha} & i_{s\beta} & 0 & 0 \end{bmatrix}^T \tag{2.59}$$

$$A(t) = \begin{bmatrix} 0 & 0 & -R_s & 0 \\ 0 & 0 & 0 & -R_s \\ \lambda R_r & \lambda L_r \omega_r(t) & -\lambda k_{sr} & -\omega_r(t) \\ -\lambda L_r \omega_r(t) & \lambda R_r & \omega_r(t) & -\lambda k_{sr} \end{bmatrix} \tag{2.60}$$

$$B(t) = \begin{bmatrix} 1 & 0 & 0 & 0 \\ 0 & 1 & 0 & 0 \\ \lambda L_r & 0 & 0 & 0 \\ 0 & \lambda L_r & 0 & 0 \end{bmatrix} \tag{2.61}$$

$$C(t) = \begin{bmatrix} 0 & 0 & 1 & 0 \\ 0 & 0 & 0 & 1 \end{bmatrix} \tag{2.62}$$

$$D(t) = [0] \tag{2.63}$$

Where $\lambda = \frac{1}{L_s L_r - L_m^2}$, $k_{sr} = R_s L_r + R_r L_s$

For the above linear time-varying system (LTV), matrix *A(t)* depends on the instantaneous value of rotor mechanical speed $w_r(t)$, the other two matrices *B(t)* and *C(t)* are constant. Since *A(t)* is LTV matrix, the realization of an exact discrete model of the system becomes complex and it is not straightforward due to the variations in $w_r(t)$ [138]. Hence, a simple forward Euler's discretization method is used to obtain the required discrete model of the induction motor. The discrete model for the continuous-time LTV system described in Eq. 2.55 and Eq. 2.56 is given as

$$X^{k+1} = A_d^k X^k + B_d^k U^k \tag{2.64}$$

$$Y^{k+1} = C_d^k X^k + D_d^k U^k \tag{2.65}$$

Forward Euler's discretization is a simple and approximate numerical differentiation method. It can be represented by the following relation

$$\frac{dx}{dt} = \frac{x^{k-1} - x^k}{T_s} \tag{2.66}$$

In the above equation, k represents present sampling instant and T_S represents sampling period.

By applying the forward Euler's discretization to Eq. 2.55 and Eq. 2.56, the discrete model can be obtained as

$$A_d^k = I + T_s A \tag{2.67}$$

$$B_d^k = T_s B \tag{2.68}$$

$$C_d^k = C \tag{2.69}$$

$$D_d^k = D \tag{2.70}$$

Hence, the discrete matrices $A_d{}^k$, $B_d{}^k$, $C_d{}^k$ and $D_d{}^k$ for electromagnetic model of the induction motor are given as follows

$$A_d^k = \begin{bmatrix} 0 & 0 & -T_s R_s & 0 \\ 0 & 0 & 0 & -T_s R_s \\ T_s \lambda R_r & T_s \lambda L_r \omega_r & 1 - T_s \lambda k_{sr} & -T_s \omega_r \\ -T_s \lambda L_r \omega_r & T_s \lambda R_r & T_s \omega_r & 1 - T_s \lambda k_{sr} \end{bmatrix} \tag{2.71}$$

$$B_k^d = \begin{bmatrix} T_s & 0 & 0 & 0 \\ 0 & T_s & 0 & 0 \\ T_s \lambda L_r & 0 & 0 & 0 \\ 0 & T_s \lambda L_r & 0 & 0 \end{bmatrix} \tag{2.72}$$

$$c_k^d = \begin{bmatrix} 0 & 0 & 1 & 0 \\ 0 & 0 & 0 & 1 \end{bmatrix} \tag{2.73}$$

$$D_k^d = [0] \tag{2.74}$$

The electromagnetic toque can be obtained by using the Eq. 2.53.

2.7. Summary

In this chapter analysis, modelling and control algorithms of three-level boost converter, boost converter is explained in detail. Operation of two-level inverter during fault condition of any one switch in any of the legs of a three-level inverter topology is explained by connecting TRAICs between DC link and Inverter poles and observed that even though supply to all the three phases of induction motor is achieved, the voltage at inverter output terminal is not same as before fault condition. To achieve balanced three-phase voltages at

the inverter output terminals a boost converter and a three-level boost converter connected at the input terminals and two Topologies are developed to obtain fault-tolerant operation for the induction motor. Modelling of three-phase induction motor in stationary reference frame is also presented. These two fault-tolerant inverter topologies are used to control the induction by applying various speed control methods are presented in the subsequent chapters.

Chapter-3
Scalar Control using Fault-Tolerant Converter Topologies

3.1. Introduction

In this chapter, the speed control of induction motor using scalar control with the help of proposed fault-tolerant two-level voltage source inverter topologies are presented for various operating conditions. Scalar v/f control scheme is implemented to observe the suitability of these converters to control the speed of the drive under faulty condition of the inverter switches and results are presented by conducting the experiments on the developed hardware setup.

3.2. Speed Control Algorithm

Speed control of squirrel cage induction motor can be obtained by various scalar methods such as supply voltage control, supply frequency control, stator resistance/ reactance control, pole changing mechanism, v/f control etc. Each method has its own limitations w.r.t motor operating conditions, insulation requirements and so on. Out of these methods v/f control is popular to get wide variation of speeds within the operating range of the motor with reasonable dynamic performance [81]. Due to advancements in the development of wide range of power semiconductor devices, converter topologies and also control techniques, the generation of variable voltage variable frequency supply become simple and easy from the available AC/DC supply. Since power converters consists of semi-conductor switches which are prone to open circuit or short circuit faults due to input supply side problems or load operating conditions. As a result the performance of drive may deteriorate and may also spoil the quality of the product particularly in case of continuous process industry. Therefore it is necessary and essential to design and develop a fault-tolerant converter. In this research work two such converter topologies are developed and observed their operation for open-circuit and short-circuit switch faults in any one leg of the three phase two-level voltage source inverter. In this process a simple scalar v/f control is applied at first stage and results are presented in this chapter.

Fig. 3.1 shows the scheme for speed control of induction motor drive fed from a voltage source inverter with sine-triangle PWM. In outer loop, the reference speed is compared with the measured speed and the error is used to obtain the slip speed. This slip speed is added to the rotor speed to obtain synchronous speed and then stator frequency to generate three-phase sinusoidal signals with a phase shift of 120^0. These reference signals are compared with the triangular carrier wave of 2 kHz to generate PWM signals for inverter

(i.e., S_a, S_b and S_c) during normal operation. Whereas in post-fault operation; two sinusoidal signals are generated with a phase shift of 60^0 and compared with the triangular carrier wave of 2 kHz to generate PWM signals for the reconfigured inverter (i.e., S_b and S_c) to achieve post-fault operation.

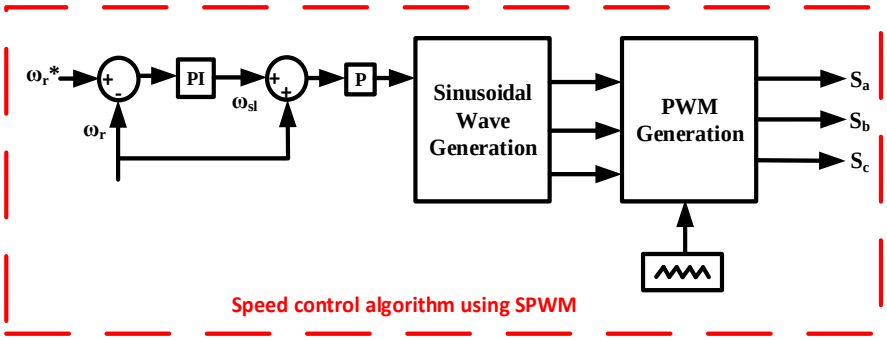

Fig. 3.1 Speed control algorithm for induction motor drive

3.3. Experimental Setup

Block diagram of proposed fault-tolerant induction motor drive is shown in Fig. 3.2. It consists of an IGBT based DC-DC converter, 2.2 kW, 4-pole, 50 Hz, three-phase squirrel-cage induction motor, a 1.5 kW separately excited DC generator along with resistive load bank, a 9.3 kVA two-level IGBT based voltage source inverter (VSI), an incremental encoder with 1024 ppr, three current sensors (LA-25 NP), two voltage sensor (LV-25) and a dSPACE-DS1104 R&D controller board. Induction motor is coupled with DC generator which in turn connected to a resistive load bank. Speed of the motor is measured at a sub-sample rate of 500 Hz in order to reduce the quantization error of the speed signal obtained from the incremental encoder [91]. The two-level VSI used to drive the induction motor and intermediate dc-link capacitors. The DC supplies of ± 15 V are used for current sensors and voltage sensor and a DC supply of 10 V is used for incremental encoder. A digital storage oscilloscope (Make: Yokogowa with model No.: DLM 4058) is used to capture the experimental results. The photograph of the experimental setup is shown in Fig. 3.3. This experimental setup is used to implement all the proposed converter topologies and control techniques presented in this thesis.

The dSPACE-DS1104 R&D controller board is used for real-time implementation of conventional and proposed control algorithms. The block diagram of this controller board is shown in Fig. 3.4. The main components of this controller board are main/master

processor (MPC8240, PowerPC 603 core, 250 MHz), four multiplexed ADCs (16 - bit), four independent ADCs (12-bit), eight DACs (16-bit), two incremental encoder interfaces, 20-bit digital I/Os, serial interface (RS232, RS485 and RS442) and one slave DSP (TMS320F240) with built-in PWM signals for both three-phase and single-phase PWM outputs. This controller board is placed in the 32-bit PCI slot of the personal computer (PC) and it requires Matlab/Simulink/RTW. In order to communicate Simulink based control algorithm with induction motor drive, it is necessary to introduce I/O interface into the model using dSPACE real-time interfacing (RTI) blocks. This will allow the simulation to interface with the hardware. A model will be created with Simulink and RTI blocks using the SimulinkCoder™. This generates the C code and the RTI build process compiles the generated C code and links the object files and libraries into an executable form. This application directly dumped to the real-time processor after the compilation (build). The build status is displayed in the MATLAB command window and generates four files namely

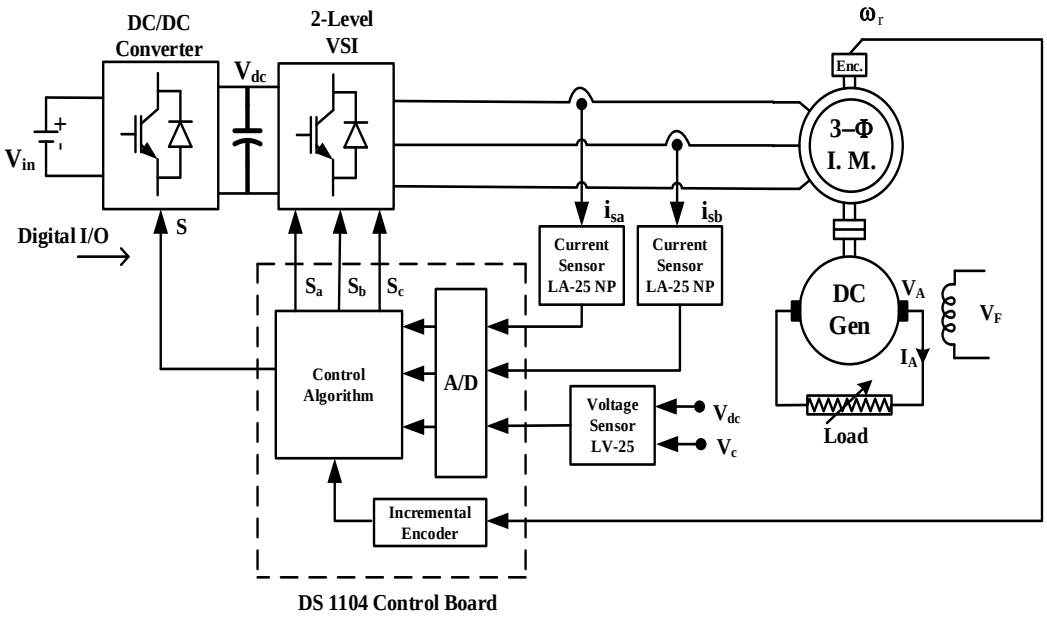

Fig. 3.2 Block diagram of proposed fault-tolerant induction motor drive

PPC: The real-time application to be downloaded to a Power PC board

MAP: Map file with address information of variables.

TRC: Variable description files to use by Control Desk.

SDF: System description files with reference to PPC, MAP and TRC files.

Using the information from the SDF, control desk will read and write the variables in real-time. Control desk provides numerous instruments to access, measure and display the various parameters in the real-time implementation.

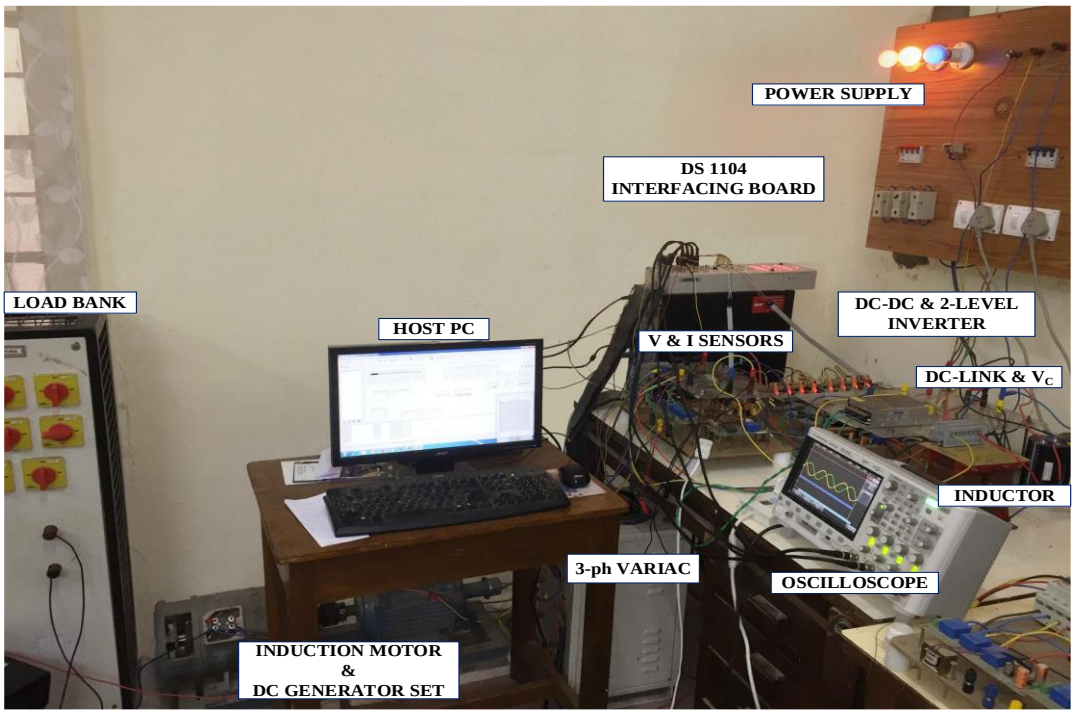

Fig. 3.3. Experimental set-up of fault-tolerant induction motor drive

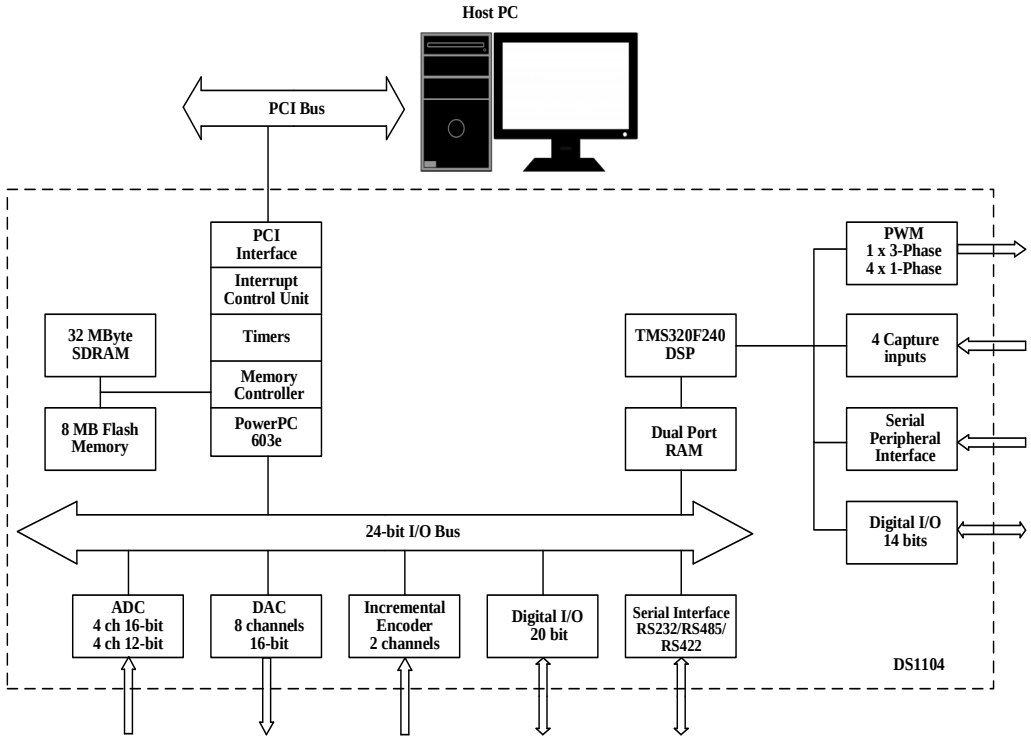

Fig. 3.4 Block diagram for dSPACE DS-1104 R&D controller board [97]

3.4. Experimental Results for Topology-A

Experiments are conducted on the designed and developed proposed converter topology by controlling in real-time with dSPACE-DS 1104 controller as shown in Fig. 3.3 for various operating conditions of the drive. As mentioned in the chapter-2, this Topology-A consists of three-level boost converter (TLBC) based fault-tolerant two-level inverter fed induction motor. Fig. 3.5 represents the results for load 8 N-m at motor speed of 80 rad/sec for the healthy inverter and proposed fault-tolerant inverter when switch fail i.e., open-circuit or short-circuit in any one leg of the VSI. Fig. 3.6 represents the results of the healthy inverter and proposed fault-tolerant inverter operating at a speed of 150 rad/sec with a load torque of 8 N-m. From the results, it is witnessed that the proposed topology with switch failure gave stator currents, torque and speed are almost similar to the healthy inverter, hence it can be assumed that the proposed control algorithm is working satisfactorily for variation in load and also for speed changes.

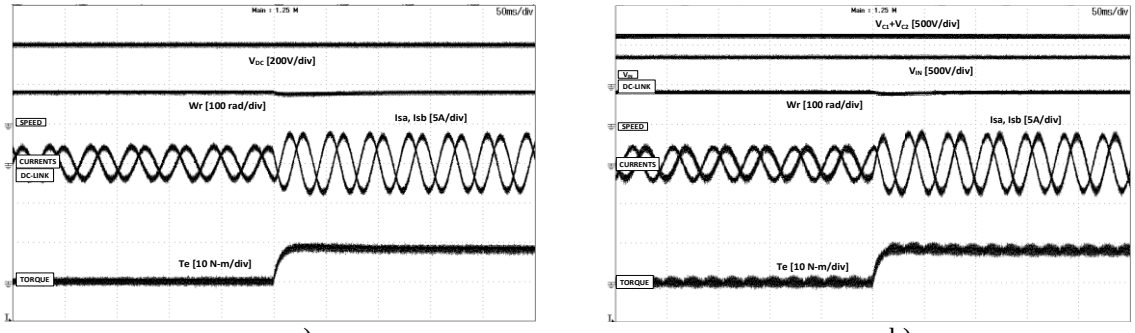

a) b)

Fig. 3.5 Speed and torque response for variation of load from 0 N-m to 8 N-m at 80 rad/sec.

a) Healthy converter topology
b) Proposed converter topology

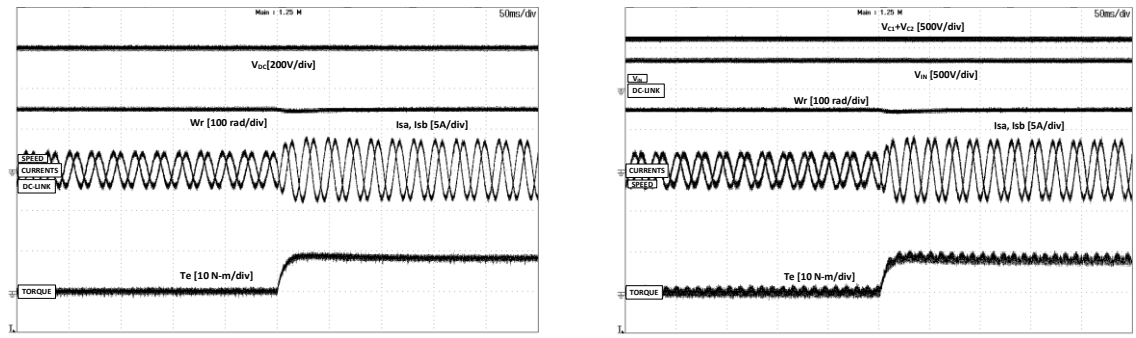

a) b)

Fig. 3.6 Speed and torque response for variation of load from 0 N-m to 8 N-m at 150 rad/sec.

a) Healthy converter topology
b) Proposed converter topology

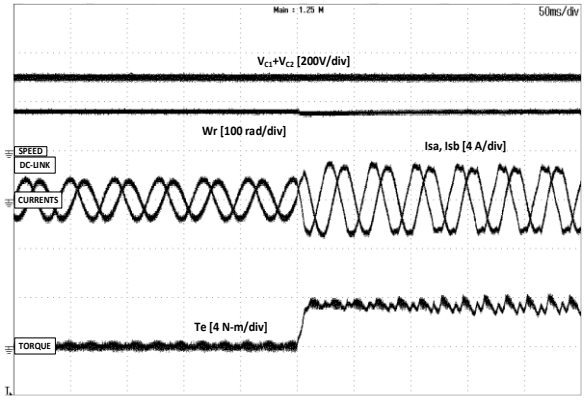

Fig. 3.7 Torque response for variation of load from 0 N-m to 4 N-m at 80 rad/sec for B4 converter.

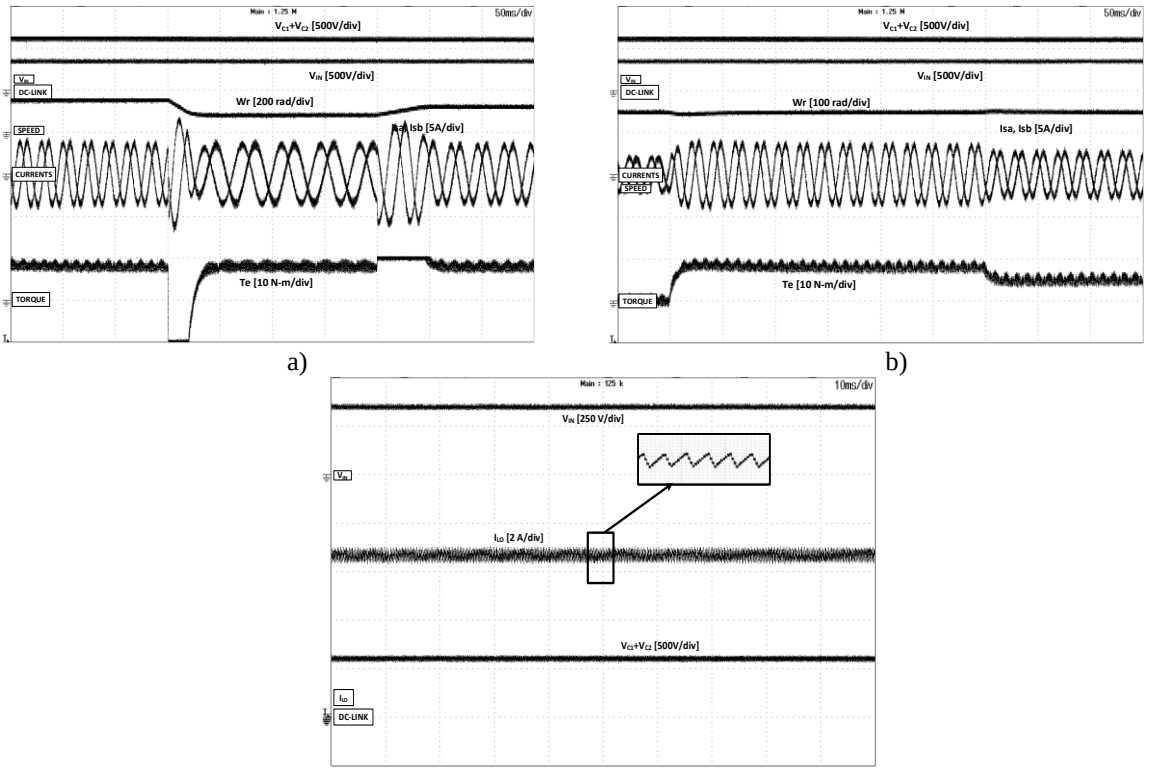

Fig. 3.8 Response of the proposed fault-tolerant inverter topology

a) Change in speed
b) Change in load
c) Output of three-level boost converter

Fig. 3.7 represents the results of conventional fault-tolerant inverter topology (B4) operating at a speed of 80 rad/sec with a load torque of 4 N-m. From the above result, it is observed that the conventional fault-tolerant inverter topology can operate with less load torque in post-fault condition; whereas the proposed topology in post-fault condition will operate in rated condition similar to the healthy inverter topology. Hence, it can be concluded that the proposed control algorithm worked satisfactorily for these operating

conditions. Fig. 3.8 represents the results of proposed fault-tolerant converter topology during change in speed, change in load and TLBC outputs respectively. From these waveform it is observed that the proposed converter topology and its control algorithm gives a better dynamic performance in a post-fault condition.

3.5. Experimental Results for Topology-B

Experiments are conducted on the designed and developed proposed converter topology by controlling in real-time with dSpace_1104 controller as shown in Fig. 3.3 for various operating conditions of the drive. As mentioned in the chapter-2, this Topology-B consists of a boost converter with fault-tolerant two-level inverter fed induction motor. The proposed converter and motor parameters are represented in Appendix.

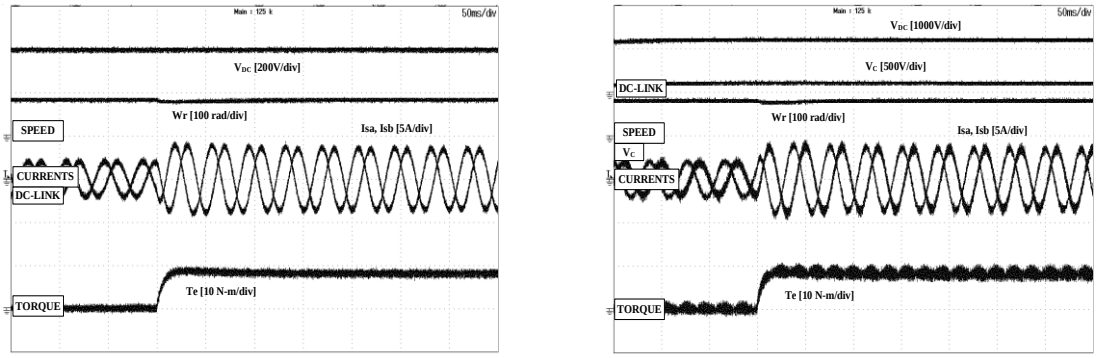

a) b)

Fig. 3.9 Speed and torque response for variation of load from 0 N-m to 8 N-m at 80 rad/sec.

a) Healthy converter topology
b) Proposed converter topology

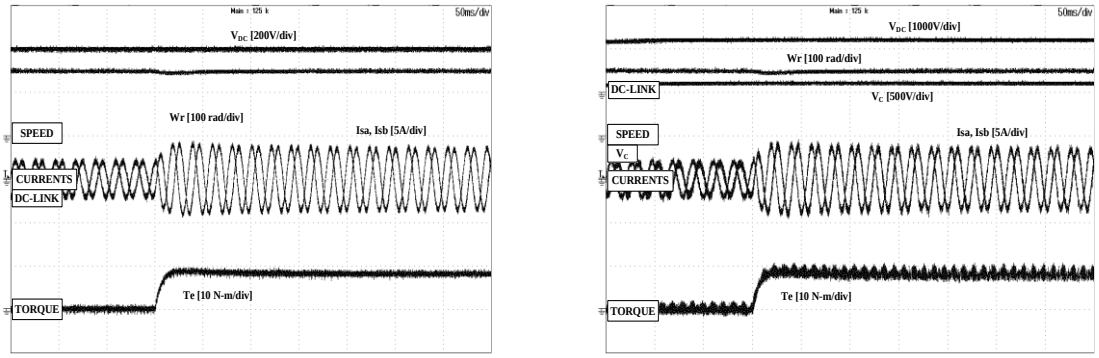

a) b)

Fig. 3.10 Speed and torque response for variation of load from 0 N-m to 8 N-m at 150 rad/sec.

a) Healthy converter topology
b) Proposed converter topology

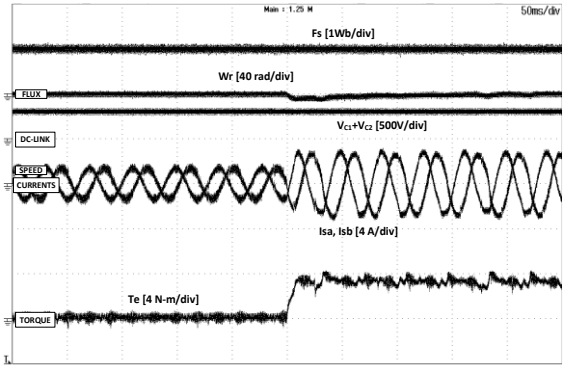

Fig. 3.11 Torque response for variation of load from 0 N-m to 4 N-m at 80 rad/sec for B4 converter.

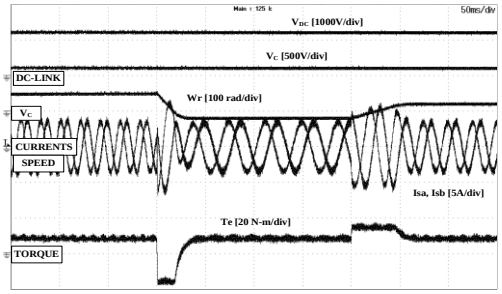

a)

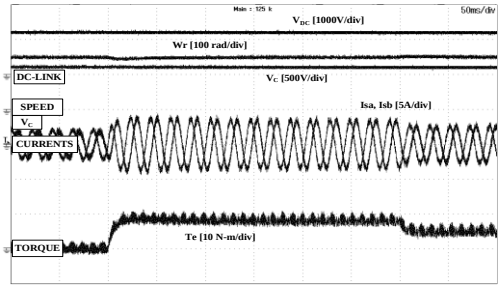

b)

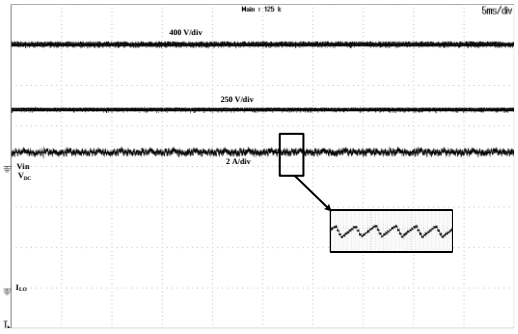

c)

Fig. 3.12 Response of the proposed fault-tolerant inverter topology

a) Change in speed
b) Change in load
c) Boost converter output

Fig. 3.9 represents the response of the healthy inverter topology and proposed fault-tolerant inverter topology operating at 80 rad/sec with 8 N-m load torque. From the results, it is examined that the proposed topology stator currents, torque and speed are almost similar to the healthy inverter. Fig. 3.10 shows the response of the healthy inverter and proposed fault-tolerant inverter operating at a speed of 150 rad/sec with a load torque of 8 N-m. From the results, it is examined that the proposed topology stator currents, torque and speed are almost similar to the healthy inverter. Fig. 3.11 shows the results of conventional fault-tolerant inverter topology at 80 rad/sec with 4 N-m load torque. From

the above result, it is observed that the conventional fault-tolerant inverter topology operate with low speed and load torque in post-fault condition; whereas the proposed topology in post-fault condition will operate in rated condition similar to the healthy inverter topology. Fig. 3.12 shows the proposed topology results during load change, speed change and boost converter outputs respectively. The proposed topology gives a better dynamic performance in a post-fault condition which is observed from the experimental results.

3.6. Summary

Two-level VSI is connected with three-level boost converter/boost converter (Topology-A/Topology-B) at the front end for induction motor with fault-tolerant capability is presented in this chapter. The proposed converter topologies operation is compared with conventional fault-tolerant converter topology and experimental results are presented. In post-fault operation, the proposed topologies can able to operate the drive in full rated capacity and also gives a better dynamic performance, eliminates the voltage balance at dc-link in the B4 operation. From the experimental results, it is witnessed that the proposed fault-tolerant topologies and its control logic with switch failure offer the stator currents; torque and speed variations almost similar as that of healthy inverter however conventional fault-tolerant topology (B4) drive operates with less capacity. Hence, it may be considered as one of the alternative solutions for operation of induction motor drives during inverter switch failures.

Chapter-4
Field Oriented Control using Fault-Tolerant Converter Topologies

4.1. Introduction

In this chapter, the brief fundamentals related to field oriented control of three-phase induction motor are discussed. Simulation and experimental results using three-level boost converter fed fault-tolerant converter and boost converter fed fault-tolerant converter are presented and results are compared with conventional fault tolerant inverter (B4) for load changes and speed changes. Detailed explanation with respect to merits of the proposed topologies is presented.

4.2. Field Oriented Control Algorithm

Induction motor operation can be studied for different operating conditions by sensing the variation in currents, voltages and speed. With the help of these measurements torque and flux are estimated. Reference frame theory is applied to convert three phase quantities into two phase quantities and vice-versa wherever required. By using park's transformation the measured stator currents are converted into rotating reference frame and shown in Fig. 4.1. The magnitude of rotor flux and electromagnetic torque is controlled by the direct and quadrature axis currents respectively [82-85].

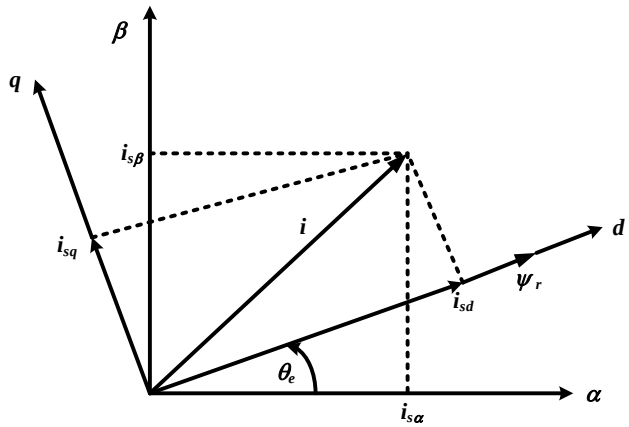

Fig. 4.1. Reference frame orientation used in FOC [85]

$$\varphi_{rd} = \frac{L_m}{\tau_{rs}+1} i_{sd} \tag{4.1}$$

$$T_e = \frac{3}{2}\frac{L_m}{L_r} p\varphi_{rd} i_{sq} \tag{4.2}$$

The reference direct and quadrature axis currents are generated with the help of rotor speed and rotor flux. The current error is given to PI controller to obtain reference voltage signals in d-q transformation and converted into three-phase reference voltages by using Inverse

Park's transformation. The three-phase reference voltages are fed to the PWM unit to generate the switching states to the two-level inverter to control the speed of induction motor. The complete mechanism is represented in Fig. 4.2. During normal operating conditions, the motor line currents are given by (4.3) – (4.5).

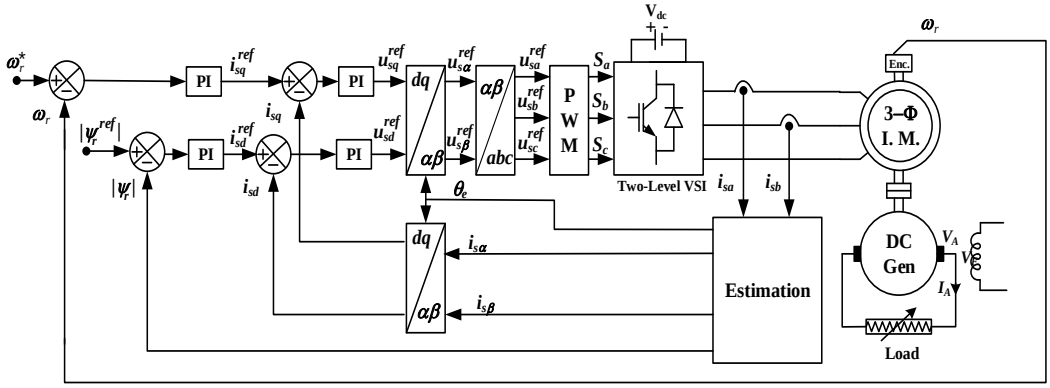

Fig. 4.2. Block diagram of FOC for induction motor drive [85]

$$I_{as} = I\cos(\omega t + \Phi) \tag{4.3}$$

$$I_{bs} = I\cos\left(\omega t + \Phi - \frac{2\Pi}{3}\right) \tag{4.4}$$

$$I_{cs} = I\cos\left(\omega t + \Phi + \frac{2\Pi}{3}\right) \tag{4.5}$$

The MMF generated by the stator currents of the three phases as

$$MMF = MMF_a + MMF_b + MMF_c$$

$$= NI_{as} + aNI_{bs} + a2NI_{cs}$$

Where a = $1\angle 120^0$ and N is the effective stator turns per phase.

For balanced operation

$$MMF = \frac{3}{2} Fe^{j0} = \frac{3}{2} F(\cos\theta + j\sin\theta)$$

Where F = NI and $\theta = (\omega t + \Phi)$.

For fault in inverter leg 'A', corresponding motor phase 'A' is isolated and connected to mid-point of the DC-link capacitors/capacitor C_2 and the line current of the motor I_{as} is sensed. After reconfiguration of inverter and modification in the control logic induction motor phase current I_{as} and also healthy phase currents I_{bs}, I_{cs} are sinusoidally distributed with a phase shift of 120^0as indicated in (4.4) and (4.5) of the normal operation of the drive controlled using FOC. Even though FOC has the drawbacks of indirect control over

flux and electromagnetic torque and require more coordinates transformation which increase the control complexity and computation burden, some application may still require this control. Therefore simulation and experimental studies are made and results are presented for feasibility of this control with the proposed two fault tolerant converter topologies.

4.3. Simulation Results of Topology-A

Simulations are carried out on the induction motor drive system with the conventional converter(B6), conventional fault-tolerant converter (B4) and proposed Topology-A consists of three-level boost converter (TLBC) based fault-tolerant two-level inverter fed induction motor.

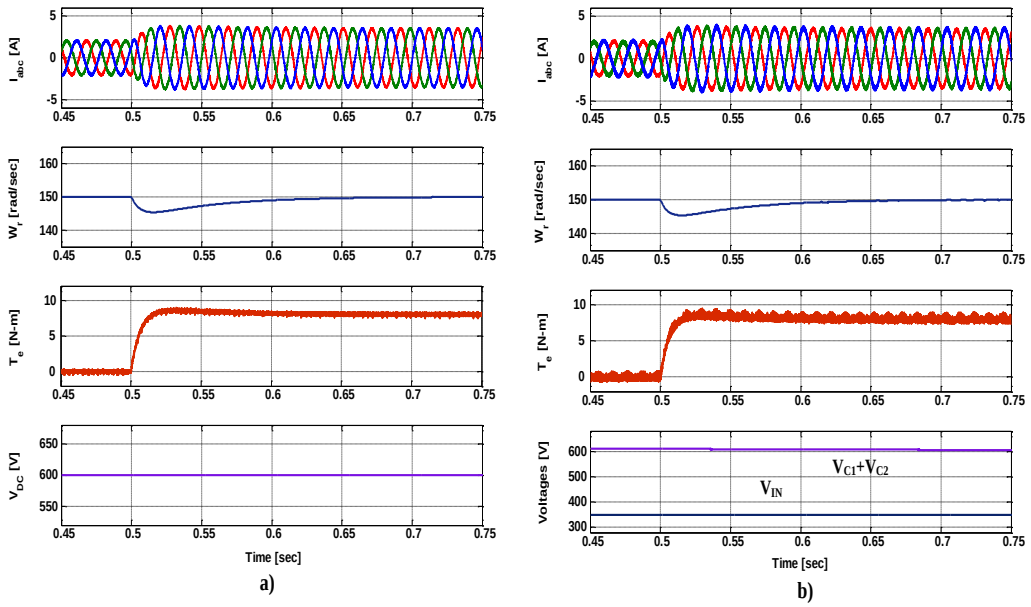

Fig. 4.3. Step-change responses of an induction motor drive at load torque of 0 N-m to 8 N-m at 150 rad/sec.

a) Conventional converter
b) Proposed 3-level boost converter fed B4 converter.

Fig. 4.3 shows the results of B6 converter (conventional two-level inverter) and proposed three-level boost converter with B4 converter configuration for induction motor drive operating at reference speed of 150 rad/sec and step-change in load torque from 0 N-m to 8 N-m. Fig. 4.4 shows the results of B6 converter, conventional fault-tolerant converter (B4) and proposed B4 converter at load torque of 8 N-m with reference speed of 80 rad/sec.

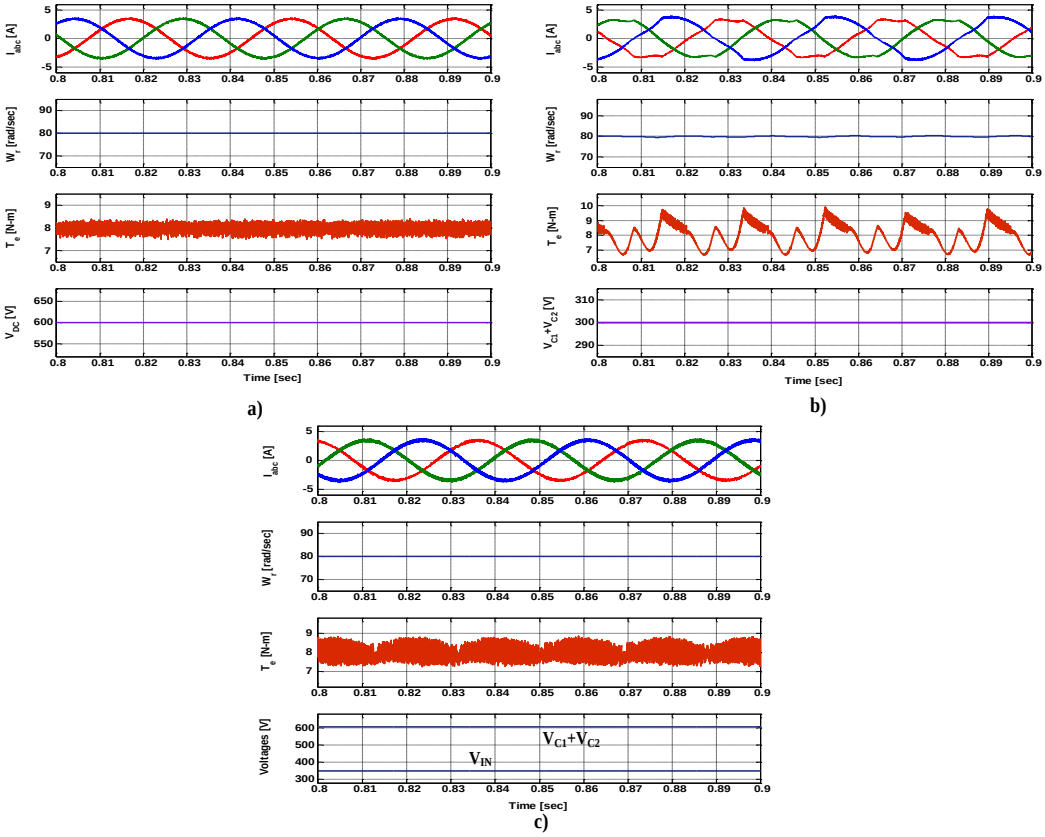

Fig. 4.4. Steady-state response of an induction motor drive at load torque of 8 N-m at 80 rad/sec
a) Conventional converter
b) Conventional B4 fault-tolerant converter
c) Proposed three-level boost converter fed B4 converter.

From Fig. 4.4, it is observed that behaviour of the B4 converter fed drive is not similar to B6 converter. Ripples in current generate ripples in the torque which in turn produce oscillations in the speed. Hence, a TLBC is proposed at front end of two-level inverter to minimize these issues. Operation of the drive system with proposed fault-tolerant topology at full load, change in speed and change in load and output of three-level boost converter are shown in Fig. 4.5. The stator phase voltages of the proposed converter in healthy and post-fault condition are shown in Fig. 4.6. From the results it is observed that the proposed converter can operate in full rated operating condition of the drive similar to conventional converter (B6). To observe the performance of the drive, a load torque of 8 N-m is considered as a test case and results are presented. During B6 converter operation, when the motor is operated at a speed of 80 rad/sec for a load torque of 8 N-m, the current THD is 6.80% and torque ripple is 1.55 N-m.

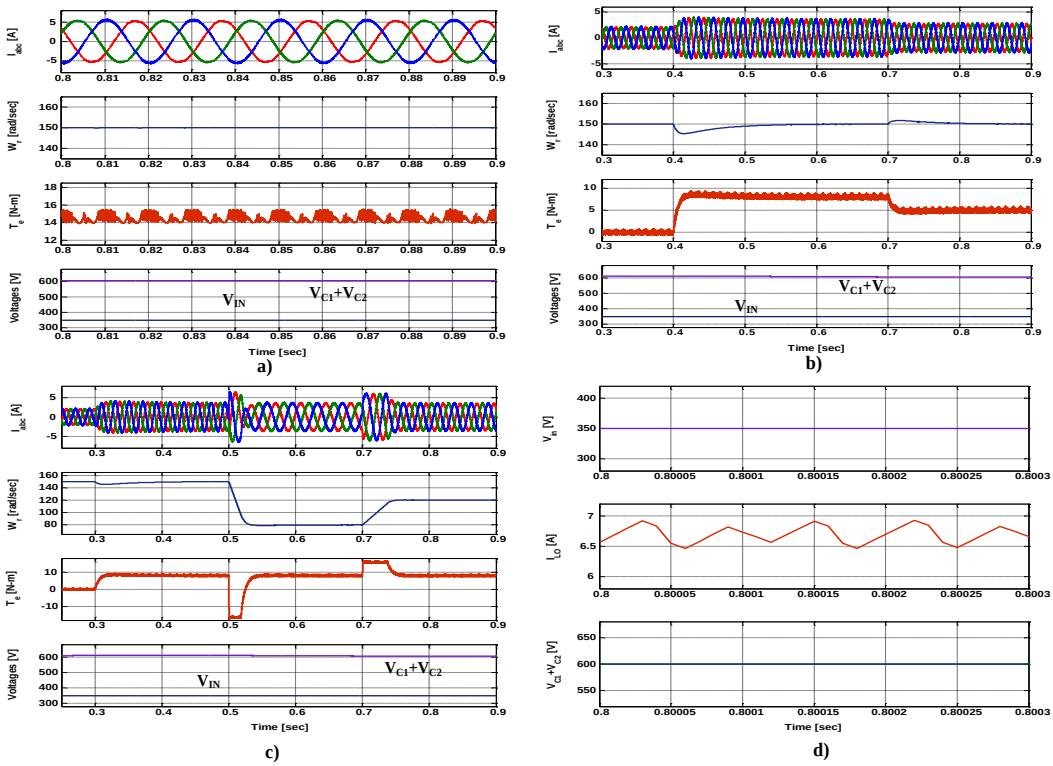

Fig. 4.5. Simulation results of the proposed 3Level-boost converter fed induction motor drive.

a) During full rated condition
b) With change in load
c) With change in speed
d) Output of three-level boost converter

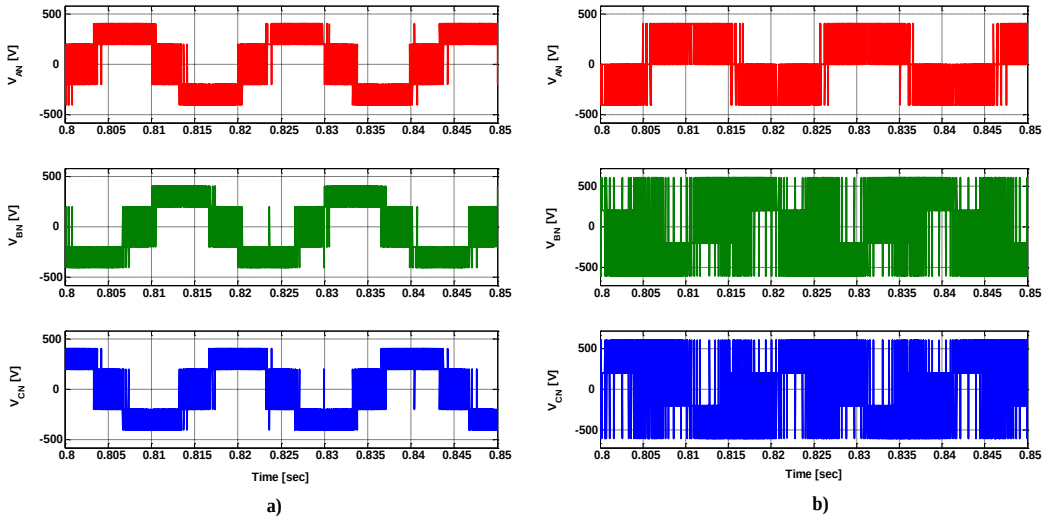

Fig. 4.6. Stator phase voltages of the proposed three-level boost converter fed induction motor drive.

a) Healthy condition
b) Post-fault condition

For the same operating conditions, during fault, the converter is re-configured as B4, the current THD is increased to 11.04% and torque ripple is increased to 2.95 N-m, however

with proposed three-level-boost converter fed B4 inverter, the current THD is 6.94% and torque ripple is 1.68 N-m which are very close to normal operation of the inverter (B6 configuration) and also the dc-link voltage is restored to in post-fault operation.

4.4. Experimental Results of Topology-A

Experiments are carried out on the developed setup as shown in Fig. 3.3. A three-level boost converter at front end of two-level voltage source inverter and control logic is shown in it. Experiments are conducted on this hardware setup for various operating conditions and results are presented.

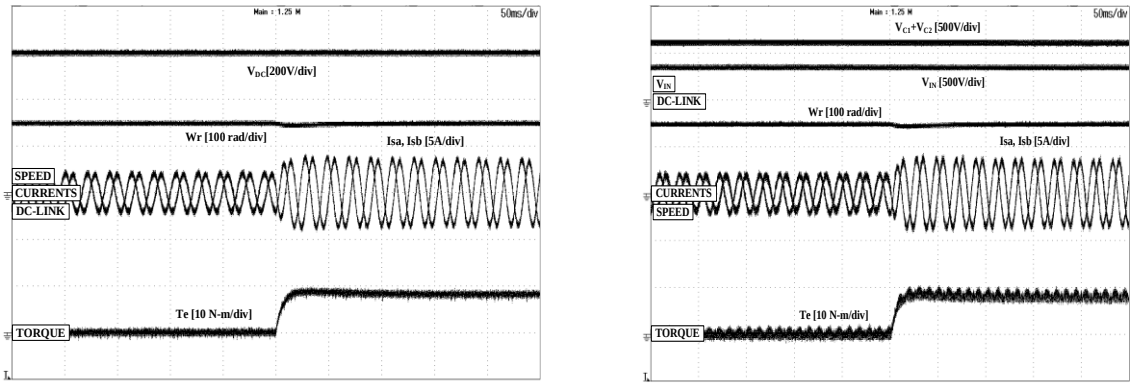

a) b)

Fig. 4.7. Experimental results of step change in load for induction motor drive

a) Conventional converter
b) Proposed 3-level boost converter fed B4 converter.

Fig. 4.7 shows results the stator currents i_{sa}, i_{sb}, speed and torque with reference speed of 150 rad/sec at a load of 8 N-m for conventional converter and the proposed three-level boost converter fed B4 converter respectively for the step change in load. Similarly Fig. 4.8 shows the results of conventional converter (B6), B4 converter and proposed B4 converter at load 8 N-m at a speed of 80 rad/sec. From the results, it is examined that three-level boost converter fed converter(proposed converter) exhibits similar behaviour as that of conventional converter during post-fault operation. With B4 converter, stator currents are not sinusoidal and the torque ripple is more as a result the motor speed is fluctuating. To overcome this problem, a three-level boost converter is proposed at front end of the two-level inverter.

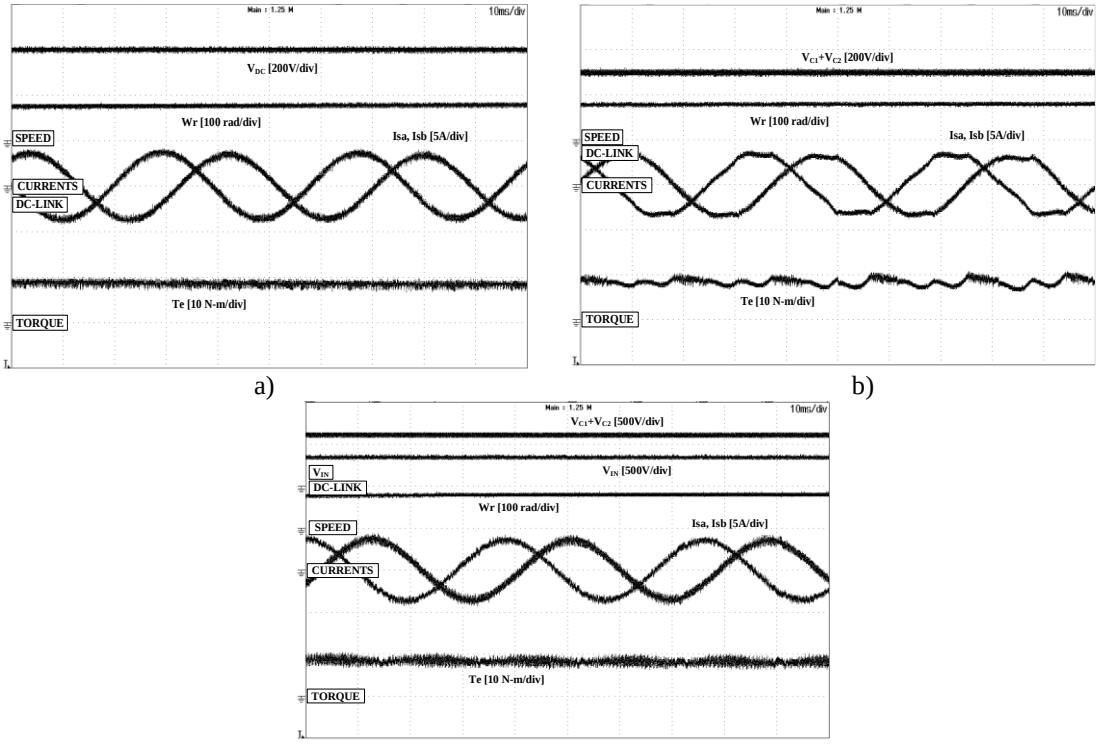

Fig. 4.8. Steady-state response of drive at load torque of 8 N-m at 80 rad/sec.

a) Conventional converter
b) Conventional fault-tolerant B4 converter
c) Proposed three-level boost converter fed B4 converter.

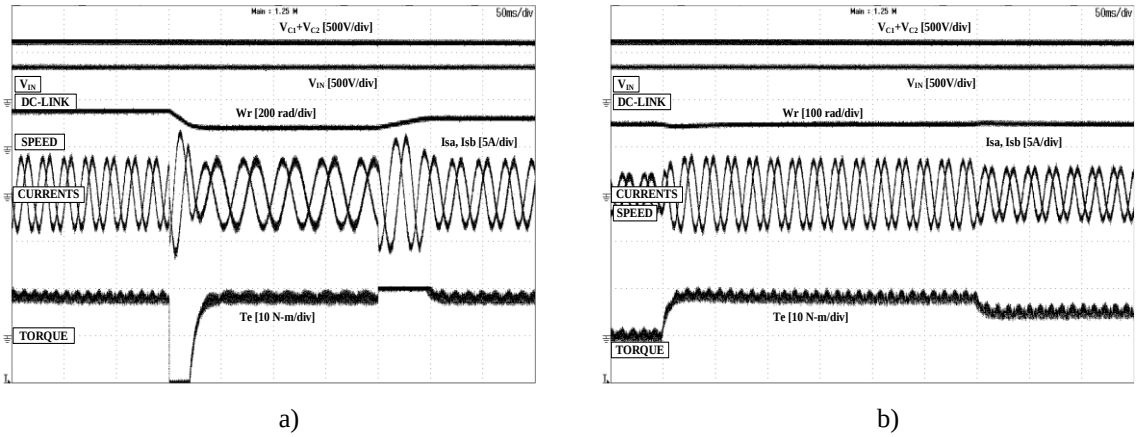

Fig. 4.9. Experimental results of the proposed converter topology

a) Speed change
b) Load change

Fig. 4.9 illustrates the variations in speed, load and performance of the proposed converter. From these results, the stator current; torque and speed of the drive system with three-level boost converter fed induction motor drive is almost similar to conventional inverter fed induction motor. Fig. 4.10 shows the stator phase voltages of the proposed converter under healthy and post-fault operation. The THD of motor current with the conventional

converter is 6.70% and torque ripple is 1.61 N-m for a load torque of 8 N-m at reference speed of 80 rad/sec. For same operating conditions, the proposed three-level boost converter inverter offered current THD is 6.90% and torque ripple is 1.72 N-m. However the conventional B4converter offered more current THD and torque ripple i.e., current THD of 11.48% and torque ripple of 3.14 N-m.

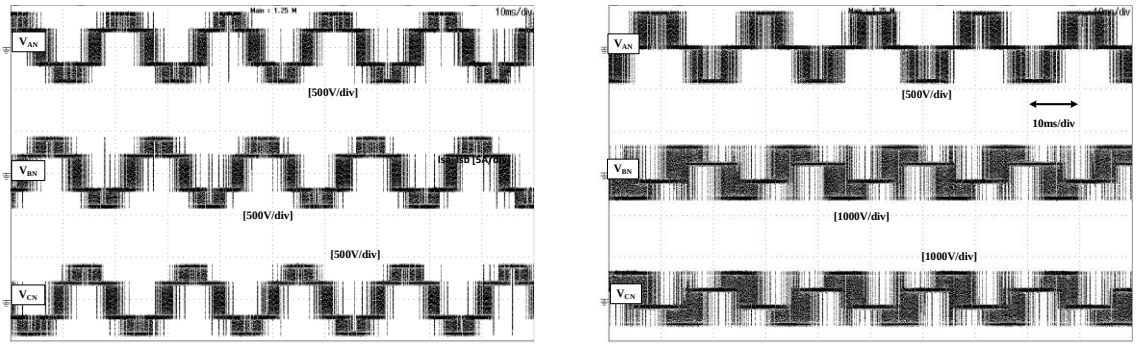

a) b)

Fig. 4.10. Stator phase voltages of the proposed three-level boost converter fed induction motor drive.

a) Healthy condition
b) Post-fault condition

4.5. Simulation Results of Topology-B

Simulation results for the converter topology consists of a simple boost converter and a single capacitor at the DC link its control strategy is shown in Fig. 3.2. Fig. 4.11 shows the steady-state operation of the induction motor drive with FOC, for a speed of 85 rad/sec and a load torque of 8 N-m for a healthy converter (B6), conventional fault-tolerant converter (B4) and proposed fault-tolerant configuration respectively. From the results it is noticed that, the stator currents of the conventional fault-tolerant converter are unbalanced, speed fluctuates and torque having more ripples. The proposed fault-tolerant converter and healthy converter results are almost the same. Fig. 4.12 shows the features of the healthy converter and proposed converter under the steady-state operation of the induction motor drive using FOC with load torque of 8 N-m at a speed of 150 rad/sec. From the results, it is observed that stator currents are balanced, torque ripple is less and speed fluctuations are nominal. Fig. 4.13 shows the phase voltages of the proposed drive in healthy and post-fault condition.

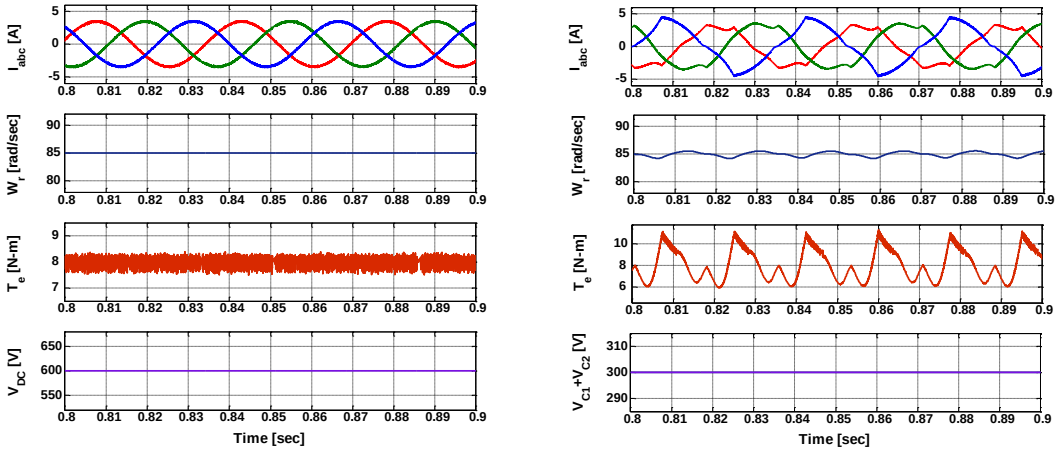

a) b)

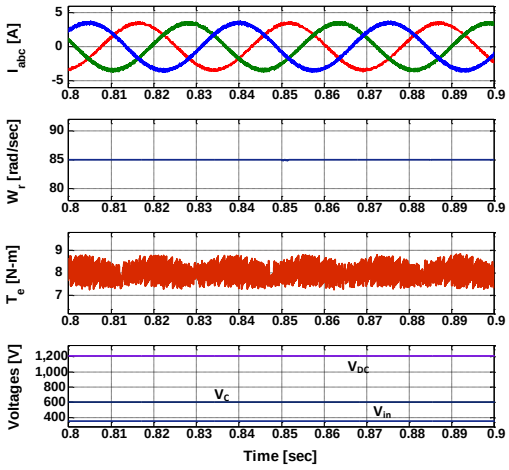

c)

Fig. 4.11 Simulation results of drive operating with speed of 85 rad/sec at a load torque of 8 N-m.

a) Conventional converter (B6)
b) Conventional fault-tolerant converter(B4)
c) Proposed fault-tolerant converter (boost conveter+B4)

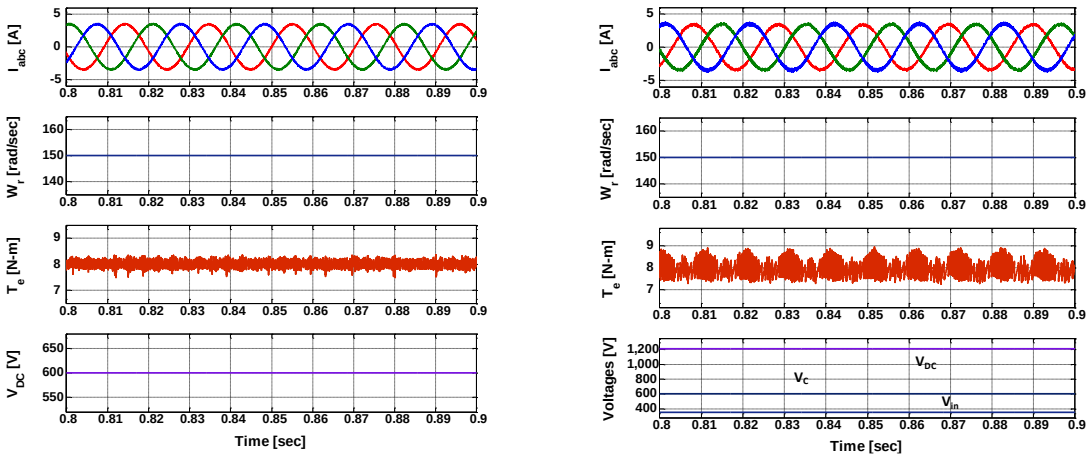

a) b)

Fig. 4.12 Simulation results of the induction motor drive at a speed of 150 rad/sec and load torque of 8 N-m.

a) Conventional Converter (B6)
b) Proposed fault-tolerant converter (boost conveter+B4)

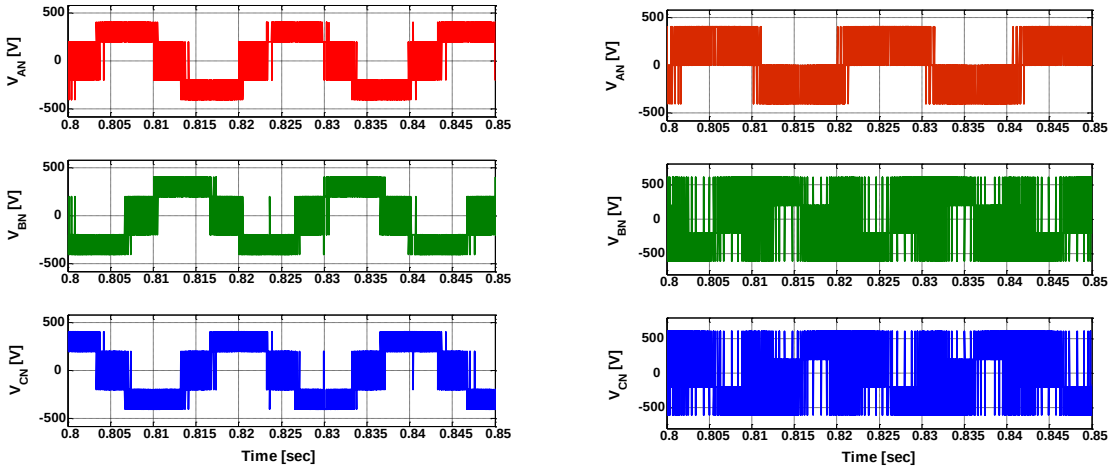

a) b)

Fig. 4.13 Phase voltages of the proposed topology with load torque 8 N-m at a speed of 150 rad/sec.

a) Healthy condition
b) Post-fault condition

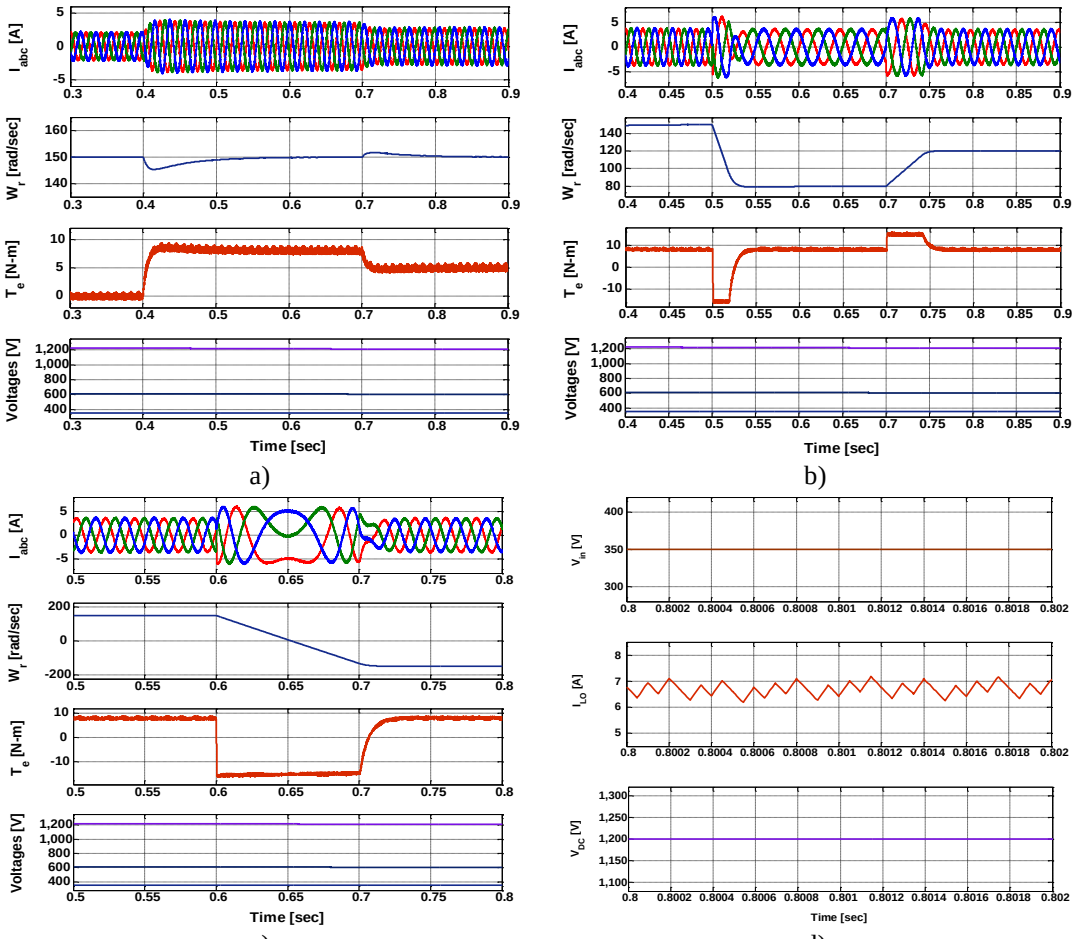

a) b)

c) d)

Fig. 4.14 Simulation results of the proposed topology of induction motor drive using FOC.

a) Change in load
b) Change in speed
c) Speed reversal
d) Waveforms of boost converter

Fig. 4.14(a), (b) and (c) shows some features of the proposed converter with change in speed, change in torque and speed reversal of the drive respectively and Fig. 4.14(d) shows the input and output waveforms of boost converter i.e. input voltage (V_{in}), inductor current (I_{LO}) and dc-link voltage (V_{DC}). From the results it is noticed that, the stator currents are balanced, ripples in load torque are less as a results speed fluctuations are nominal.

4.6. Experimental Results of Topology-B

Experiments are carried out on the developed setup consists of a boost converter at front end of two-level voltage source inverter and control logic as shown in Fig. 3.3. On this experimental setup tests are conducted for various operating conditions and results are presented. Fig. 4.15 shows the waveforms of stator currents i_{sa}, i_{sb}, speed and torque with reference speed of 85 rad/sec at a load of 8 N-m for conventional converter (B6), conventional fault-tolerant converter (B4) and the proposed boost converter fed B4 configuration respectively.

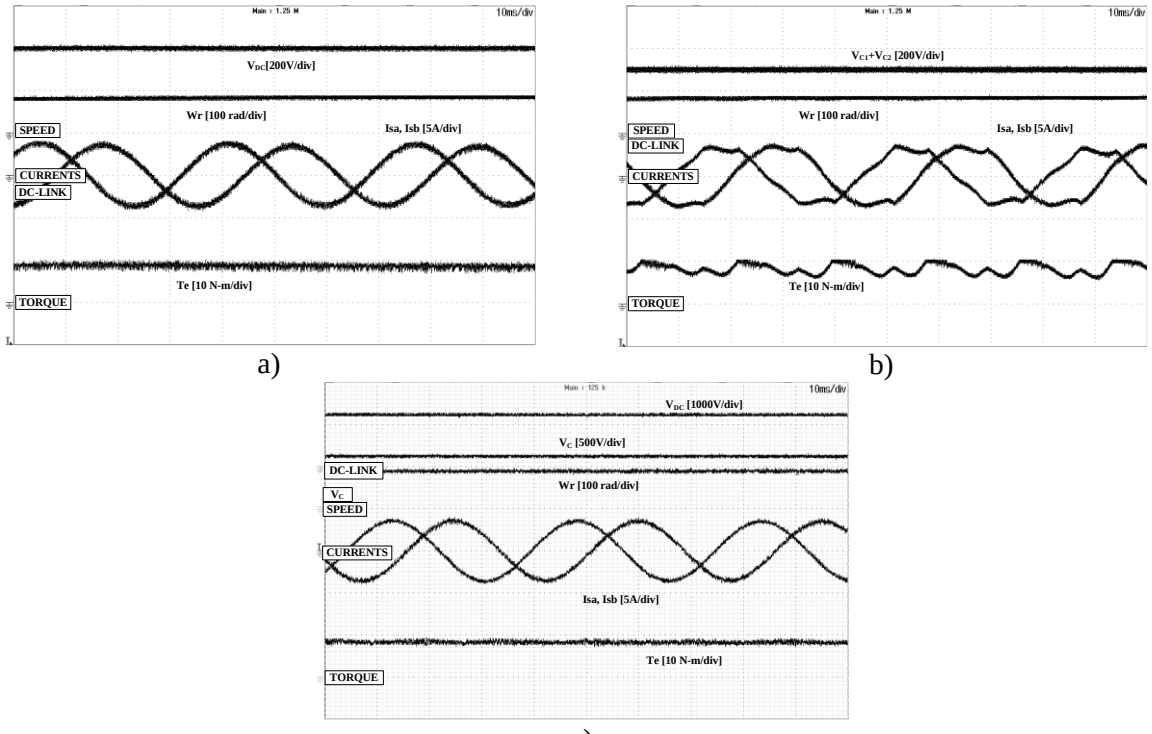

Fig. 4.15 Experimental results of drive operating with speed of 85 rad/sec at a load torque of 8 N-m.

a) Conventional converter (B6)
b) Conventional fault-tolerant converter (B4)
c) Proposed fault-tolerant converter (B4+ Boost Converter)

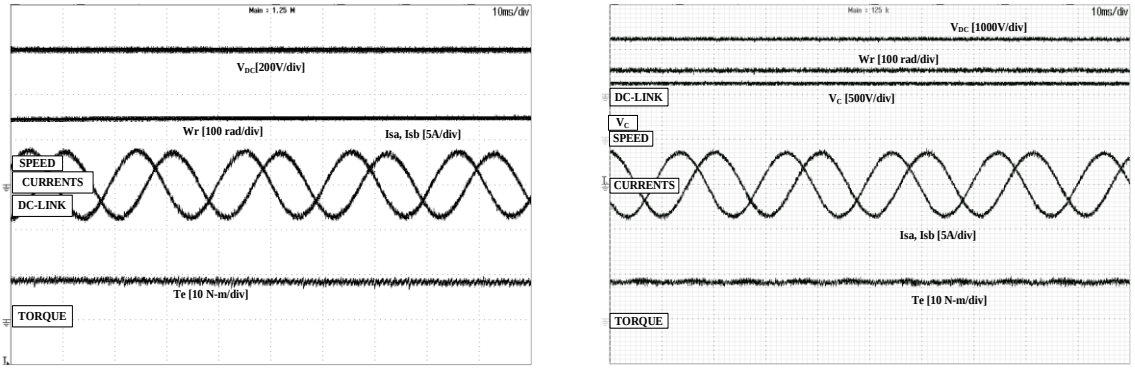

a) b)

Fig. 4.16 Experimental results of the induction motor drive at a speed of 150 rad/sec and load torque 8N-m.

a) Conventional converter(B6)
b) Proposed fault-tolerant converter (B4+ Boost Converter)

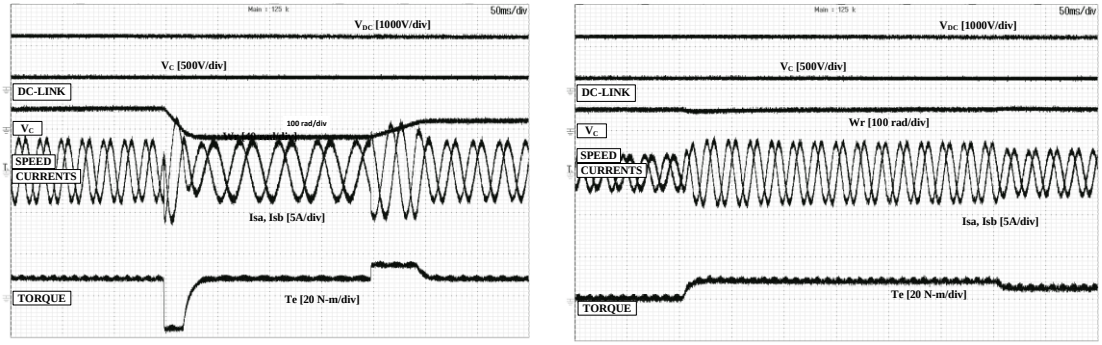

a) b)

Fig. 4.17 Experimental results of the proposed topology of induction motor drive using FOC.

a) Change in speed
b) Change in load

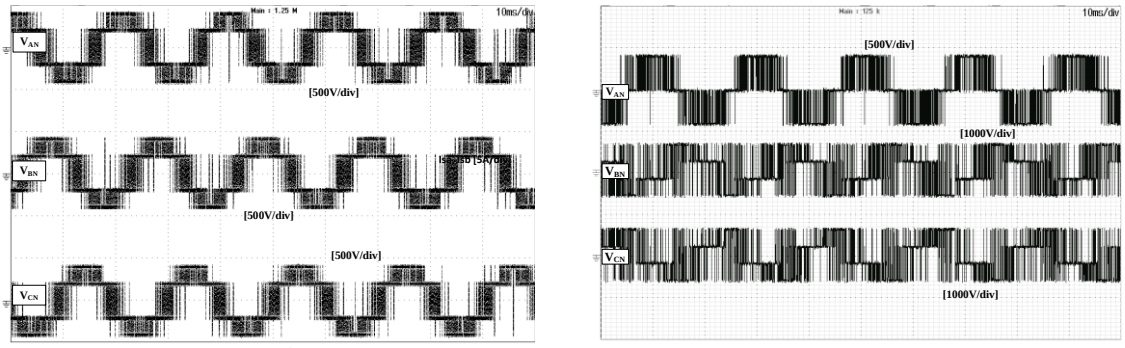

a) b)

Fig. 4.18 Phase voltages of the proposed topology with load torque 8 N-m at a speed of 150 rad/sec.

a) Healthy condition
b) Post-fault condition

Similarly Fig. 4.16 shows the results of conventional converter (B6) and proposed B4 converter at load 8 N-m for speed of 150 rad/sec. From the results, it is examined that boost converter fed induction motor drive converter configuration (proposed converter)

exhibits similar behaviour as that of conventional converter during post-fault operation. With B4 converter, the drive speed is fluctuating, stator currents are not sinusoidal and the torque ripple is more. To overcome this problem, a boost converter is proposed at front end of the two-level inverter. Fig. 4.17 illustrates the speed changes and load changes. From these results, the stator current; torque and speed of the drive system with boost converter fed induction motor drive is almost similar to healthy inverter fed induction motor. Fig. 4.18 shows the stator phase voltages of the proposed converter under healthy and post-fault operation. The performance indices of the boost converter fed induction motor drive topology using FOC are compared with healthy converter and conventional fault-tolerant converter (B4), for load torque of 8 N-m and operating at a speed of 85 rad/sec are explained in detail. The drive fed with healthy converter (B6) offered stator current THD 6.75 % with a torque ripple of 1.62 Nm, whereas with conventional fault-tolerant converter (B4) offered stator current THD 12.28 % with a torque ripple of 3.31 Nm and with the proposed fault-tolerant converter offered stator current THD 6.98 % with a torque ripple of 1.88 Nm. From the above results, it is observed that torque ripple and stator current THD of the proposed converter values are closer to the healthy converter values. From the results it is observed that the drive system with proposed converter topology offered results very close to conventional fault-tolerant converter (B4).

4.7. Summary

Three-level boost converter/Boost converter fed fault-tolerant inverter for induction motor with filed oriented control is presented in this chapter. Results are presented for conventional inverter configuration (B6), conventional fault-tolerant inverter (B4) configuration and B4 configuration with three-level boost converter/boost converter fed fault-tolerant inverter on the developed hardware setup at a load torque of 8 N-m using field oriented control for three-phase induction motor drive. From the results it is concluded that the operation of proposed three-level boost converter/boost converter fed induction motor drive in post-fault operation is very close to the conventional two-level inverter (B6) fed induction motor drive. These proposed drive systems has offered considerable improvement in the torque ripple, current THD and balanced dc-link voltage of capacitors compared to a conventional two-level fault-tolerant inverter (B4). Hence proposed drive system may be considered as one of the alternatives for the field oriented controlled fault-tolerant induction motor drives.

Chapter-5

Direct Torque Control using Fault-Tolerant Converter Topologies

5.1. Introduction

In this chapter, the brief fundamentals related to direct torque control of three-phase induction motor, simulation and experimental results using three-level boost converter fed fault-tolerant converter and boost converter fed fault-tolerant converter are presented. These results are compared with conventional fault tolerant inverter (B4) for load changes and speed changes. Detailed explanation with respect to merits of the proposed topologies are presented.

5.2. Direct Torque Control Algorithm

The DTC offer control over stator flux and electromagnetic torque to generate a suitable switching states for the inverter. The DTC is implemented in stationary reference frame [83], [85]-[88]. Fig. 5.1 represents the block diagram of the control technique. The estimation of stator flux, stator flux vector positon and electromagnetic torque is required to implement the DTC algorithm. The stator flux estimation expression for induction motor is

$$\frac{d\varphi_s}{dt} = V_s - R_s i_s \tag{5.1}$$

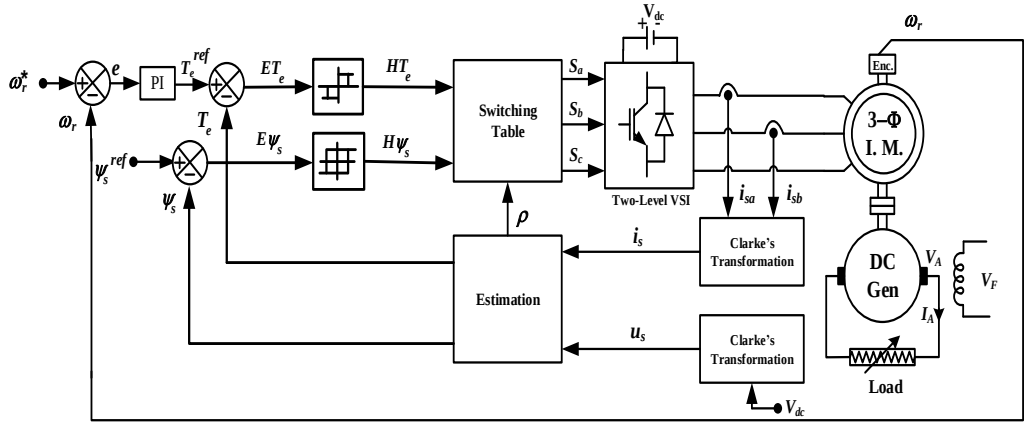

Fig. 5.1. Block diagram of DTC for induction motor drive [88]

In a sample time of *Ts*, the change in stator flux by neglecting the stator resistance in the Eq. 5.1 is modified as

$$\Delta\varphi_s \cong V_s T_s \tag{5.2}$$

The change in voltage vector in a particular sample time will directly impact on the stator flux; which is observed from the Eq. 5.2. Hence, by selecting a proper voltage vector will directly control over the stator flux. Stator and rotor flux complex plane is divided into six

equal sectors. In complex plane the variation of rotor flux and stator flux in one sample period is shown in Fig. 5.2. The stator flux position in the complex plane is obtained as

$$\rho = tan^{-1}\langle\frac{\varphi_{s\beta}}{\varphi_{s\alpha}}\rangle \tag{5.3}$$

Since rotor dynamics are much slower than the stator dynamics, ~~in~~ one sampling period is considered to estimate the electromagnetic torque [85] as

$$T_e = \frac{3}{2}p\frac{L_m}{L_sL_r - L_m^2}|\varphi_s||\varphi_r|\sin(\theta_{sr}) \tag{5.4}$$

The difference of the reference and estimated flux is given as the input to the two level hysteresis band. $2HB_\varphi$ is selected as the hysteresis band width. The stator flux is rotated in a circular path by application of active voltage vectors [88]. Two digital outs 1 and -1 is generated from the controller based on the trajectory of the stator flux (i.e., decrement or increment of stator flux) as per the below conditions

$$H\varphi_s = 1 \text{ for } E\varphi_s > +HB\varphi_s \tag{5.5}$$

$$H\varphi_s = -1 \text{ for } E\varphi_s < -HB\varphi_s \tag{5.6}$$

Reference speed is compared with the measured speed to generate the reference to torque using PI controller. This reference torque and measured torque are compared and the error is given as input to the three-level hysteresis band to control the torque. Based on the torque requirement (i.e., decrement, increment or no change of the torque), the output of the controller is

$$HT_e = 1 \text{ for } ET_e > +HBT_e \tag{5.7}$$

$$HT_e = 0 \text{ for } -HT_e > +HBT_e \tag{5.8}$$

$$HT_e = -1 \text{ for } ET_e < -HBT_e \tag{5.9}$$

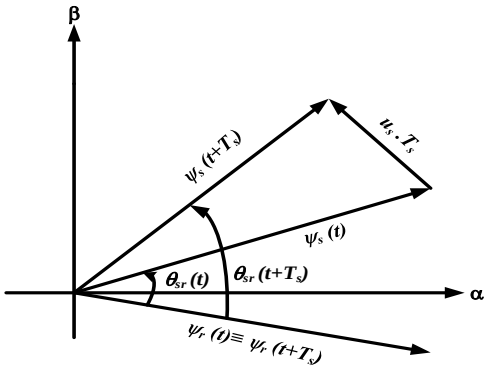

Fig. 5.2.Variation of stator flux and rotor flux in complex plane [85]

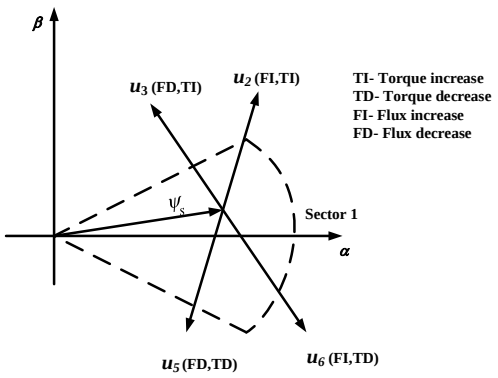

Fig. 5.3. Switching state selection for stator flux in sector 1 [83]

Based on the stator flux position in the complex plane outputs from the hysteresis controllers generates a suitable switching state. For example, if stator flux position is in sector 1, the criterion for the corresponding switching state selection is shown in Fig. 5.3. The different combinations of hysteresis outputs and the sector locations will generate the overall switching states for the induction motor drive which is represented in Table. 5.1.

Table-5.1 DTC switching table

$H\varphi_s$	HT_e	ρ					
		1	2	3	4	5	6
1	1	V_2	V_3	V_4	V_5	V_6	V_1
	0	V_7	V_0	V_7	V_0	V_7	V_0
	-1	V_6	V_1	V_2	V_3	V_4	V_5
-1	1	V_3	V_4	V_5	V_6	V_1	V_2
	0	V_0	V_7	V_0	V_7	V_0	V_7
	-1	V_5	V_6	V_1	V_2	V_3	V_4

Switching states: V_0 (0 0 0), V_1 (1 0 0), V_2 (1 1 0), V_3 (0 1 0), V_4 (0 1 1),V_5 (0 0 1), V_6 (1 0 1) and V_7 (1 1 1).

Under fault condition, a modified DTC with four voltage vectors are calculated as per Eq. 5.10 and applied. The motor phase voltages V_{AN}, V_{BN}, and V_{CN} are determined based on inverter switching states and hence DC-link voltage is also balanced. The voltage vectors of re-configured inverter for fault in leg A are presented in Table. 5.2.

$$V^R \text{ or } V_R{}^1 = \frac{2}{3}(V_{AN} + a*V_{BN} + a^2*V_{CN}) \tag{5.10}$$

Table-5.2 Inverter switching states and motor phase voltages after inverter re-configuration

States	$\mathbf{V_{AO}}$	$\mathbf{V_{BO}}$	$\mathbf{V_{CO}}$	$\mathbf{V_{AN}}$	$\mathbf{V_{BN}}$	$\mathbf{V_{CN}}$	**V**
00	$\frac{V_{DC}}{2}$	0	0	$\frac{V_{DC}}{3}$	$-\frac{V_{DC}}{6}$	$-\frac{V_{DC}}{6}$	$V_R{}^1 = \frac{V_{DC}}{3} e^{j0}$
10	$\frac{V_{DC}}{2}$	V_{DC}	0	0	$\frac{V_{DC}}{2}$	$-\frac{V_{DC}}{2}$	$V_R{}^2 = \frac{V_{DC}}{\sqrt{3}} e^{j\frac{\pi}{2}}$
11	$\frac{V_{DC}}{2}$	V_{DC}	V_{DC}	$-\frac{V_{DC}}{3}$	$\frac{V_{DC}}{6}$	$-\frac{V_{DC}}{6}$	$V_R{}^3 = \frac{V_{DC}}{3} e^{j\pi}$
01	$\frac{V_{DC}}{2}$	0	V_{DC}	0	$-\frac{V_{DC}}{2}$	$-\frac{V_{DC}}{2}$	$V_R{}^4 = \frac{V_{DC}}{\sqrt{3}} e^{j\frac{3\pi}{2}}$

Speed (ω) is sensed by an incremental encoder and given to encoder slot in dSpace to implement control algorithm. The reference speed is compared with sensed speed to generate error signal

$$e = \omega^* - \omega_m \tag{5.11}$$

This error signal generates reference torque as

$$T_e^{ref} = k_p e + k_i e \tag{5.12}$$

Where, k_p and k_i are controller gains.

The output of PI controller is compared with estimated Torque (T_e)

$$T_e = \frac{3}{2} p\left((f_{s\alpha} * i_{s\beta}) - (f_{s\beta} * i_{s\alpha})\right) \tag{5.13}$$

Torque error (ET_e) is given to hysteresis controller with a band of ± 0.1 to generate torque vector (HT_e).

Similarly, stator flux is estimated based on stator voltages and currents. The expression is

$$f_{s\alpha} = \int (v_{s\alpha} - R_s i_{s\alpha}) \tag{5.14}$$

$$f_{s\beta} = \int (v_{s\beta} - R_s i_{s\beta}) \tag{5.15}$$

From the above equations the resultant flux is estimated as

$$\psi_s = \sqrt{(f_{s\alpha})^2 + \left(f_{s\beta}\right)^2} \tag{5.16}$$

Table-5.3 Inverter switching states after re-configuration of inverter at fault in leg A

$H\varphi_s$	HT_e	**Flux position (0^0 - 90^0)**	**Flux position (90^0 - 180^0)**	**Flux position (180^0 - 270^0)**	**Flux position (270^0 - 360^0)**
F^+	T^+	V_R^2	V_R^3	V_R^4	V_R^1
	T^-	V_R^1	V_R^2	V_R^3	V_R^4
F^-	T^+	V_R^3	V_R^4	V_R^1	V_R^2
	T^-	V_R^4	V_R^1	V_R^2	V_R^3

The reference stator flux (ψ_s^{ref}) is compared with estimated stator flux (ψ_s) to generate flux error ($E\psi_s$). This flux error is given to hysteresis controller with a band of ± 0.01 to generate flux vector ($H\psi_s$). The stator flux is also used to generate flux position (ρ), which indicates the sector number. Finally, selection of inverter switching states is based on stator flux vector ($H\varphi_s$), torque vector (HT_e) and position of flux vector (ρ). If $H\varphi_s$ is increased, the HT_emay increase or decrease and based on flux position the inverter switching state is generated. Similarly, $\Delta\varphi$ is decreased, the HT_e may increase or decrease and based on flux position the inverter switching state is generated and represented in Table-5.3.

5.3. Simulation Results using Topology-A

Simulations are carried out on the induction motor drive system with the conventional converter (B6), conventional fault-tolerant converter (B4) and proposed Topology-A consists of three-level boost converter (TLBC) based fault-tolerant two-level inverter fed induction motor for various operating conditions.

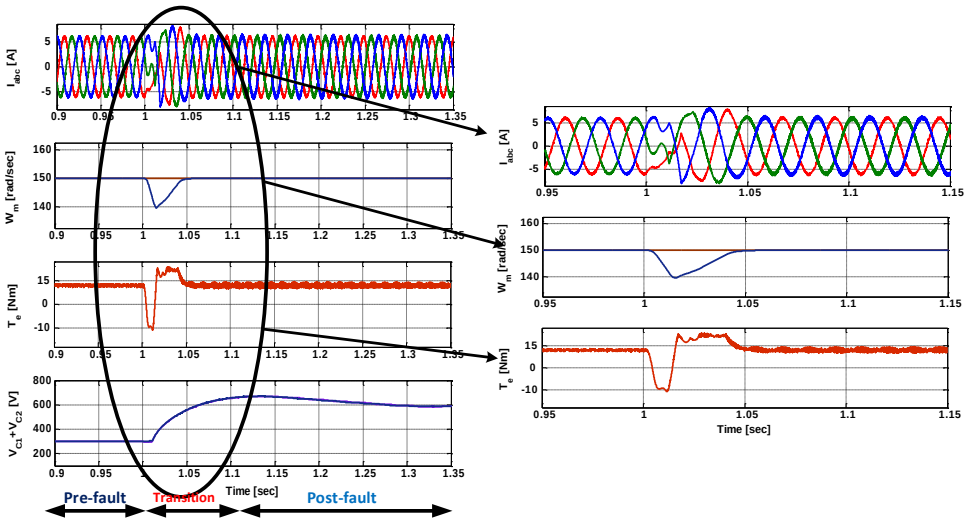

Fig. 5.4 Simulation results of an induction motor drive for pre-fault to post-fault transition.

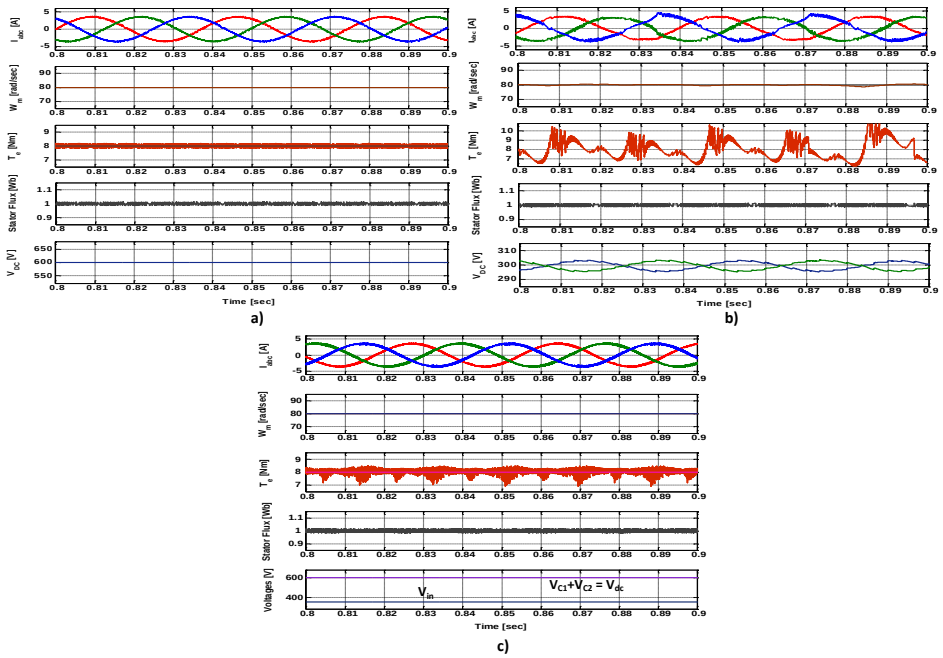

Fig. 5.5 Simulation results of an induction motor drive for speed 80 rad/sec at load torque of 8 N-m.

a) Conventional converter (B6)
b) Conventional fault-tolerant converter (B4)
c) Proposed fault-tolerant converter (B4+ TLBC)

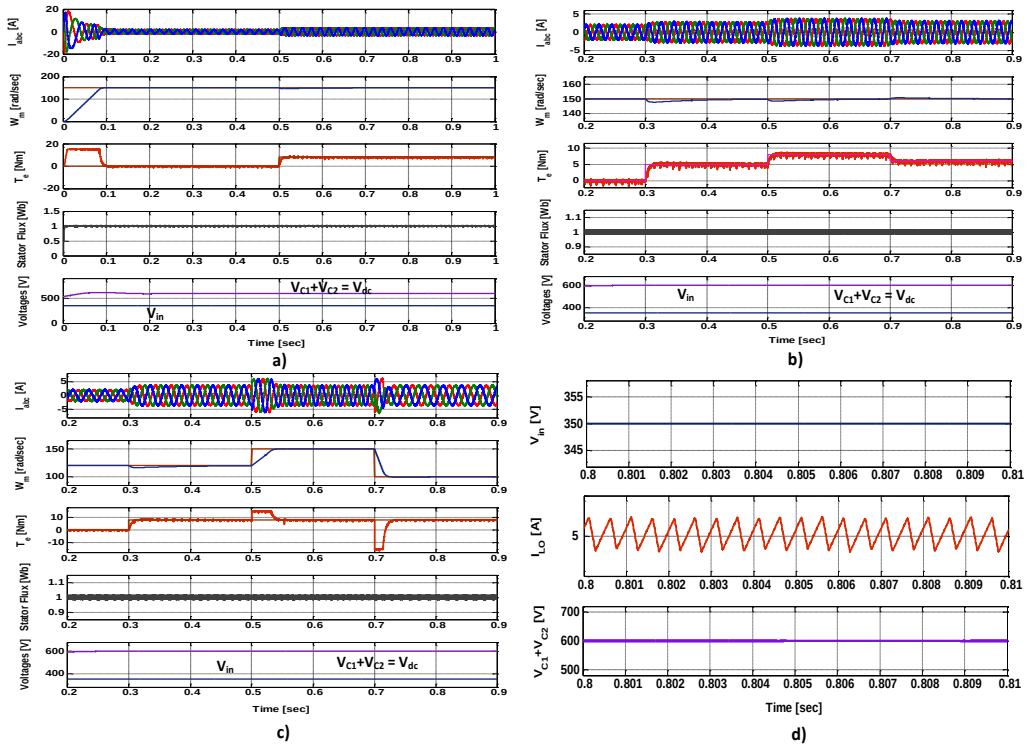

Fig. 5.6 Simulation results of proposed TLBC fed induction motor drive

a) During starting
b) Change in load
c) Change in speed
d) Response of TLBC

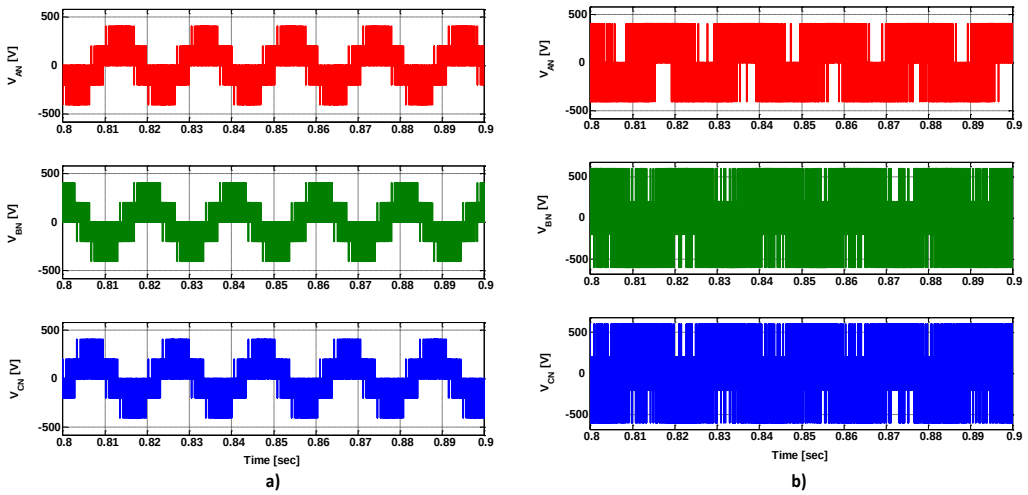

Fig. 5.7 Stator phase voltages of proposed fault-tolerant induction motor drive during

a) Pre-fault
b) Post-fault

Results for pre-fault to post-fault condition of the proposed converter is shown in Fig. 5.4 and results at a speed of 80 rad/sec with a load torque of 8 Nm are shown in Fig. 5.5. It illustrates that, torque ripple of the proposed converter under post-fault condition is same as

the conventional converter under normal operation, but B4 converter having ripples in the dc-link voltage and torque and also fluctuations in speed. Response of proposed converter at starting, during load change, speed change and TLBC response of the drive with current control and DTC algorithm during post fault-condition are presented in Fig. 5.6. From results it is observed that, proposed converter operation is almost similar to conventional converter and also operates in full rated condition during post-fault operation. Finally, from the above results it is observed that proposed converter configuration has less torque ripples, stator currents are sinusoidal and also the voltage across the dc-link capacitors are balanced. Stator phase voltages of the proposed converter during pre-fault and post-fault operation are presented in Fig. 5.7.

5.4. Experimental Results using Topology-A

Experiments are carried out on the developed setup as shown in Fig. 3.3. A three-level boost converter at front end of two-level voltage source inverter and control logic is shown in it.

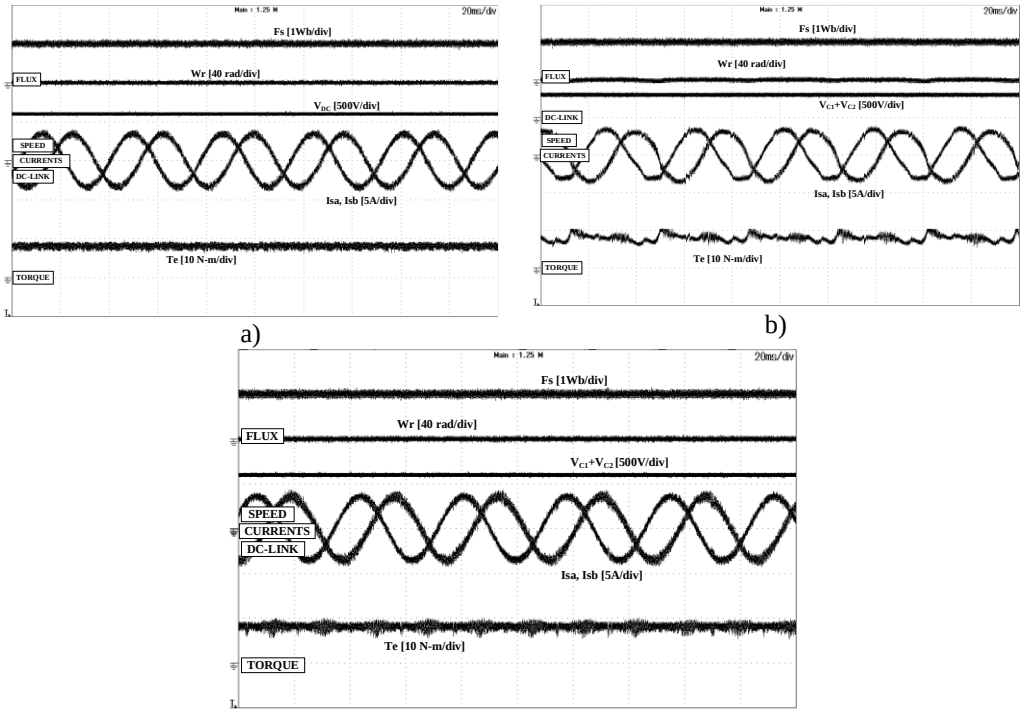

Fig. 5.8 Experimental results of an induction motor drive for speed 80 rad/sec at load torque of 8 N-m.

a) Conventional converter
b) Conventional fault-tolerant converter
c) Proposed fault-tolerant converter

On this experimental setup tests are performed for various operating conditions and results are presented. Fig. 5.8 shows the steady-state behaviour of conventional converter, conventional fault-tolerant converter and proposed fault-tolerant converter at 8 Nm load for a speed of 80 rad/sec. From the results it is observed that, stator currents are not sinusoidal and ripples in the torque are more with conventional B4 converter. Further increase in speed and load may lead to halt the drive system. The faulty phase voltage of the B4 converter is decreases by $\sqrt{3}$ times. Due to this, B4 converter is restricted to 50 % of full rated condition. To overcome the issue, a proposed converter is implemented.

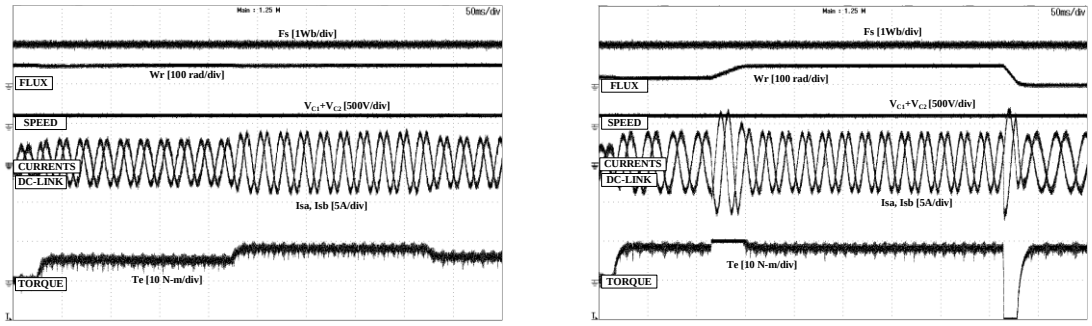

a) b)

Fig. 5.9 Experimental results of the proposed TLBC fed induction motor drive during
a) Change in load
b) Change in speed

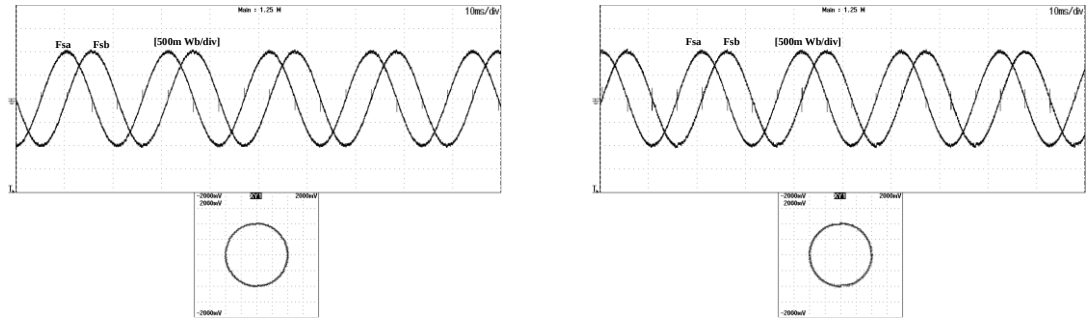

a) b)

Fig. 5.10 Stator flux of the proposed fault-tolerant induction motor drive
a) Pre-fault
b) Post-fault

The response of stator currents i_{sa}, i_{sb} [A], speed [w_m], torque [N-m] of a drive for conventional converter under normal operation and the proposed converter for post-fault operation are almost same. Fig. 5.9 shows the experimental results of proposed converter for a change in load and change in speed. From results, it is observed that proposed topology having better dynamic response. Fig. 5.10 shows the lissajous stator flux response in healthy and post-fault condition. Fig. 5.11 illustrates stator phase voltages of the proposed fault-

tolerant induction motor drive in pre-fault and post-fault operation. Fig. 5.12 shows the results of conventional converter, conventional B4 converter and proposed converter for a step-change in load from No-load to 8 Nm for a speed of 80 rad/sec.

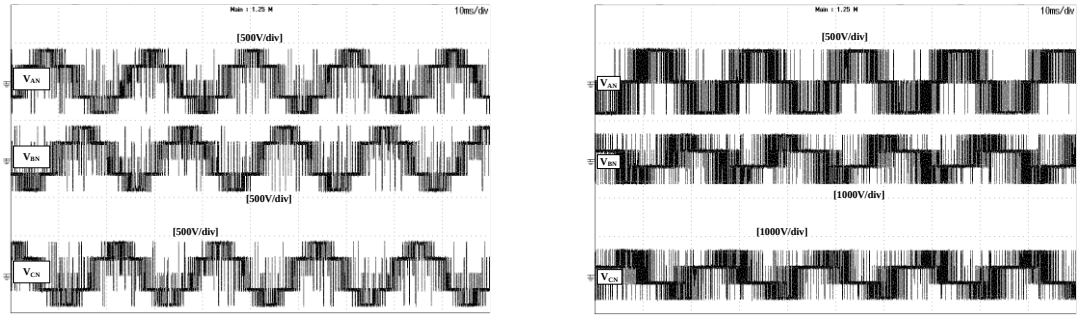

a) b)

Fig. 5.11 Stator phase voltages of the proposed fault-tolerant induction motor drive

a) Pre-fault
b) Post-fault

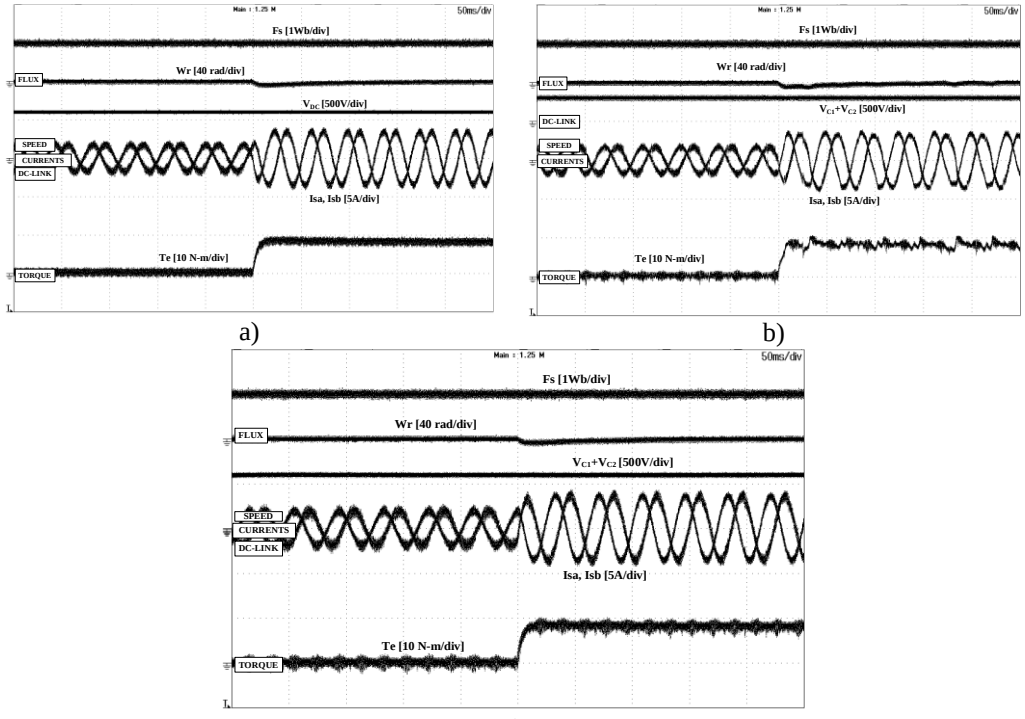

a) b)

c)

Fig. 5.12 Experimental results of the drive for Wr=80 rad/sec at step change in load torque 8 N-m

a) Conventional B6 converter
b) Conventional B4 converter
c) Proposed TLBC fed induction motor drive

Fig. 5.13 shows step-change in load and steady-state behaviour of the drive for conventional converter and proposed fault-tolerant converter at a load torque of 8 Nm for a speed of 150

rad/sec. From results it is observed that, conventional converter at normal operation and proposed converter at post-fault operation behaves in similar manner. The proposed fault-tolerant converter fed induction motor drive offers balanced stator currents, dc-link voltage and also the drive is able to operate in full rated condition during post-fault operation. When the drive is operating with a load torque of 8 N-m at 80 rad/sec for a conventional two-level inverter with DTC offered a stator current THD of 6.92 % and torque ripple of 1.46 N-m. For conventional fault-tolerant converter in post-fault operation with same operating conditions offered a stator current THD of 9.81 % and torque ripple of 2.26 N-m, whereas proposed fault-tolerant converter topology with modified DTC offered a stator current THD of 7.02 % and torque ripple of 1.54 N-m. From results it is observed that; torque ripple and %THD of stator current of a proposed TLBC fed induction motor operating in post-fault condition is very close to the conventional converter fed drive system. Hence, it is observed that drive is operating satisfactorily with the proposed fault tolerant converter topology.

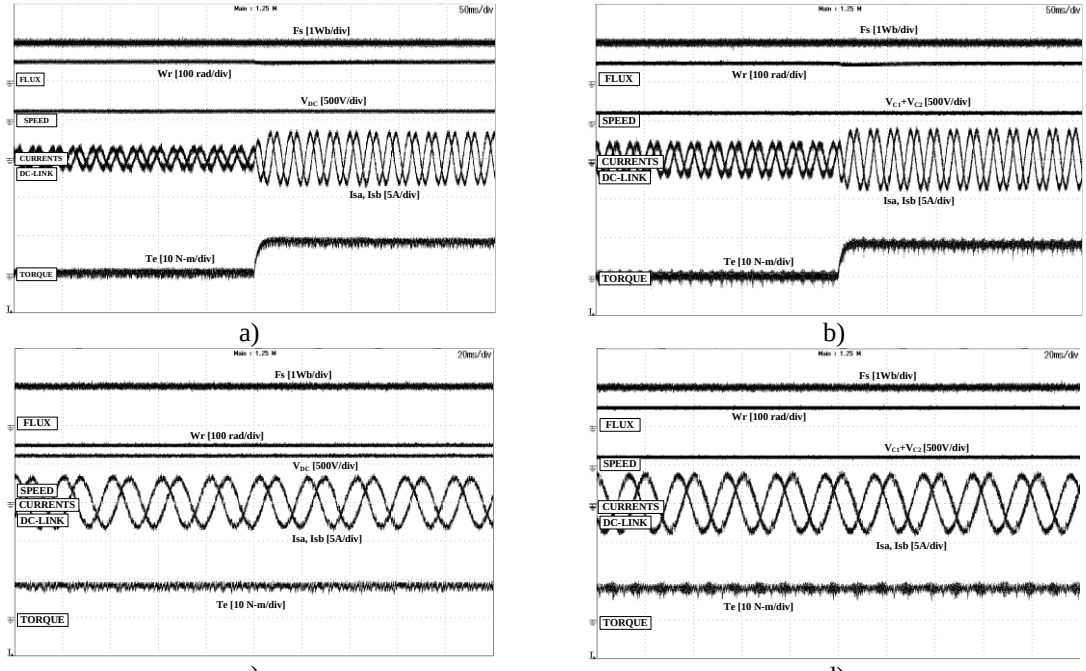

Fig. 5.13 Experimental results of the drive for Wm=150 rad/sec.

a) Conventional B6 converter with No-load to 8 N-m
b) Proposed TLBC fed induction motor drive with No load to 8 N-m
c) Steady–state response of conventional B6 converter
d) Steady–state response of proposed TLBC fed induction motor drive.

5.5. Simulation Results using Topology-B

Simulation results are presented for the proposed fault-tolerant converter fed induction motor drive and compared with the conventional fault-tolerant converter (B4) fed drive to show its effectiveness. Induction motor fed from conventional converter, conventional fault-tolerant converter (B4) and proposed fault-tolerant converter operating with a load torque of 8 N-m at a speed of 85 rad/sec is shown in Fig. 5.14. From the results it is observed that the conventional fault-tolerant converter has fluctuations in speed, more torque ripple and stator currents are non-sinusoidal when compared with proposed fault-tolerant converter. The normalized root mean square deviation (NRMSD) expression used for calculation of torque ripple, flux ripple is

$$NRMSD = \sqrt{\sum_{i=1}^{l} \frac{(x_i - \hat{x})^2}{(l-1)}} \tag{5.17}$$

Where $\hat{x} = \frac{1}{l}\sum_{i=1}^{l} x_i$, $l =$ number of samples i.e., 1000 samples are considered to calculate the torque ripple.

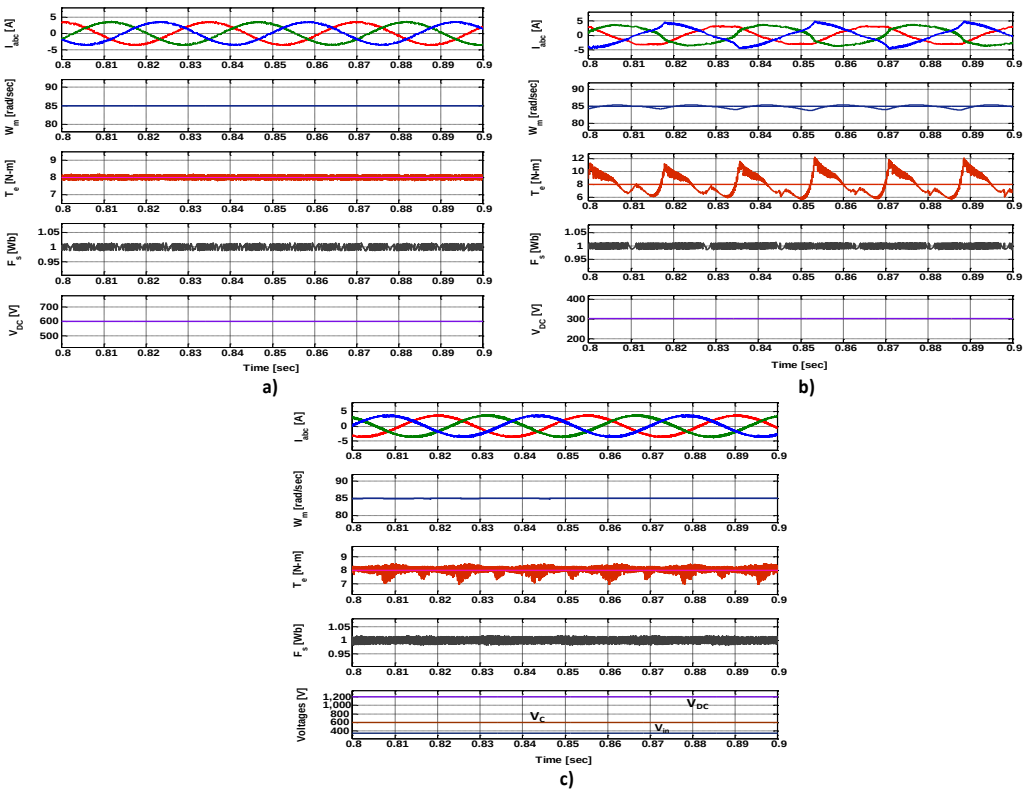

Fig. 5.14 Simulation results of the drive with a load torque of 8 N-m at 85 rad/sec.

a) Conventional converter
b) Conventional fault-tolerant converter
c) Proposed fault-tolerant converter

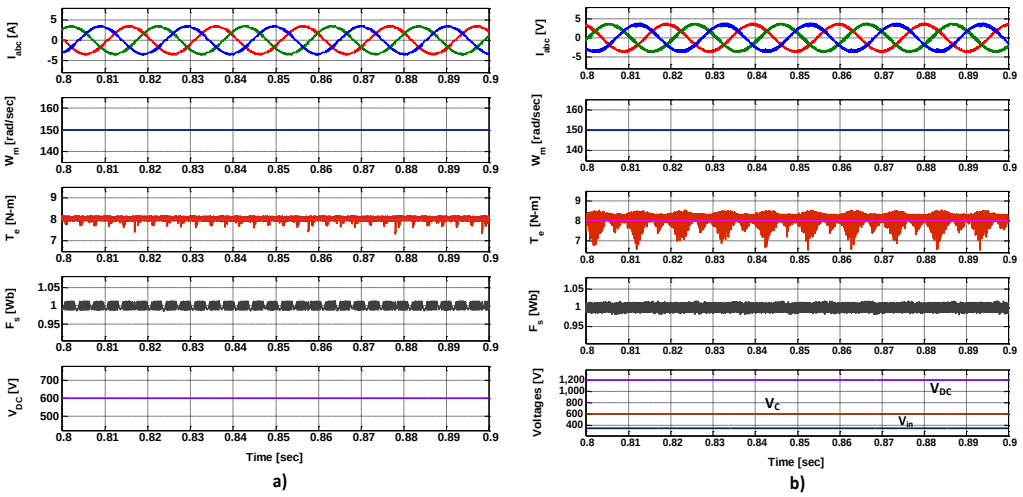

Fig. 5.15 Simulation results of the drive with a load torque of 8 N-m at 150 rad/sec.

a) Conventional converter
b) Proposed fault-tolerant converter

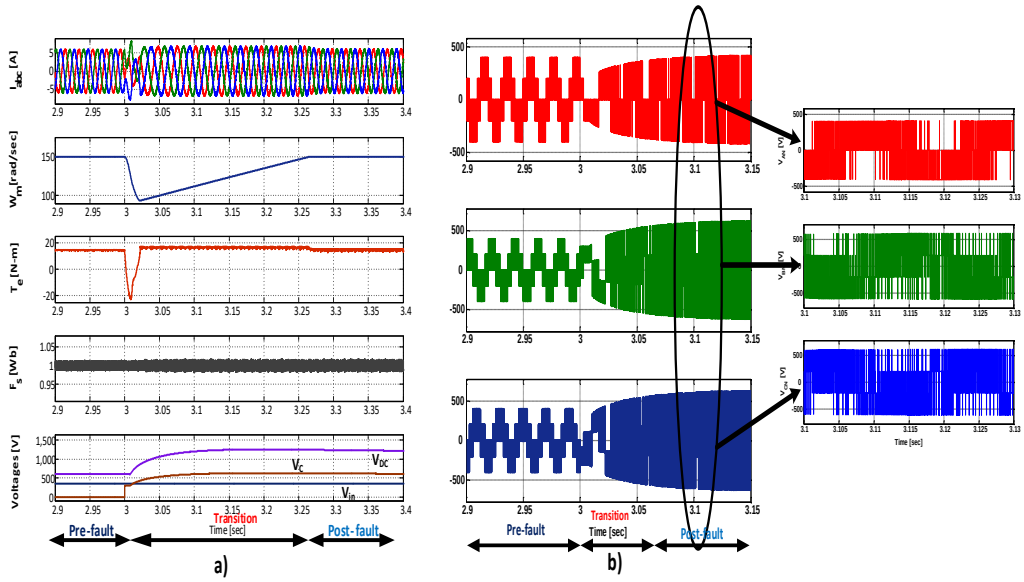

Fig. 5.16 Simulation results of proposed topology for pre-fault to post-fault transition.

a) Induction motor speed, torque, current and flux
b) Motor phase voltages

Fig. 5.15 shows the results of conventional converter and proposed fault-tolerant converter operating with a load torque of 8 N-m at 150 rad/sec. From the results, it is observed that the proposed converter topology performance is almost similar to the conventional converter and also eliminates the drawback of conventional fault-tolerant converter. To show the full rated operation (150 rad/sec, 14.5 N-m) of the proposed fault-tolerant converter fed induction motor drive, simulation results are presented for pre-fault operation, pre-fault to post-fault transition and post-fault operation and shown in Fig. 5.16.

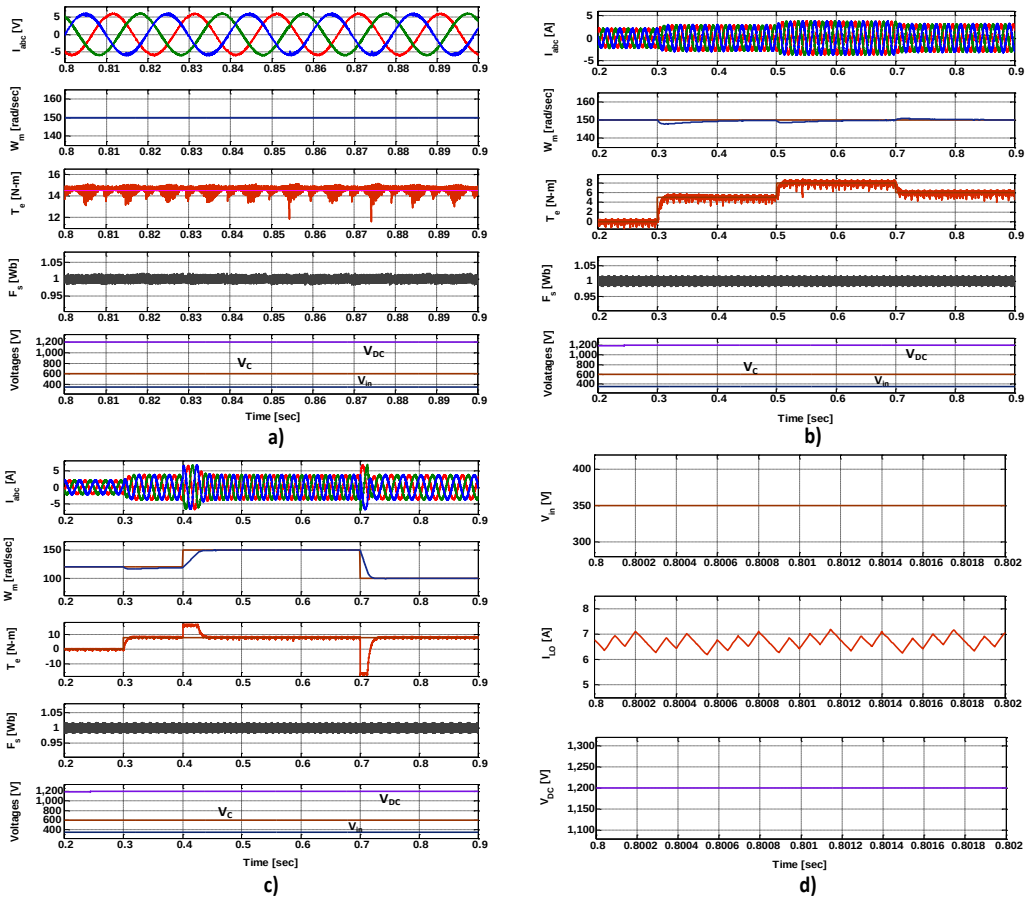

Fig. 5.17 Simulation results for post-fault-operation of proposed fault-tolerant converter

a) Full rated operation
b) Load change
c) Speed change
d) Output of boost converter

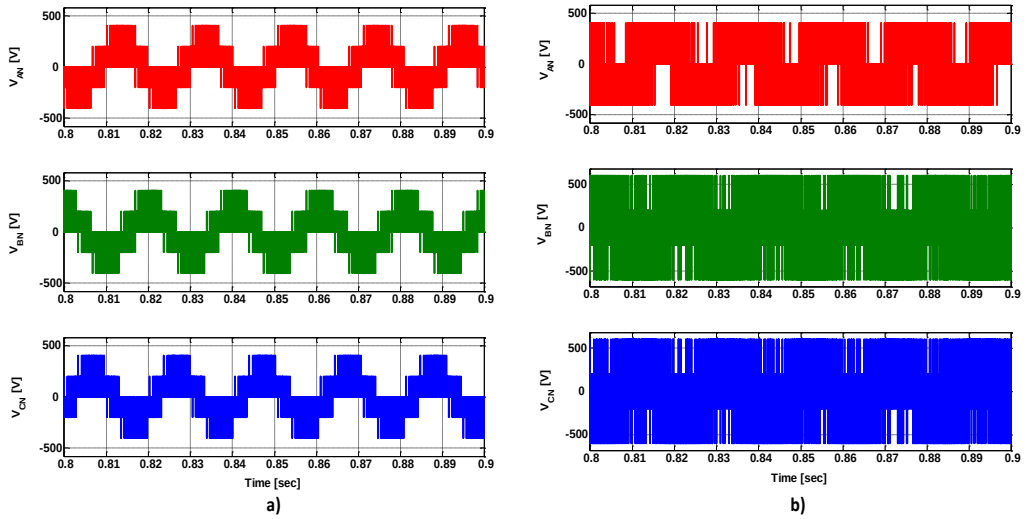

Fig. 5.18 Simulation results of an induction motor drive

a) Pre-fault phase voltages
b) Post-fault phase voltages

Fig. 5.17 (a-d) illustrates the operation of proposed fault-tolerant drive at rated load, change in load, change in speed and the output of boost converter. From the results it is observed that the proposed topology operating at full load also have dynamic performance similar to that of conventional converter. Fig. 5.18 shows the stator phase voltages of the proposed converter in pre-fault and post-fault condition.

5.6. Experimental Results using Topology-B

Experiments are carried out on the developed setup as shown in Fig. 3.3. A boost converter at front end of two-level voltage source inverter and control logic is shown in it. On this experimental setup tests are performed to observe the response of the drive system for various operating conditions and results are presented for variations in stator currents, speed, torque, dc-link voltage, and stator flux.

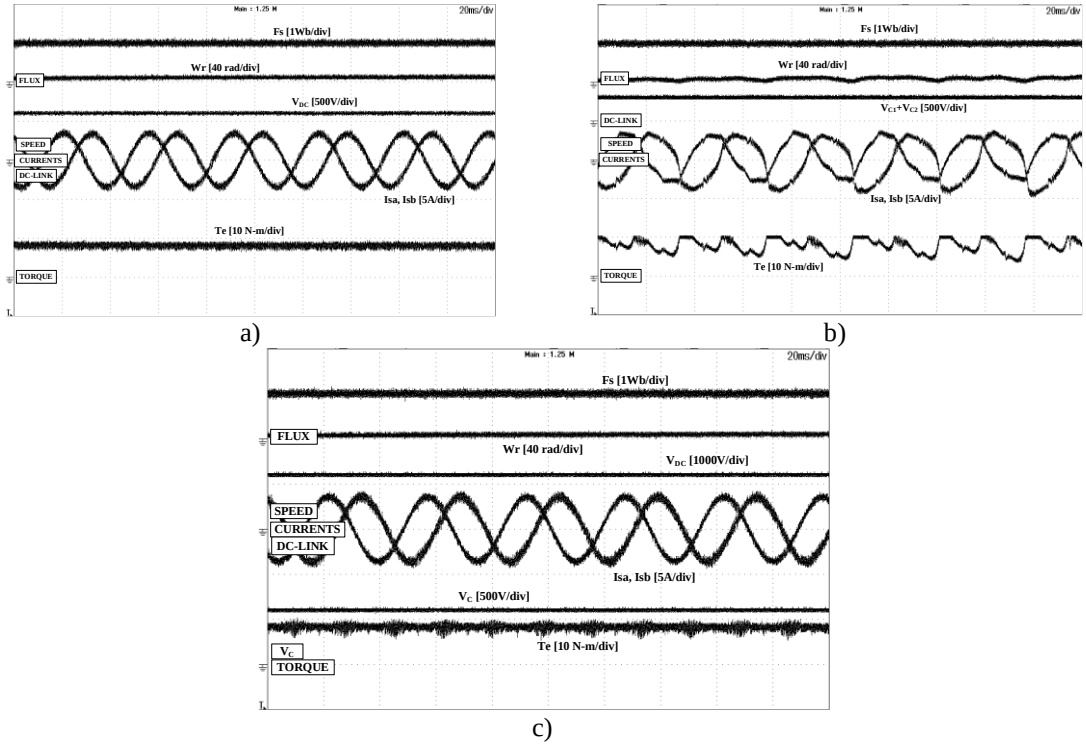

Fig. 5.19 Experimental results of the drive with load torque 8 N-m at 85 rad/sec.

a) Conventional converter
b) Conventional fault-tolerant converter
c) Proposed fault-tolerant converter

Fig. 5.19 shows the operation of induction motor with load torque of 8 N-m at 85 rad/sec fed with conventional converter (B6), conventional fault-tolerant converter (B4) and proposed fault-tolerant converter in post-fault condition. From the results of the proposed

fault-tolerant converter it is observed that stator currents are sinusoidal; torque ripples are less and fluctuations in the speed compared with conventional fault-tolerant converter (B4).

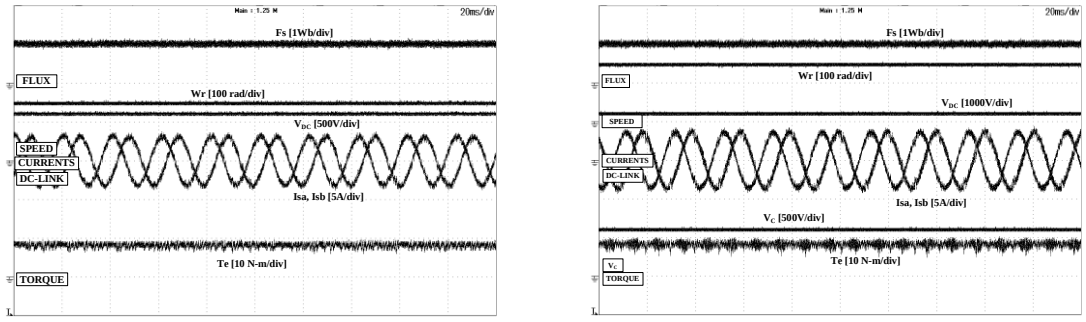

a) b)

Fig. 5.20 Experimental results of the drive with load torque 8 N-m at 150 rad/sec

a) Conventional inverter
b) Proposed fault-tolerant converter

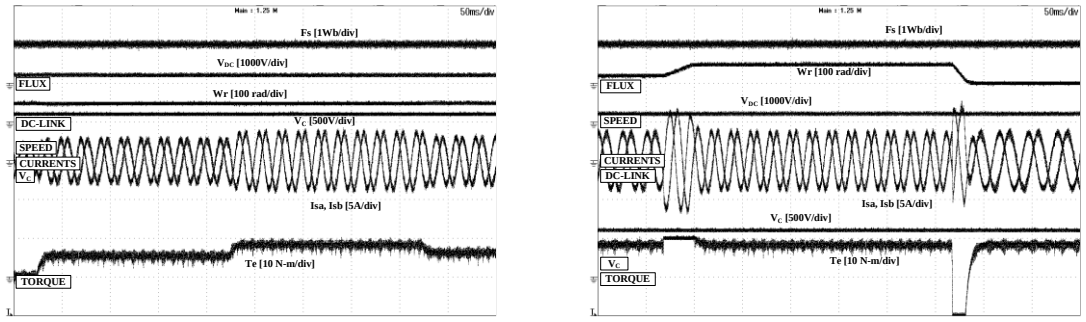

a) b)

Fig. 5.21 Experimental results of proposed fault-tolerant converter fed drive

a) Load change
b) Speed change

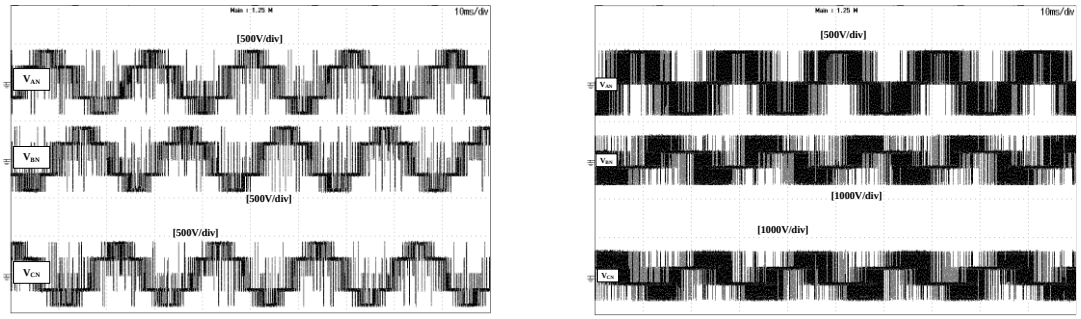

a) b)

Fig. 5.22 Experimental results of proposed fault-tolerant converter fed drive

a) Pre-fault phase voltages
b) Post-fault phase voltages

When the drive is operating with a load torque of 8 N-m at 85 rad/sec for a conventional two-level inverter with DTC offered a stator current THD of 6.97 % and torque ripple of 1.62 N-m. For conventional fault-tolerant converter in post-fault operation with same

operating conditions offered a stator current THD of 10.21 % and torque ripple of 3.12 N-m, whereas proposed fault-tolerant converter topology with modified DTC offered a stator current THD of 7.01% and torque ripple of 1.51 N-m. From these results, it is noted that stator current THD and torque ripple for a proposed two-level inverter with DTC in post-fault operation is almost the same as the conventional converter topology. Fig. 5.20 shows the drive operating with load torque of 8 N-m at 150 rad/sec for conventional converter (B6) as well as proposed fault-tolerant converter. From these results, it can be identified that the proposed topology operating at rated speed has less torque ripple, less speed fluctuations and stator currents are sinusoidal. Fig. 5.21 shows the dynamic operation of the proposed topology in post-fault operation, which is found to satisfactory w.r.t torque and flux ripples and also profile of stator currents. The pre-fault and post-fault phase voltages of the motor are presented in Fig. 5.22. Fig. 5.23shows the Lissajous pattern of stator flux in pre-fault and post-fault condition. From the results, it is observed that the stator flux pattern is almost similar.

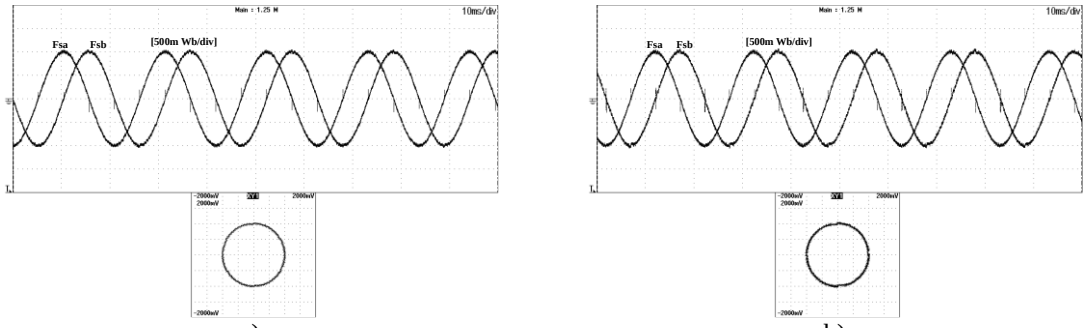

a) b)

Fig. 5.23 Stator flux Lissajous pattern of proposed converter fed drive

a) Pre-fault
b) Post-fault

5.7. Summary

Three-level boost converter/Boost converter fed fault-tolerant inverter for induction motor with direct torque control is presented in this chapter. Results are presented for conventional inverter configuration (B6), conventional fault-tolerant inverter (B4) configuration and B4 configuration with three-level boost converter/boost converter fed fault-tolerant inverter on the developed hardware setup at a load torque of 8 N-m using direct torque control for three-phase induction motor drive. From the results it is concluded that the operation of proposed three-level boost converter/boost converter fed induction motor drive in post-fault operation is very close to the conventional two-level inverter (B6) fed

induction motor drive. These proposed drive systems has offered considerable improvement in the torque ripple, current THD and balanced dc-link voltage of capacitors compared to a conventional two-level fault-tolerant inverter (B4). The proposed fault-tolerant converter topologies and fault-tolerant topologies existing in the literature are carried out for a load torque of 8 N-m at 85 rad/sec and results are presented in Table-5.4 w.r.t the number of components used, Open-Circuit (OC) and Short-Circuit (SC) fault, control complexity, torque ripple, flux ripple, %THD of stator current. From the results, it is concluded that the proposed fault-tolerant converter topology operates the drive at rated values during post-fault operation with less control complexity when compare with the existing converter topologies. Hence proposed drive system may be considered as one of the alternatives for the direct torque controlled fault-tolerant induction motor drives.

Table-5.4 Comparison of proposed converters with conventional fault-tolerant converters

Topologies	No. of Switches (IGBT's)	Diodes & Inductors	Capacitors	No. of Redundant Switches	Switches		Leg		Control Complexity	Ripple at 85 rad/sec and 8 N-m		%THD	Performance
					SC	OC	SC	OC		Torque (N-m)	Flux (Wb)		
Proposed Converter-A	8	2 &1	2	3	Yes	Yes	Yes	Yes	Average	1.55	0.0176	7.03	100 % of operation.
Proposed Converter-B	7	1& 1	2	3	Yes	Yes	Yes	Yes	Average	1.51	0.0176	7.01	100 % of operation.
Faulty phase connected to midpoint of dc-link	6	--	2	3	Yes	Yes	Yes	Yes	Complex	3.12	0.0790	10.21	Restricted to 50 % of operation, dc-link voltage fluctuations.
Additional leg	8	--	2	3	Yes	Yes	Yes	Yes	Complex	1.48	0.0169	6.98	100 % of operation.
Motor neutral terminal connected to midpoint of dc-link	6	--	2	3	Yes	Yes	Yes	Yes	Complex	3.92	0.095	11.32	Restricted to 50 % of operation, Extra Neutral terminal required & Motor operates in Two phase mode.
Motor neutral terminal connected to extra leg	8	--	2	3	Yes	Yes	Yes	Yes	Complex	4.12	0.105	12.23	Restricted to 50 % of operation, Extra Neutral terminal required & Motor operates in Two phase mode.
Quasi z-source inverter	6	1 & 2	2	3	Yes	Yes	Yes	Yes	Complex	1.65	0.0182	7.42	100 % of operation.

Chapter-6
Predictive Torque Control using Fault-Tolerant Converter Topologies

6.1. Introduction

In this chapter, the brief fundamentals related to predictive torque control of three-phase induction motor, its simulation and experimental results using three-level boost converter fed fault-tolerant converter and boost converter fed fault-tolerant converter are presented. Studies carried out from the results obtained for possible operating conditions and conclusions are presented.

6.2. Model Predictive Control

The MPC concept was introduced for optimal control theory in 1960s and it was completely implemented in industrial process by the end of 1970s [115]. The predictive control for power electronics was made in early 1980s as first attempt [117], [118]. In this method, high amount of calculations are required in each sampling period of time. Hence it is not popular at that time but in recent past the advanced digital control platform with high computational capabilities enabled the implementation of complex control techniques like MPC with more precision and ease. This control concept explicitly uses the model of a system to select an optimal control action by using receding horizon policy which is shown in Fig. 6.1. From this illustration, it can be observed that the input signal u_k at the beginning of the present sampling period k is obtained by predicting the future behaviour of the output y_k for a given range of prediction horizon ($k+NP$).

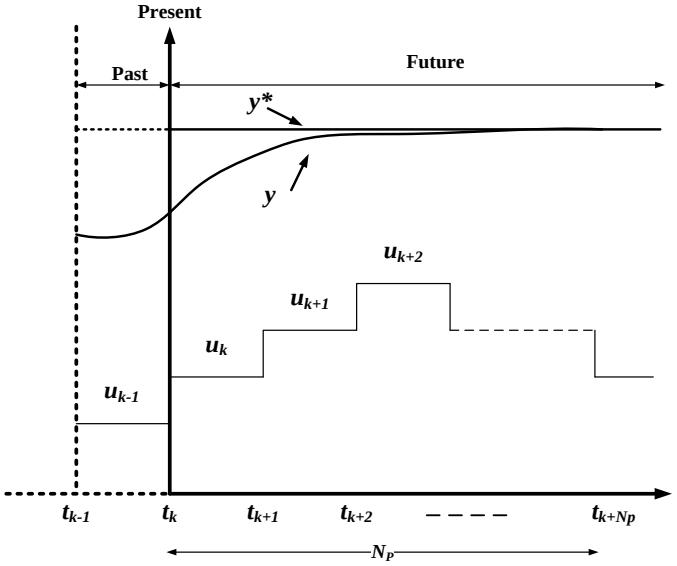

Fig. 6.1. Receding horizon polocy for model predictive control

Similarly, an input signal for the next sampling period is obtained by predicting the future behaviour of output for a prediction horizon of (*k+NP+1)*. Hence, this is known as receding horizon policy [114]. The basic structure for implementation of MPC is shown in Fig. 6.2. The input and output values of past and present status are given to the model of the system to predict the future behaviour of the outputs. The errors obtained from the reference trajectory and the predicated outputs are given to the optimizer. Future inputs for the system will be selected depending upon the objectives and constraints given to the optimizer.

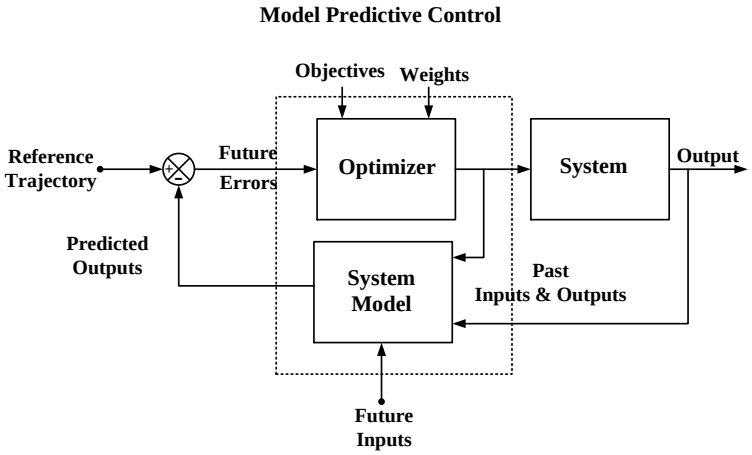

Fig. 6.2. Structure for implementing model predictive control

6.3. Finite Set Model Predictive Control

Continuous Control Set Model Predictive Control (CCS-MPC) and Finite Control Set Model Predictive Control (FCS-MPC) are the MPC control techniques used for power electronics and drives [85], [105], [111], [119]. In CCS-MPC to obtain desire control action from the modulation stage,a control signal is computed in a continuous time (usually duty ratio of voltage). On the other hand, FCS-MPC directly selects the control signals by optimizing the objective-function which contains the error terms of control parameters and uses the inherent discrete nature of the converters. For power converters and drives, finite number of control actions are implemented in straight forward by using FCS-MPC. There are several advantages by using this technique such as easy to understand and provision to include nonlinearities into objective function and addition of control parameters [111], [119].

The generic principle of FCS-MPC for two-level Voltage Source Inverter (VSI) with short prediction horizon (i.e., NP=1) is shown in Fig. 6.3. Here, $y^k{}_0$ is considered as a control

parameter for the present sampling instant *k* and it can be estimated based on the past data. As the two-level VSI has eight switching states, the response of control parameter for all these eight switching states can be predicted for the next sampling period *(k+1)*.

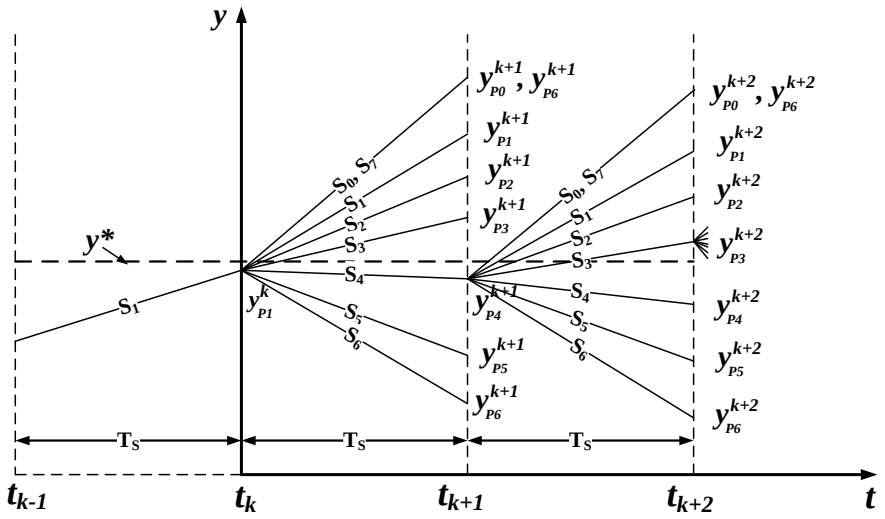

Fig. 6.3. Principle of finite control set model predictive control

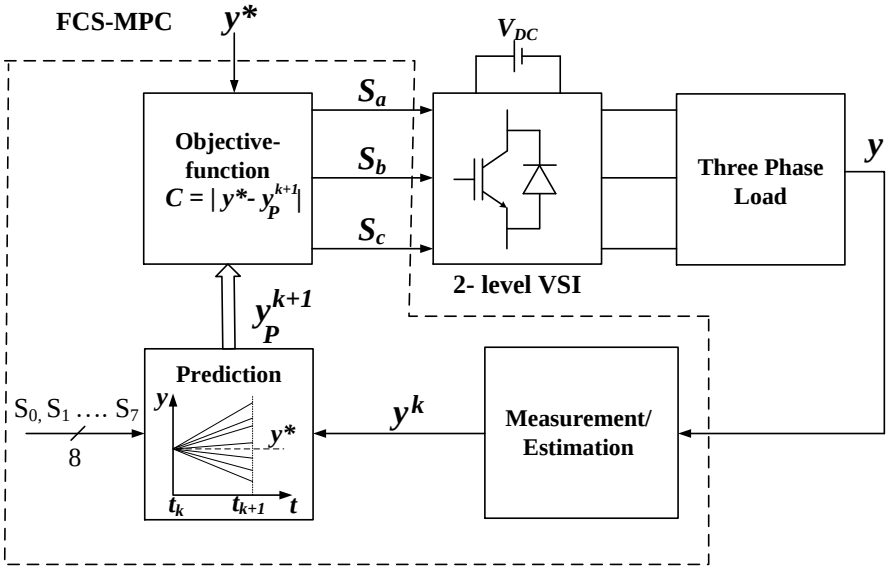

Fig. 6.4. Block diagram for finite control set model predictive control

The switching state which results in close tracking of predicted control parameter with respect to the reference of control parameter *y** (i.e., $|y^*-y^{k+1}|$ is minimum) is considered as an optimal control action for the next sampling period. From Fig. 6.3, at the sampling instant *(k+1)*, switching state S_4 leads to close tracking of y^k with respect to *y**. Based on this measure, $S_4$is applied at *k* to obtain the optimal control action. Similarly, S_3 is the suitable control action at *(k+1)* [111]. The block diagram of FCS-MPC for a typical two-level VSI

connected to a three phase load is shown in Fig. 6.4. Initially, control parameter y^k is measured for present sampling instant *k*. If the direct measurement of the control parameter is not possible, then estimation of control parameter has to be done based on the model of the system and past history of the control parameter. Based on the measured/estimated values, prediction of control parameter can be done for all available inverter control actions. An objective function is formulated by using these predicted values and the corresponding reference value. A suitable control action for two-level VSI is selected based on the minimization of this objective-function. However, in power electronics and drive applications; the inclusion of diverse control parameters like current, stator flux, torque, speed and common mode voltage into single objective-function requires a suitable selection of weighting factors to maintain the relative balance between them.

CCS-MPC and FCS-MPC are the two MPC techniques used for power electronics and electric drive applications. Out of these two, FCS-MPC is widely used technique for power electronic applications due to its advantages such as concepts are easy to understand, optimizations are greatly simplified due to finite number of switching states and simultaneous control over all control parameters can be achieved with the help of single objective-function [105], [111], [119].

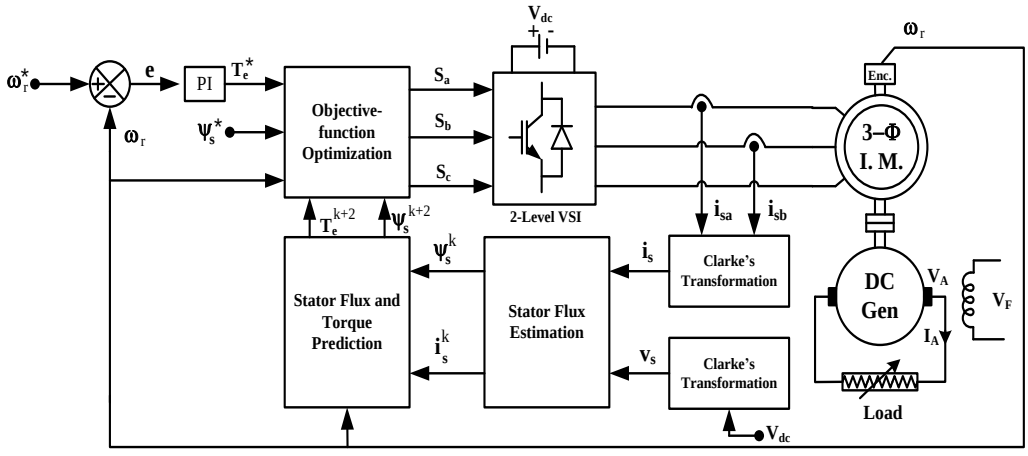

Fig. 6.5. Block diagram for PTC of induction motor drive [120]

FCS-MPC based techniques used for induction motor drives are classified into two types; Predictive Current Control (PCC) and Predictive Torque Control (PTC). Block diagrams of PTC for induction motor drive is shown in Fig. 6.5. The control structure of PTC is similar to DTC. In PCC, stator currents in the stationary reference frame are used as control

parameters. Prediction of stator currents can be done for all available inverter actuations based on the stator measured currents and estimated rotor flux for the present sampling period. A cost function is formulated by using the predicted stator currents and corresponding reference values. By minimizing this cost function, a suitable control actuation will be selected for the converter. The required reference currents can be obtained from outer speed loop and rotor flux loop [121], [122]. In PTC, torque and stator flux are used as control parameters. Prediction of torque and stator flux can be done for all available inverter actuations based on the stator measurements, estimated stator and rotor fluxes. A cost function (also known as objective-function) is formulated by using the predicted toque and stator flux and corresponding reference values. Finally by minimizing this cost function, an optimal actuation is selected for the converter. The reference torque required for cost function is obtained from outer speed loop. The comparative analysis of PTC and PCC for induction motor drives was given in [120]. Since the selection of control action directly depends on the error terms of torque and stator flux, PTC achieves the lower torque ripple and better dynamic response compared to PCC. Hence, PTC is becoming as an effective alternative for DTC based control techniques and also allows the flexibility of adding extra control parameters into the cost function with ease [121]–[130].

6.4. Algorithm for Predictive Torque Control

PTC is used to control the induction motor drive in pre-fault and post-fault operation is explained in detail. Fig. 6.5 shows the schematic of the control algorithm. As shown in the figure, the comparison of reference speed with the measured mechanical speed, then speed error is given to the PI controller to generate reference torque. Finally, the switching pulses are generated by predictive control, which is implemented in three stages; (i) flux estimation, (ii) prediction stage and (iii) formulation of the cost function.

6.4.1. Flux Estimation

Stator currents are obtained by direct measurement at stator terminals of the motor. Stator flux at present sampling period can be estimated by using first-order forward Euler discretizing method as follows:

$$\psi_s^k = \psi_s^{k-1} + T_s(-R_s i_s^{k-1} + V_s^{k-1}) \tag{6.1}$$

Where T_s is sampling time period, V_s is stator voltage vector, i_s is stator current vector, R_S is stator resistance and ψ_s is a stator flux vector.

6.4.2. Prediction Stage

To implement predictive torque control, the torque and stator flux predictions for all the switching states for a two-level inverter are obtained by one step ahead prediction. In healthy condition of the two-level inverter, seven vectors are sufficient to operate the drive in healthy condition (two null vectors generate the same voltage), but in the post-fault operation of the inverter, six active voltage vectors are reduced to four active vectors, which are presented in Table-2. Based on this, the stator flux at (k+1) is predicted as

$$(\psi_s^{k+1})_m = \psi_s^k + T_s(-R_s i_s^k + (V_s^k)_m) \tag{6.2}$$

The stator current at (k+1) instant is

$$(i_s^{k+1})_m = T_s\lambda(R_r - jL_r\omega_r)\psi_s^k + (1 + T_s(-\lambda k_{sr} + j\omega_r^k))i_s^k + T_s\lambda L_r(V_s^k)_m \tag{6.3}$$

Where $\lambda = \frac{1}{(L_s L_r - L_m^2)}$

From the stator flux and stator current torque at (k+1) is obtained as

$$(T_e^{k+1})_m = \frac{3}{2} PI_m((\psi_s^{k+1*})_m \times (i_s^{k+1})_m) \tag{6.4}$$

Where 'm' is switching states of healthy and post-fault converter, 'T_S' is sampling time, 'V_S' is stator voltage, 'L_S' is stator inductance, 'L_r' is rotor inductance, 'L_m' is magnetising inductance, 'w_r' is rotor speed and 'P' is pole pairs. Predictions are obtained for all possible switching sates and corresponding resultant voltage vectors.

6.4.3. Formulation of Cost Function

After the predictions of torque and stator flux, cost function is formulated as

$$C_m = |T_e^* - (T_e^{k+1})_m| + \lambda_o \left| |\psi_s^*| - |(\psi_s^{k+1})_m| \right| \tag{6.5}$$

Where λ_0 is the weighting factor to maintain the relative relation between stator flux and torque. In [126-127], the general procedure for obtained the weighting factor is explained and is given as

$$\lambda_o = \frac{T_e^{nom}}{|\psi_s^{nom}|} \tag{6.6}$$

Where T_e^{nom} = 14.6 N-m & $|\psi_s^{nom}|$ = 1.

From the above expression, the optimal torque and stator flux is obtained by minimizing the cost function to select the optimal switching state for the next sampling period (k+1). Optimal switching states for the inverter is obtained by minimizing the cost function

$$S_{opt} = arg \min_{(S_1 \ldots\ldots S_6)} C_m \qquad \text{For healthy inverter}$$

$$S_{opt} = arg \min_{(S_1 \ldots\ldots S_4)} C_m \qquad \text{For post-fault inverter}$$

6.4.4. Delay Compensation

One step ahead prediction of flux and torque is sufficient for optimization of the cost function in simulation studies. Whereas, in real-time implementation of PTC requires a considerable time for sensing feedback signals such as motor currents and speed, prediction of torque and flux causes a time delay in obtaining the optimal switching states. Hence, the delay concept is introduced in the PTC algorithm to overcome the delay caused by the digital control platform. This delay is compensated by using a two step ahead prediction. Accordingly, eq. (4), (5) and (6) are modified and re-written as follows.

$$(\psi_s^{k+2})_m = \psi_s^{k+1} + T_s(-R_s i_s^{k+1} + (V_s^k)_m) \tag{6.7}$$

$$(i_s^{k+2})_m = T_s\lambda(R_r - jL_r\omega_r)\psi_s^{k+1} + (1 + T_s(-\lambda k_{sr} + j\omega_r^k))i_s^{k+1} + T_s\lambda L_r(V_s^k)_m \tag{6.8}$$

$$(T_e^{k+2})_m = \frac{3}{2}PI_{img}((\psi_s^{k+2*})_m \times (i_s^{k+2})_m) \tag{6.9}$$

Based on this, the cost function is modified as

$$C_m = |T_e^* - (T_e^{k+2})_m| + \lambda_o\left||\psi_s^*| - |(\psi_s^{k+2})_m|\right| \tag{6.10}$$

In post-fault operation, the phase terminal of the motor connected to the inverter faulty leg is removed and connected to the mid-point of the dc-link. After the inverter is reconfigured to operate the drive in normal operation, current imbalance in the capacitors creates an issue of dc-link voltage offset. To eliminate the voltage offset in post-fault operation, capacitor voltage predictions are required to be added as the third term in the cost function. Due to this, the cost function becomes complex and requires more computational time. To overcome these issues, the faulty phase terminal of the motor connected to the inverter is isolated and connected to midpoint of the dc-link/positive terminal of capacitor C_2 and the negative terminal of the capacitor is connected to the negative rail of the dc-link in the proposed topology. As a result dc-link voltage offset suppression is eliminated in the proposed topologies. Due to this, the cost function in post-fault operation remains same as (6.10).

6.5. Simulation Results using Topology-A

Simulations of predictive torque controlled induction motor drive with the conventional converter (B6), conventional fault-tolerant converter (B4) and proposed converter topology consists of three-level boost converter (TLBC) based fault-tolerant two-level inverter fed

induction motor are presented. Results of pre-fault to post fault operation is shown in Fig. 6.6.

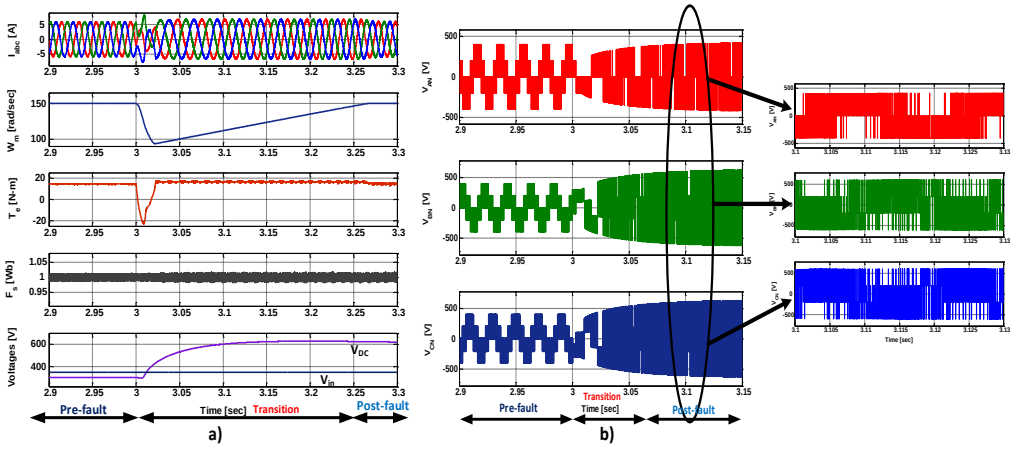

Fig. 6.6 Simulation results of the proposed fault-tolerant drive during pre-fault to post-fault transition

a) Stator currents, Speed, Torque, Flux and DC-link voltage
b) Phase Voltages of the induction motor

Response of the drive operating with a speed of 80 rad/sec at a load torque of 8 N-m is compared with healthy two-level inverter, conventional fault-tolerant inverter (B4) and proposed fault-tolerant inverter are shown in the Fig. 6.7. From the results, it is witnessed that the stator currents, stator flux and torque of proposed fault-tolerant inverter are almost same as the normal two-level inverter. However the stator currents are unbalance, torque ripples are more for the conventional fault-tolerant inverter. As a result the drive system may halt when further speed increases.

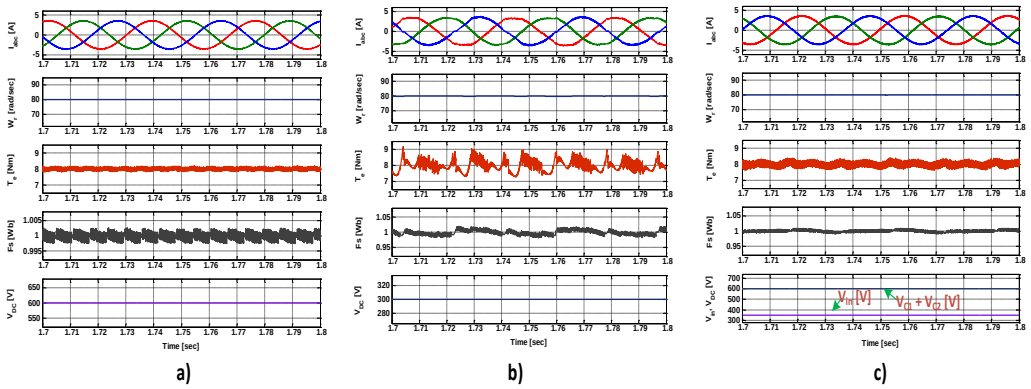

Fig. 6.7 Simulation results of the drive at load torque of 8 N-m and operating at80 rad/sec.

a) Conventional Two-level inverter (B6)
b) B4 converter
c) Proposed fault-tolerant inverter

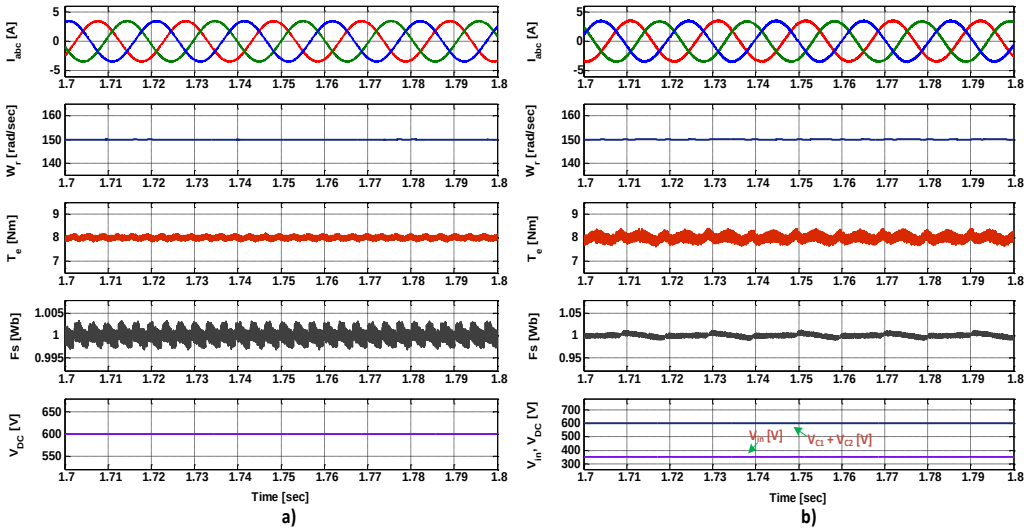

Fig. 6.8 Simulation results of the drive at load torque of 8 N-m and operating at150 rad/sec.

a) Healthy two-level converter
b) Proposed fault-tolerant converter

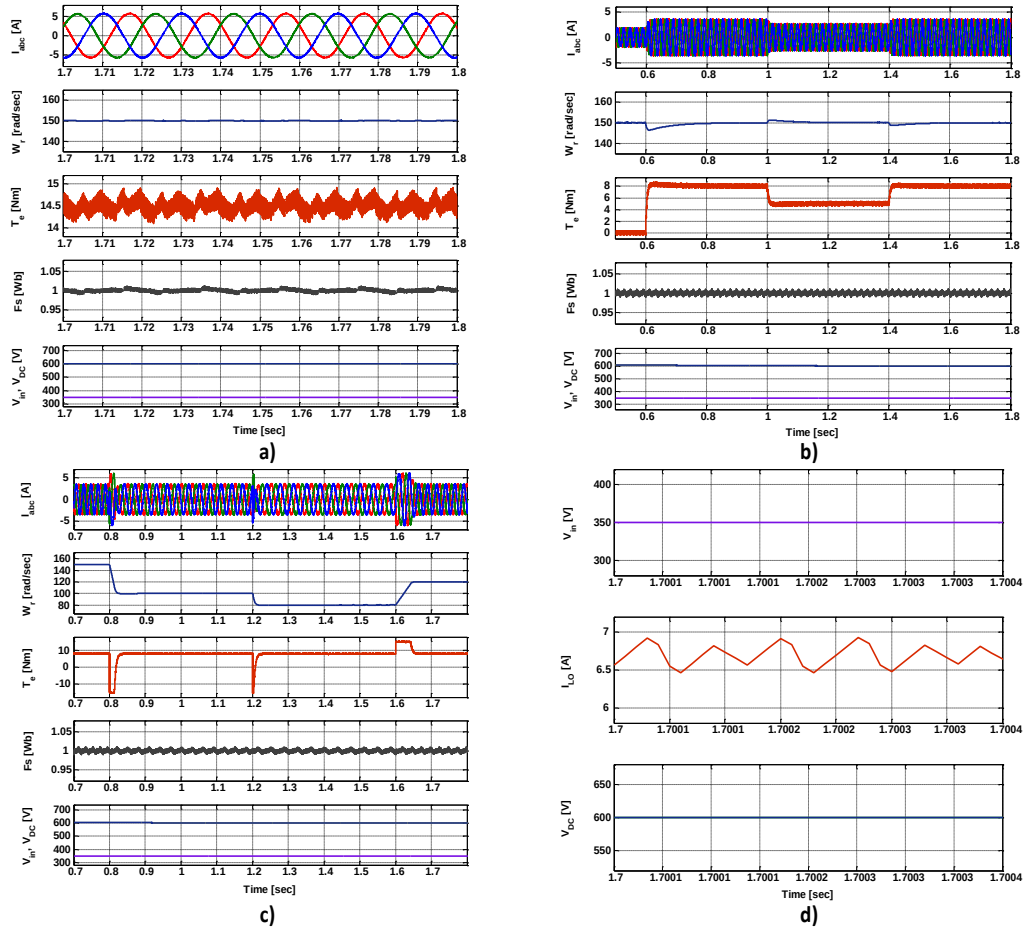

Fig. 6.9 Simulation results of the proposed fault-tolerant inverter in post-fault condition

a) Steady-state operation
b) Load change
c) Speed change
d) Output of TLBC

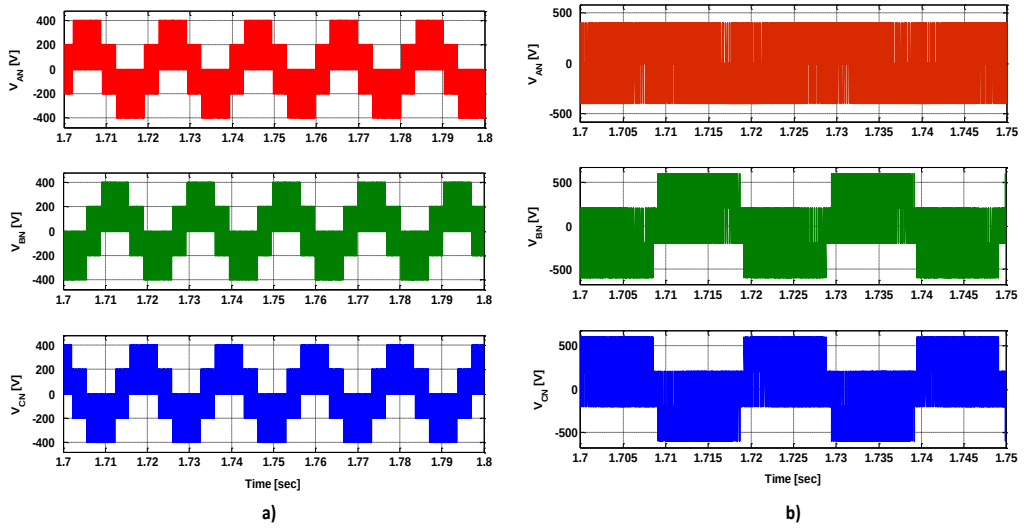

Fig. 6.10 Simulation results of the proposed fault-tolerant converter fed induction motor drive.

a) Phase voltages in healthy condition
b) Phase voltages in post-fault condition

To avoid this, a conventional fault-tolerant inverter is operated at less than 50% of its full rated capacity. Whereas the proposed fault-tolerant inverter operates with full rated capacity in post-fault operation by boosting the dc-link voltage with the help of a three-level boost converter. The normal two-level inverter and proposed fault-tolerant inverter at load torque 8 N-m and operate with full rated speed i.e. 150 rad/sec are shown in Fig. 6.8. From the results it is witnessed that the stator currents are sinusoidal and balanced, torque and flux also have fewer ripples for the proposed fault-tolerant inverter. Fig. 6.9 illustrates the behaviour of the drive at the steady-state, load change, speed change and output of three-level boost converter for proposed fault-tolerant converter topology. From the results, it is witnessed that the dynamic response is reasonably and the voltage across the dc-link is balanced for load and speed changes. The proposed fault-tolerant converter phase voltages in healthy and post-fault converter operation are presented in Fig. 6.10.

6.6. Experimental Results using Topology-A

Experiments are carried out for various operating conditions and results are presented on the developed setup consists of a three-level boost converter at front end of two-level voltage source inverter and control logic as shown in Fig. 3.3. The steady-state operation of the induction motor with a load torque of 8 N-m at a speed of 80 rad/sec for conventional two-level inverter (B6), conventional fault-tolerant inverter (B4) and proposed fault-tolerant inverter are presented in Fig. 6.11. From the results it is witnessed that the stator currents

are sinusoidal and balanced, torque and stator flux ripples are reduced in proposed fault-tolerant inverter in post-fault operation when compared with a conventional fault-tolerant inverter.

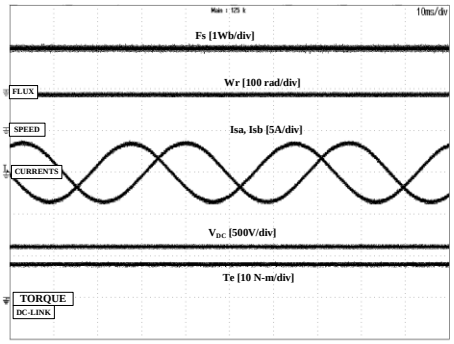

a)

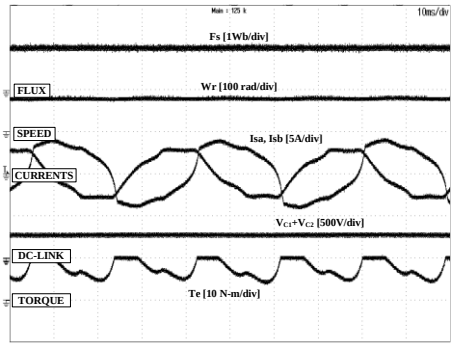

b)

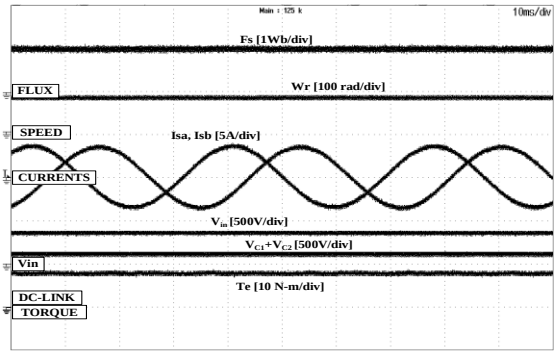

c)

Fig. 6.11 Experimental results of the drive at load torque of 8 N-m and operating at 80 rad/sec.

a) Two-level inverter (B6)
b) B4 inverter
c) Proposed fault-tolerant inverter

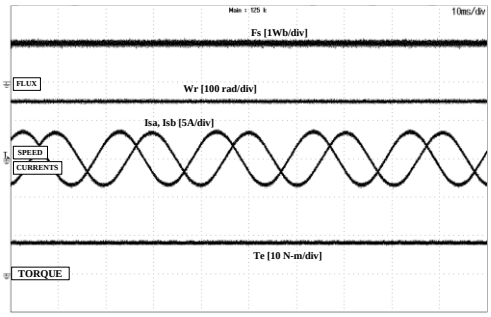

a)

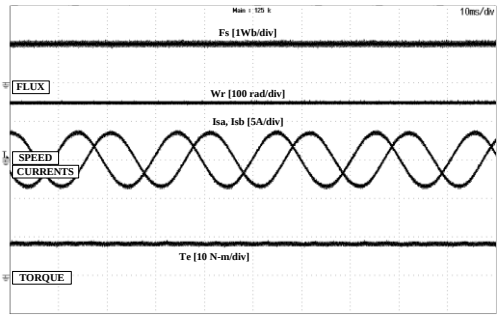

b)

Fig. 6.12 Experimental results of the drive at load torque of 8 N-m and operating at 150 rad/sec.

a) Two-level inverter
b) Proposed fault-tolerant inverter

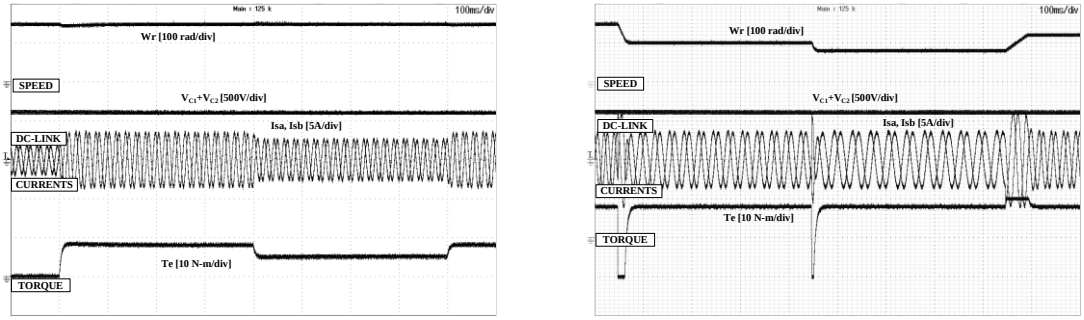

a) b)

Fig. 6.13 Experimental results of the proposed fault-tolerant inverter in post-fault condition for
a) Load change
b) Speed change

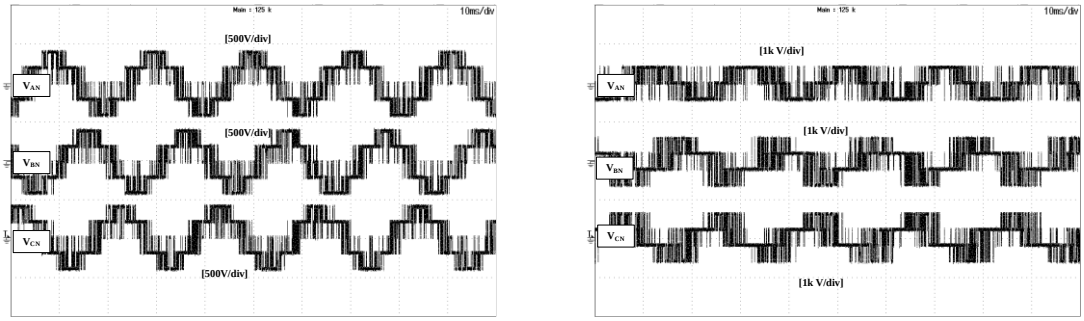

a) b)

Fig. 6.14 Experimental results of the proposed fault-tolerant converter fed induction motor drive.
a) Phase voltages in healthy condition
b) Phase voltages in post-fault condition

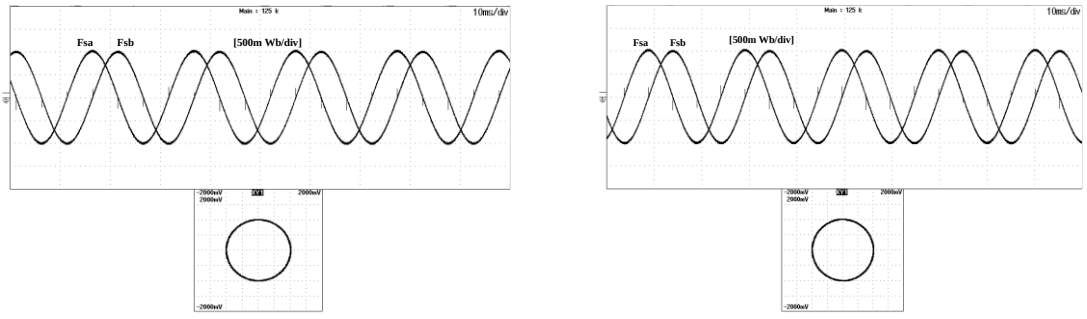

a) b)

Fig. 6.15 Lissajous pattern of stator flux from the experimental results
a) Healthy operation
b) Post-fault operation

The two-level healthy inverter and proposed fault-tolerant inverter operate with full rated speed of 150 rad/sec and a load torque of 8 N-m is shown in Fig. 6.12. From the results, it is witnessed that the proposed converter can operate in full rated speed and the operation is similar to the healthy inverter. The results for load change, speed change and response of three-level boost converter are presented in Fig. 6.13. From the results, it is observed that the dynamic response is satisfactory and the voltage across the dc-link is also balanced in

load and speed changes. Fig. 6.14 illustrates the inverter phase voltages in healthy operation and post-fault operation. The steady-state operation of the drive at a 80 rad/sec and at load torque of 8 N-m for healthy two-level inverter offered 6.82 % stator current THD, 0.042 N-m of torque ripple and 1.40 Wb of stator flux ripple. Whereas, the convention fault-tolerant inverter operated in post-fault operation offered stator current THD of 13.8 %, torque ripple of 4.04 N-m and stator flux ripple of 0.153 Wb. For the same operating conditions, the proposed fault-tolerant inverter in post-fault operation offered stator current THD of 6.91 %, torque ripple of 1.46 N-m and stator flux ripples of 0.062 Wb. Fig. 6.15 illustrates the lissajous pattern of the stator flux in pre and post-fault operation of the proposed fault-tolerant inverter.

6.7. Field Weakening Operation using Topology-A

Behaviour of induction drive with the proposed topology is observed in the field weakening region by running above its base speed. Stator flux reference is chosen based on the speed and is inversely proportional to the rotor speed as follows as

$$\varphi_s^{ref} = \varphi_s^{rated} * \frac{\omega_{rated}}{\omega_r} \tag{6.11}$$

Where ω_{rated} is the induction motor rated speed.

Whenever speed of the drive increases to above its rated value, accordingly the stator currents will exceed their rated values. To limit this, the maximum torque reference is adjusted with the help of stator flux reference as follows

$$T_e^{ref} = T_e^{rated} * \frac{\varphi_s^{ref}}{\varphi_s^{rated}} = T_e^{rated} * \frac{\omega_{rated}}{\omega_r} \tag{6.12}$$

Where T_e^{rated} is the rated torque of the induction motor.

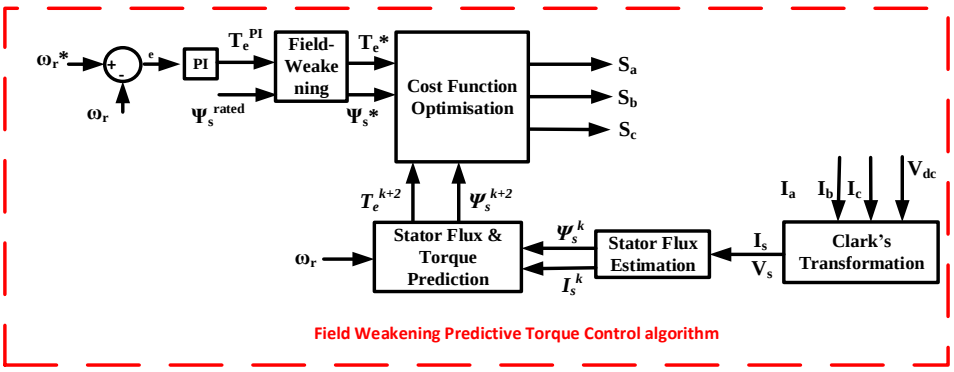

Fig. 6.16 Control algorithm for field weakening region

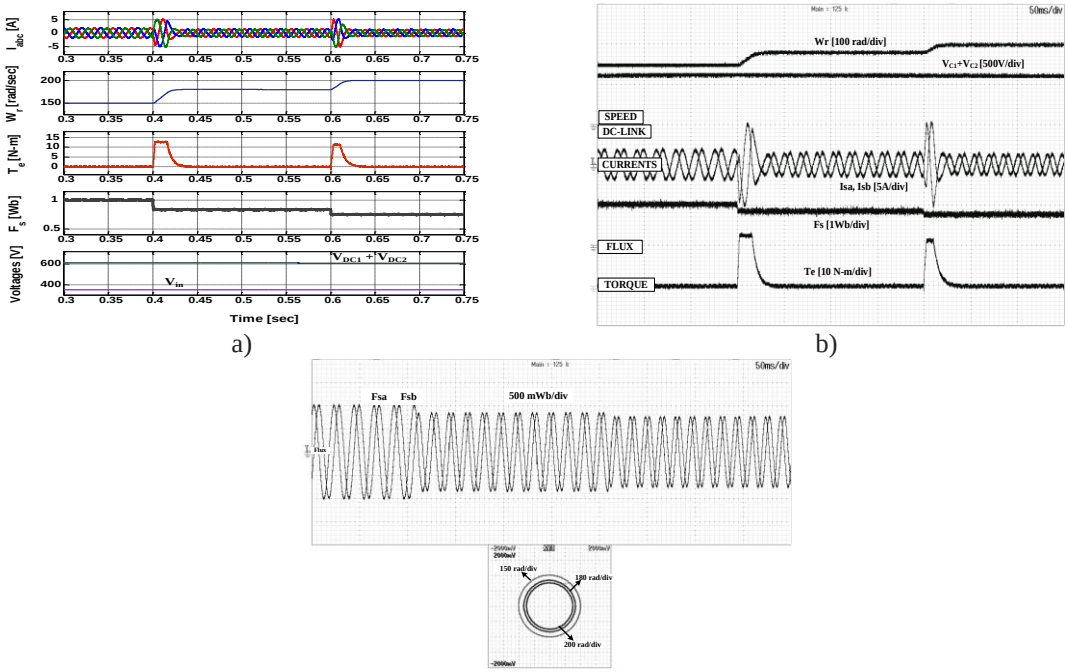

a) b)

c)

Fig. 6.17 Field weakening operation in the speed of 150 rad/sec to 200 rad/sec.

a) Simulation results of the proposed topology
b) Experimental results of the proposed topology
c) Lissajous pattern of stator flux for the proposed topology

The control algorithm for the filed weakening region is shown in Fig. 6.16. Simulation and experimental results of the proposed fault-tolerant converter operating above its rated speed of 150 rad/sec to 180 rad/sec and then to 200 rad/sec are shown in Fig. 6.17 (a) and Fig. 6.17 (b) respectively to observe the field weakening mode of operation. From the results it is observed that the drive is able to operate satisfactorily for this increase in speeds. The Lissajous pattern of stator flux results for the proposed topology with speed changes from 150 rad/sec to 180 rad/sec and then to 200 rad/sec is shown in Fig. 6.17 (c).

6.8. Simulation Results using Topology-B

Simulations of predictive torque controlled induction motor drive with the conventional converter (B6), conventional fault-tolerant converter (B4) and proposed converter topology consists of boost converter based fault-tolerant two-level inverter fed induction motor are presented. From the results result of the pre-fault to post-fault condition shown in Fig. 6.18 it is observed that, the proposed topology operate the drive in full rated condition under pre-fault and post-fault condition. Fig. 6.19 shows the steady-state operation of the drive with PTC for a speed 85 rad/sec at a load torque of 8 N-m for a healthy converter (Conventional three-leg Inverter), conventional fault-tolerant converter (two-leg inverter B4) and proposed

fault-tolerant converter respectively. From Fig. 6.19 (b), it is noticed that the stator currents of the conventional fault-tolerant converter are not balanced; speed oscillates and torque having more ripples. The healthy converter and proposed fault-tolerant converter results are almost same as shown in Fig 6.19 (a) & (c). Fig. 6.20 shows the operation of the drive with healthy converter and proposed reconfigured converter at steady-state with PTC, for a speed 150 rad/sec and a load torque of 8 N-m. From the results, it is observed that stator currents are balanced; torque ripples and speed oscillations are less.

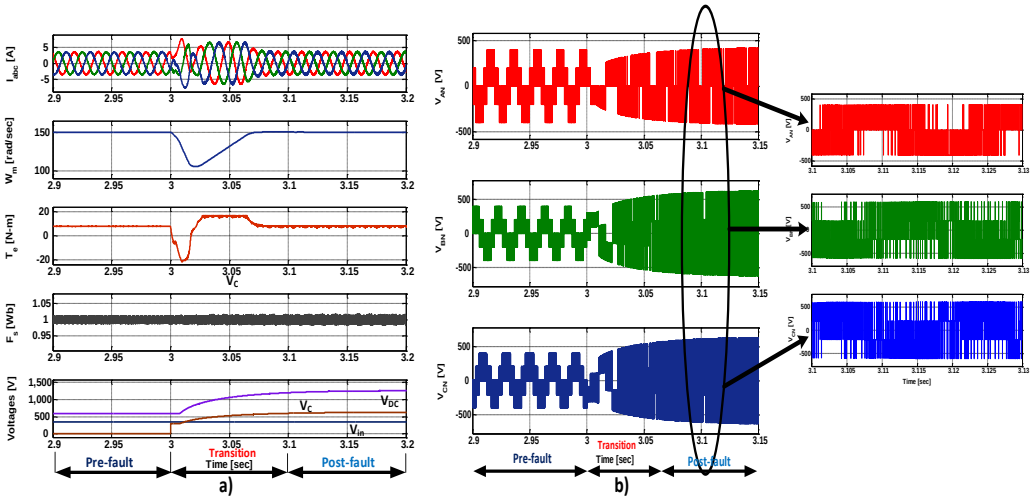

Fig. 6.18 Pre-fault to post-fault simulation results of the proposed topology
a) Current, speed, torque, flux and voltages of the proposed topology
b) Phase voltages of the induction motor drive

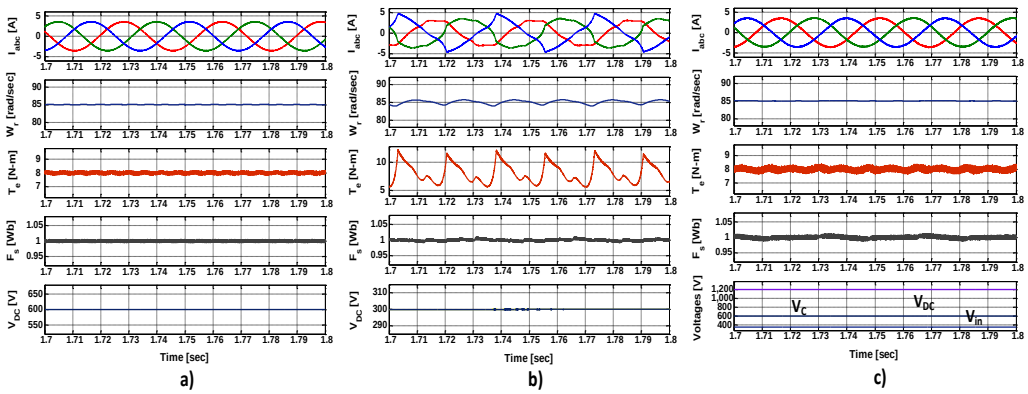

Fig. 6.19 Simulation results of the induction motor drive using PTC at load torque 8 N-m and speed 85 rad/sec.
a) Normal operation of drive
b) Conventional fault-tolerant operation of the drive
c) Proposed fault-tolerant operation of a drive

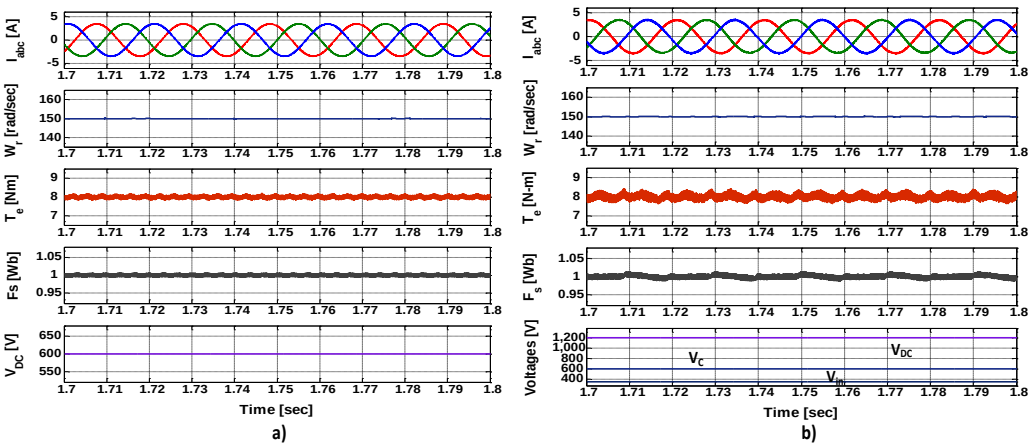

Fig. 6.20 Simulation results of the induction motor drive using PTC at load torque 8 N-m and speed 150 rad/sec.

a) Normal operation of a drive
b) Proposed fault-tolerant operation of a drive

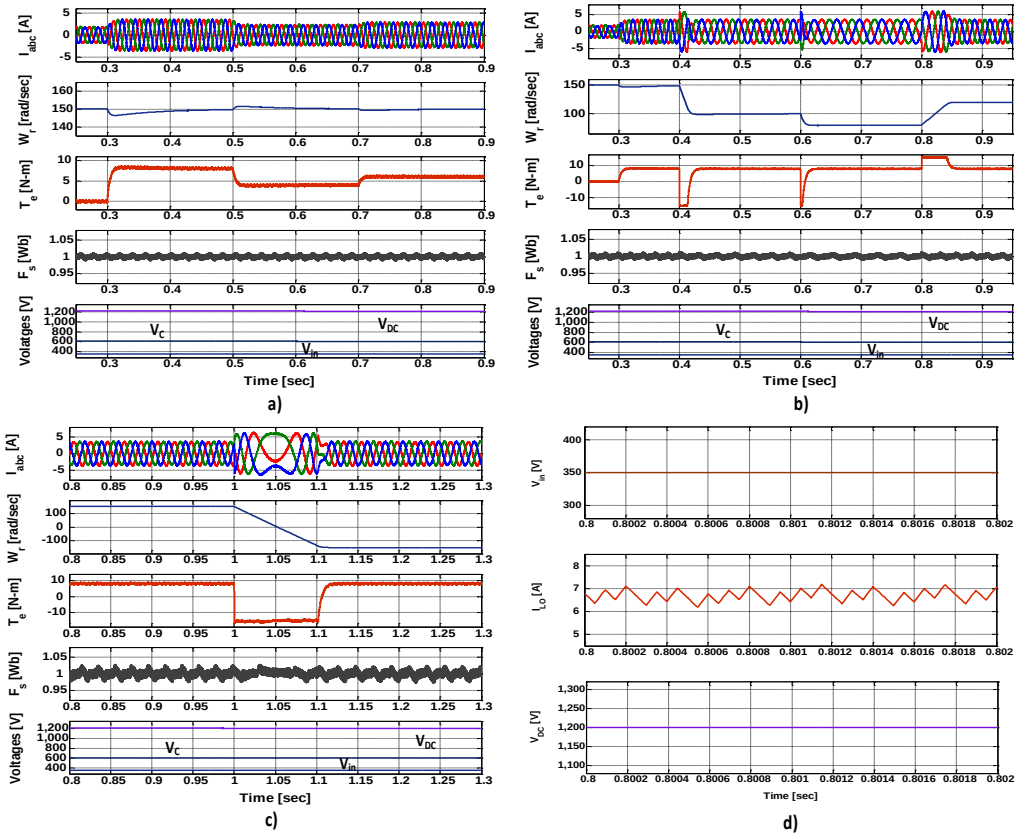

Fig. 6.21 Simulation results of the proposed fault-tolerant induction motor drive using PTC

a) Change in load
b) Change in speed
c) Speed reversal
d) Response of the Boost converter

Fig. 6.21 (a) and (b) illustrate the operation of the proposed converter with change in torque and change in speed respectively. Fig. 6.21 (c) shows the speed reversal of the proposed topology. Fig.

6.21 (d) shows input voltage (V_{in}), inductor current (I_{LO}) and dc-link voltage (V_{DC}) of the boost converter. From these results it is noticed that, the stator currents are balanced, speed and load torque are having less ripples under dynamic conditions. Fig. 6.22 illustrates the inverter phase voltages in healthy and post-fault operation.

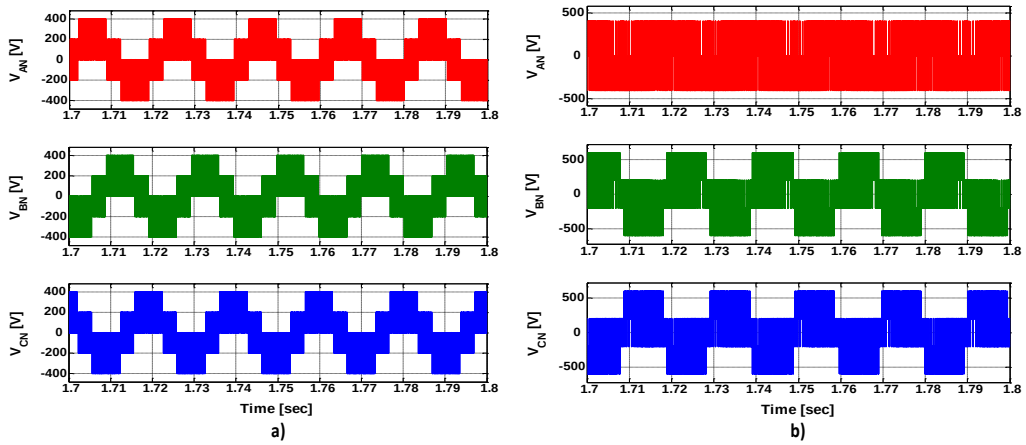

Fig. 6.22 Stator phase voltages of the induction motor drive
a) Healthy Inverter
b) Post-fault Inverter

6.9. Experimental Results using Topology-B

Experiments are carried out for various operating conditions and results are presented on the developed setup consists of a boost converter at front end of two-level voltage source inverter and control logic as shown in Fig. 3.3. Fig. 6.23 shows the stator currents, speed, torque, stator flux and dc-link voltage of the healthy converter (Conventional three-leg Inverter), conventional fault-tolerant converter (two-leg inverter B4) and proposed fault-tolerant converter operating the drive at a speed of 85 rad/sec at a load torque of 8 N-m. From the results it is observed that, in conventional fault-tolerant converter stator currents are not sinusoidal, speed fluctuates and torque have more ripples. Whereas, in proposed fault-tolerant converter the variations in stator currents, speed, torque and stator flux are almost similar to conventional converter. The dynamic behaviour of the proposed converter at load and speed changes are shown in Fig. 6.24 (a-b). From these results it is noticed that, the stator currents are balanced, speed and load torque ripples are less under dynamic conditions. The pattern of stator flux in α-β plane is shown in Fig. 6.25 (a -b). The phase voltages of the drive in healthy mode and post-fault mode are presented in Fig. 6.25 (c-d). Fig. 6.26 shows the results of healthy converter and proposed fault-tolerant converter operating the drive at a speed of 150 rad/sec at a load torque of 8 N-m. The proposed fault-

tolerant converter can operate the drive in full rated speed in post-fault operation and the results are similar to the conventional healthy converter. From the results it is observed that, in conventional fault-tolerant converter stator currents are not sinusoidal, speed fluctuates and torque have more ripples. Whereas, in proposed fault-tolerant converter the variations in stator currents, speed, torque and stator flux are almost similar to conventional converter.

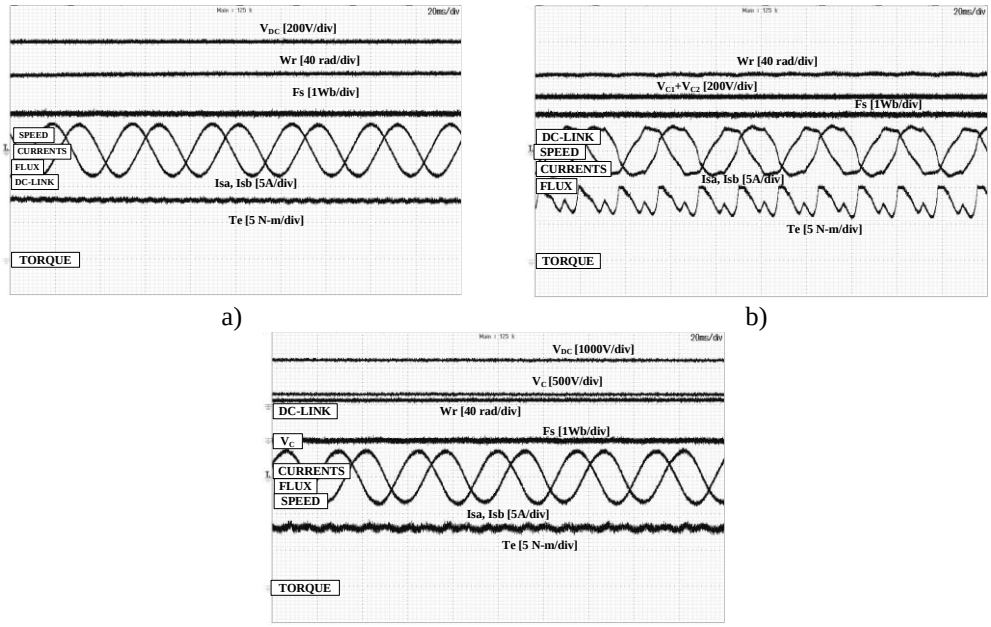

Fig. 6.23 Experimental results of the drive operating at a speed of 85 rad/sec with a load torque of 8 N-m

a) Healthy converter
b) Conventional fault-tolerant converter
c) Proposed fault-tolerant converter

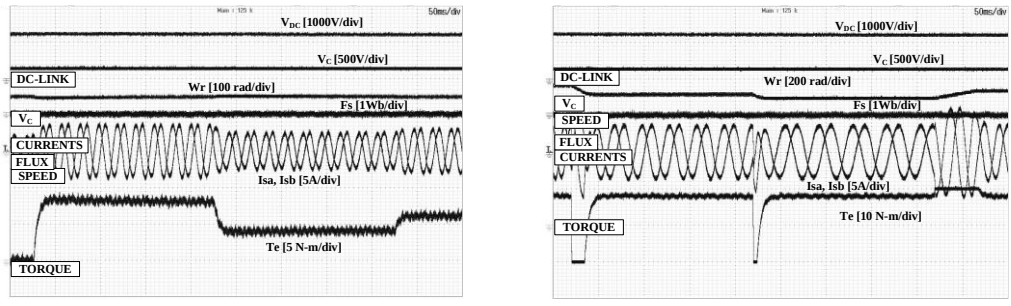

Fig. 6.24 Experimental results of the proposed fault-tolerant induction motor drive in post-fault operation

a) Load change
b) Speed change

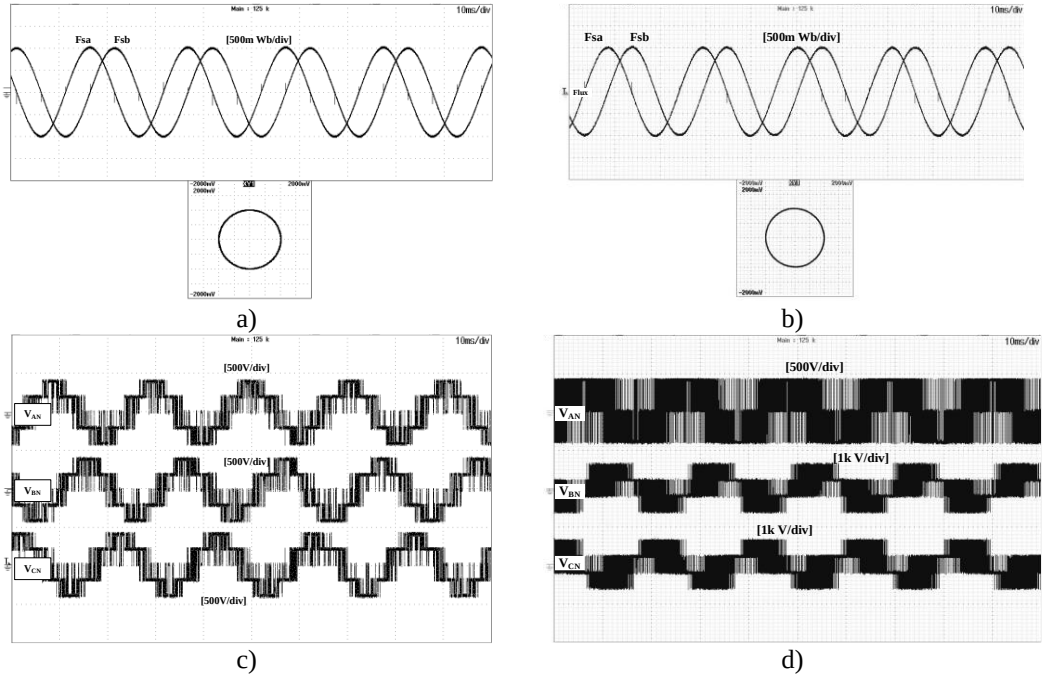

a) b)

c) d)

Fig. 6.25 Experimental results of the proposed fault-tolerant induction motor drive

a) Stator flux during pre-fault operation
b) Stator flux during post-fault operation
c) Phase voltages during pre-fault operation
d) Phase voltages during post-fault operation

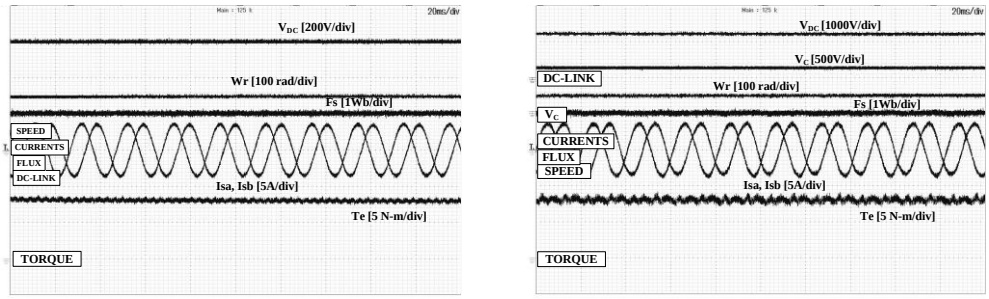

a) b)

Fig. 6.26 Experimental results of the drive operating at a speed of 150 rad/sec having a load torque of 8 N-m.

a) Healthy converter (B6)
b) Proposed fault-tolerant converter (B4+Boost Converter)

The dynamic behaviour of the proposed converter at load and speed changes are shown in Fig. 6.24 (a-b). From these results it is noticed that, the stator currents are balanced, speed and load torque ripples are less under dynamic conditions. The pattern of stator flux in α-β plane is shown in Fig. 6.25 (a -b). The phase voltages of the drive in healthy mode and post-fault mode are presented in Fig. 6.25 (c-d). Fig. 6.26 shows the results of healthy converter and proposed fault-tolerant converter operating the drive at a speed of 150 rad/sec at a load torque of 8 N-m. The proposed fault-tolerant converter can operate the drive in full rated speed in post-fault operation and the results are similar to the conventional healthy converter.

The performance indices of the proposed converter topology (B4+boost converter) are compared with healthy converter (B6) and conventional fault-tolerant converter (B4) operation of the induction motor drive with PTC for speed 85 rad/sec and a load torque of 8 N-m are presented. The healthy converter stator current THD is 6.8 %, torque ripple is 1.25 N-m and flux ripple is 0.042 Wb, whereas the conventional fault-tolerant converter stator current THD is 14.2 %, torque ripple is 4.12 N-m, flux ripple is 0.153 Wb and also for the proposed fault-tolerant converter stator current THD is 6.95 % having torque ripple of 1.48 N-m and flux ripple of 0.062 Wb. From the above results, it is observed that torque ripple, flux ripple and stator current THD of the proposed converter is almost similar to the healthy converter.

6.10. Field Weakening Mode using Topology-B

To verify the proposed topology in the field weakening region, the estimation of torque reference and stator flux reference is consider based on the below equations.

$$\varphi_s^{ref} = \varphi_s^{rated} * \frac{\omega_{rated}}{\omega_r} \tag{6.13}$$

Where ω_{rated} is the rated speed of the induction motor.

$$T_e^{ref} = T_e^{rated} * \frac{\varphi_s^{ref}}{\varphi_s^{rated}} = T_e^{rated} * \frac{\omega_{rated}}{\omega_r} \tag{6.14}$$

Where T_e^{rated} is the rated torque of the induction motor.

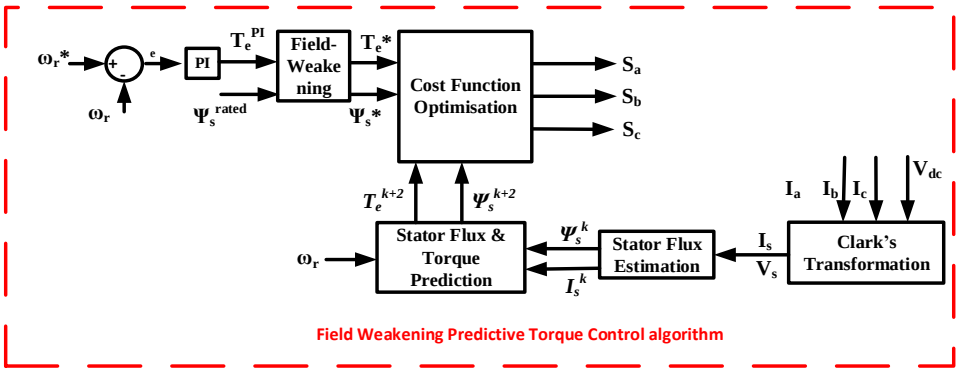

Fig. 6.27 Control algorithm for field weakening region

The control algorithm for the field weakening region is shown in Fig. 6.27. Simulation and experimental results of the proposed fault-tolerant converter operating above its rated speed of 150 rad/sec to 180 rad/sec and then to 200 rad/sec to observe the field weakening mode of operation are shown in Fig. 6.28 (a) and Fig. 6.28 (b) respectively. From the results it is

observed that the drive is able to operate satisfactorily for this increase in speeds. The Lissajous pattern of stator flux results for the proposed topology with speed changes from 150 rad/sec to 180 rad/sec and then to 200 rad/sec is shown in Fig. 6.28 (c).

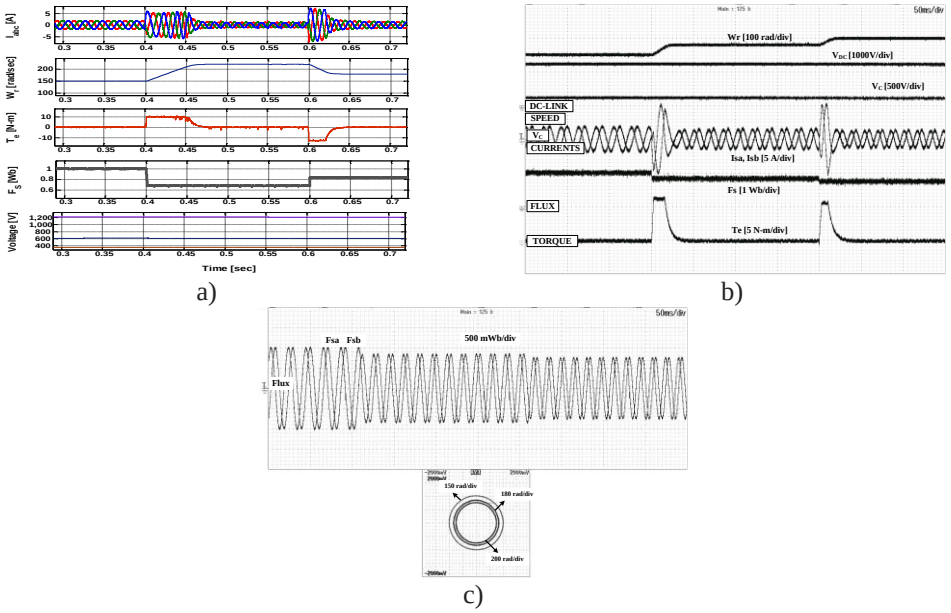

Fig. 6.28 Simulation and experimental results of the proposed topology in the field weakening region

a) Simulation results of the proposed topology operating at a speed of 150 rad/sec to 200 rad/sec.
b) Experimental results of the proposed topology operating at a speed of 150 rad/sec to 200 rad/sec.
c) Lissajous pattern for stator flux for the proposed topology operating at a speed of 150 rad/sec to 200 rad/sec.

6.11. Summary

Three-level boost converter/Boost converter fed fault-tolerant inverter for induction motor with predictive torque control is presented in this chapter. Results are presented for conventional inverter configuration (B6), conventional fault-tolerant inverter (B4) configuration and B4 configuration with three-level boost converter/boost converter fed fault-tolerant inverter on the developed hardware setup at a load torque of 8 N-m using predictive torque control for three-phase induction motor drive. From the results it is observed that the operation of proposed three-level boost converter/boost converter fed induction motor drive in post-fault operation is very close to the conventional two-level inverter (B6) fed induction motor drive. These proposed drive systems has offered considerable improvement in the torque ripple, current THD and balanced dc-link voltage of capacitors compared to a conventional two-level fault-tolerant inverter (B4). The

proposed topologiesare validated in field weakening region of operation and also verified by using simulation and experimental results. From the results it is observed that, the drive is operating satisfactorily even above the rated speeds with proposed converter topologies and control algorithm.The proposed fault-tolerant converter topologies and fault-tolerant topologies existing in the literature are carried out for a load torque of 8 N-m at 85 rad/sec and results are presented in Table-6.1 w.r.t the number of components used, Open-Circuit (OC) and Short-Circuit (SC) fault, control complexity, torque ripple, flux ripple, %THD of stator current. From the results, it is concluded that the proposed fault-tolerant converter topology operates the drive at rated values during post-fault operation with less control complexity when compare with the existing converter topologies. Hence proposed drive system may be considered as one of the alternatives for the direct torque controlled fault-tolerant induction motor drives.

Table-6.1 Comparison of proposed converters with conventional fault-tolerant converters

Topologies	**Switches**	**Diodes**	**Redundant Switches**	**Switches**		**Leg**		**Control Complexity**	**Ripple at (85 rad/sec &8 N-m)**		**THD (%)**	**Performance**
									Torque (N-m)	Flux (Wb)		
				SC	**OC**	**SC**	**OC**					
Proposed Topology-A	8	2	3	Yes	Yes	Yes	Yes	Average	1.47	0.062	6.92	100 % operation.
Proposed Topology-B	7	1	3	Yes	Yes	Yes	Yes	Average	1.48	0.062	6.95	100 % operation.
Faulty phase connected to midpoint of dc-link	6	--	3	Yes	Yes	Yes	Yes	Complex	4.12	0.153	11.65	Restricted to 50 % of operation, dc-link voltage fluctuations.
Additional leg	8	--	3	Yes	Yes	Yes	Yes	Complex	1.45	0.045	6.75	100 % of operation.
Motor neutral terminal connected to midpoint of dc-link	6	--	3	Yes	Yes	Yes	Yes	Complex	4.45	0.221	12.13	Restricted to 50 % of operation, Extra Neutral terminal required & Motor operates in Two phase mode.
Motor neutral terminal connected to extra leg	8	--	3	Yes	Yes	Yes	Yes	Complex	4.25	0.191	11.89	Restricted to 50 % of operation, Extra Neutral terminal required & Motor operates in Two phase mode.

Chapter-7
Conclusion and Future Scope

7.1. Overview and Summary of Results

Most of the industrial applications in the continuous process industry demand continuous and trouble free operation without interruption for different operating conditions and speeds depending on the requirement. In modern industry most of the drives are AC drives with induction motors controlled with power electronic converters and there is a possibility of occurrence of fault due to open-circuit or short-circuit of power electronic devices in the converter. Many drives are operating with three phase two-level voltage source inverter consists of three legs with two devices in each leg (B6 Configuration). Due to failure of any device in one leg, it becomes B4 configuration and it will not support full rated operating conditions of the drive along with other draw backs. To overcome the drawbacks in the conventional fault-tolerant converter topology (B4), two topologies are developed for induction motor drive i.e., three-level boost converter (TLBC) based two-level fault-tolerant converter topology and boost converter (BC) based two-level fault-tolerant converter topology for three-phase induction motor drive. These topologies can operate the drive in full rated condition along with balancing the dc-link voltage across the capacitors in pre-fault and post-fault conduction for various operating conditions such as change in speed and variations in load. Further, these topologies improves the stator current % THD, stator flux ripple, torque ripple and also reduce the speed fluctuations when compare with conventional fault-tolerant converter topology (B4). The simulation and experimental results shows the effective operation of the proposed drive. From the results it is observed that its operation under faulty condition is closely match with the healthy converter topology (B6) with the proposed converter configurations and their control strategy. The two proposed fault-tolerant converter topologies for induction motor drive is controlled by various control algorithms i.e., speed control using V/f method, field oriented control (FOC), direct torque control (DTC) and predictive torque control (PTC).

The two proposed fault-tolerant converter topologies operation with the control algorithms are examined in experimentation along with simulations for healthy converter (B6) and conventional fault-tolerant converter (B4). In post-fault operation, the proposed fault-tolerant converter topologies can operate the drive in full rated capacity and also eliminates the voltage balance at dc-link. From the simulation and experimental results, it is also witnessed that the proposed fault-tolerant topologies with switch failure capability and

its control logic; stator currents, torque and speed are almost gives similar results as that of healthy converter.

Using field oriented control algorithm, results are presented for healthy inverter configuration (B6), conventional fault-tolerant inverter (B4) configuration and proposed fault-tolerant converter topologieson developed hardware setup for induction motor drive. From the results it is concluded that the operation of proposed fault-tolerant converter topologies fed induction motor drive in post-fault operation is very close to the conventional two-level inverter (B6) fed induction motor drive. Proposed drive systems has offered considerable improvement (reduction) in the torque ripple, current THD and balanced dc-link voltage of capacitors compared to a two-level inverter (B4).

Using direct torque control algorithm, the proposed converter topologies operation is compared in real-time with healthy inverter topology (B6) and conventional fault-tolerant converter topology (B4). Proposed converter topologies under post-fault condition balance the dc-link capacitor voltages, operates the drive in full rated load condition with less stator flux ripple and torque ripple indeed with stator current THD. From simulation and experimental results, it is observed that proposed converter topologies operate the drive system satisfactorily during open-circuit and short-circuit faults in the inverter for all practical conditions and also prove that the proposed fault-tolerant converter topology offer better performance than conventional fault-tolerant converter topology (B4).

Using predictive torque control algorithm, the proposed fault-tolerant converter topologies operation is compared in real-time with healthy inverter topology and B4 converter topology. In post-fault operation, the proposed fault-tolerant converter topologies can operate the drive in full rated capacity and also gives a better dynamic performance, eliminates the voltage balance at dc-link in the B4 converter. From the simulation and experimental results, it is witnessed that the proposed fault-tolerant topologies with switch failure capability and its control logic gives stator currents, torque and speed are almost similar results as that of healthy inverter (B6). However conventional fault-tolerant topology (B4) drive operates with less capacity in all the operating conditions tested. The proposed topologies are validated in field weakening region of operation and also verified by using simulation and experimental results. From the results it is observed that, the drive is

operating satisfactorily even above the rated speeds with proposed converter topologies and control algorithm.

Table-7.1 Summary of experimental results for proposed Topology-A at a steady-state

Methodology	Speed [rad/sec]	Torque [Nm]	Torque ripple [Nm]			Stator current THD (%)		
			FOC	DTC	PTC	FOC	DTC	PTC
Conventional Converter (B6)	150	8	1.68	1.58	1.44	6.98	7.35	7.25
	80	8	1.61	1.46	1.40	6.70	6.92	6.82
Conventional Fault-Tolerant Converter (B4)	80	8	3.14	2.26	4.04	11.48	9.81	13.8
Proposed Fault-Tolerant Topology-A	150	8	1.78	1.70	1.56	7.21	7.73	7.45
	80	8	1.72	1.54	1.46	6.90	7.02	6.91

Table-7.2 Summary of experimental results for proposed Topology-B at a steady-state

Methodology	Speed [rad/sec]	Torque [Nm]	Torque ripple [Nm]			Stator current THD (%)		
			FOC	DTC	PTC	FOC	DTC	PTC
Conventional Converter (B6)	150	8	1.68	1.58	1.44	6.98	7.35	7.25
	85	8	1.62	1.48	1.25	6.75	6.97	6.8
Conventional Fault-Tolerant Converter (B4)	85	8	3.31	3.12	4.12	12.28	10.21	14.2
Proposed Fault-Tolerant Topology-B	150	8	1.84	1.70	1.59	7.61	7.73	7.45
	85	8	1.88	1.51	1.48	6.98	7.01	6.95

7.2. Conclusions

In this research work, two-fault tolerant converter topologies are proposed with four control algorithms such as scalar v/f control, field oriented control, direct torque control and field oriented control for induction motor drive. These topologies can operate the drive in full rated condition along with the dc-link voltage across the capacitors are balanced in pre-fault and post-fault conduction over speed and load changes. Further, these topologies improves the stator current % THD, stator flux ripple, torque ripple and also reduce the speed oscillations when compare to the conventional fault-tolerant converter topology (B4). The simulation and experimental results shows the effective performance of the proposed drive and from the results it is observed that it is closely match with the healthy converter topology (B6). Hence the proposed converter topologies with four control algorithms may be considered as some of the alternatives for the fault-tolerant induction motor drives.

7.3. Future scope

- Investigation of novel control algorithms for two-level fault-tolerant induction motor drive to obtain the still better results of the drive system in terms of w.r.t stator flux, torque and stator current % THD.
- Investigation on fault-tolerant converter topologies for four quadrant operation of induction motor drive.
- Investigation of multi-level fault-tolerant converter topologies for three-phase induction motor drive.

Appendix-A

Appendix A: Experimental Setup Specifications

A1: Induction motor specifications and parameters

Rated Power	2.2 kW
Supply Voltage	415 V
Rated Current	4.6 A
Number of Poles	4
Rated Speed	1430 RPM
Rated Torque	14.66 N-m
Rated Stator Flux	1 Wb
Stator Resistance (R_s)	2.23 Ω
Rotor Resistance (R_r)	1.17 Ω
Stator Inductance (L_s)	0.23 H
Rotor Inductance (L_r)	0.23 H
Mutual Inductance (L_m)	0.198 H
Moment of Inertia (J)	0.051 Kg-m^2

A2: DC generator specifications

Rated Power	1.5 kW
Rated Speed	1500 RPM
Armature Voltage	220 V
Armature Current	6.0 A
Field Voltage	220 V
Field Current	0.6 A
Winding	Shunt

A3: Two-level VSI specifications

Rated Power	9.3 KVA
Input Voltage	415 V
Input Current	13.8 A
Input Frequency	50 Hz
Output Voltage	0 - 415 V
Output Current	13.0 A
Output Frequency	0 - 200 Hz

A4: Incremental Encoder Specifications

Voltage Supply Range	10 to 30 V
Pulses per Revolution	1024
Starting torque	0.01 N-m
Maximum RPM	6000 RPM
Pulse Frequency	300 kHz
Low Signal Level	0.5 V
High Signal Level	V_{cc} - 1 V
Channel $A/\bar{A}$	Green/ Yellow
Channel $B/\bar{B}$	Grey/ Pink
Channel $Z/\bar{Z}$	Blue/Red
V_{cc} and Ground	Brown/White

A5: Sensor Board Parameters

Voltage Sensing Board	
Supply Voltage	± 15 V
Maximum DC Voltage	800 V
DC link Voltage Gain, ADC 8	465
Current Sensing Board	
Supply Voltage	± 15 V
Maximum Current	25 A
Current Gain, Phase “a”, ADC 6	19
Current Gain, Phase “b”, ADC 7	19

A6: dSPACE 1104 Specifications

Processors	
Primary Processor	MPC8240, PowerPC 603e core, 250 MHz
Slave Processor	Texas Instruments’ DSP TMS320F240
Inputs and Outputs	
Muxed ADCs	4 Multiplexed ADCs, 16 Bit
ADCs	4 ADCs, 12 Bit
DACs	8 DACs, 16 Bit
Digital I/O	20-bit digital I/O
Peripherals	
Incremental Encoder	2, 24-bit digital incremental encoders
Serial Interface	Serial UART (RS232, RS485 and RS422)
PCI Slot	32-bit PCI slot
PWM	1, 3-Φ PWM 4, 1-Φ PWM

Appendix-B

Appendix B: Simulation and Experimental Parameters

B1: Simulation Parameters

Start time	0.0 sec
Stop time	5.0 sec
Solver type	Fixed step
Solver	Ode 1 (Euler)
Tasking mode	Single tasking

B2: Experimental Parameters

Start time	0.0 sec
Stop time	Infinite
Solver type	Fixed step
Solver	Ode 1 (Euler)
Tasking mode	Single tasking

References

References

[1] A. M. Trzynadlowski, *Control of induction motors*. New York: Academic Press, 2001.

[2] H. Abu-rub, A. Iqbal, and J. Guzinski, *High performance control of AC drives with Matlab/Simulink models*, 1st ed. John Wiley & Sons Ltd, 2012.

[3] M. L. Sin, W. L. Soong, and N. Ertugrul, "Induction machine on-line condition monitoring and fault diagnosis – A survey," *Australian Universities Power Engineering Conference*, Chrischurch, New Zeland, 2003.

[4] IEEE Committee Report, "Report of large motor reliability survey of industrial and commercial installation, part I and part II," *IEEE Transactions on Industry Applications*, Vol. IA-21, pp. 853-872, July/August 1985.

[5] Military Handbook 217F, *Reliability prediction of electronic euipment*, Feb. 28, 1995.

[6] A. Lahyani, P. Venet, G. Grellet, and P.-J. Viverge, "Failure prediction of electrolytic capacitors during operation of a switchmode power supply," *IEEE Transactions on Power Electronics*, Vol. 13, No. 6, pp. 1199-1207, Nov. 1998.

[7] B. A. Welchko, T. A. Lipo, T. M. Jahns, and S. E. Schulz, "Fault tolerant three-phase AC motor drive topologies: A comparison of features, cost, and limitations," *IEEE Transactions on Power Electronics*, Vol. 19, No. 4, pp. 1108-1116, Jul. 2004.

[8] T. M. Jahns, "Improved reliability in solid-state ac drives by means of multiple independent phase-drive units," *IEEE Transactions on Industry Applications*, Vol. IA-16, No. 3, pp. 321-331, May/Jun. 1980.

[9] R. Spée and A. K. Wallace, "Remedial strategies for brushless dc drive failures," *IEEE Transactions on Industry Applications*, Vol. 26, No. 2, pp. 259-266, Mar./Apr. 1990.

[10] J. R. Fu and T. A. Lipo, "Disturbance-free operation of a multiphase current-regulated motor drive with an open phase," *IEEE Transactions on Industry Applications*, Vol. 30, No. 5, pp. 1267-1274, Sept./Oct. 1994.

[11] S. Bolognani, M. Zordan, and M. Zigliotto, "Experimental fault-tolerant control of a PMSM drive," *IEEE Transactions on Industrial Electronics*, Vol. 47, No. 5, pp. 1134- 1141, Oct. 2000.

[12] N. Bianchi, S. Bolognani, M. Zigliotto, and M. Zordan, "Innovative remedial strategies for inverter faults in IPM synchronous motor drives," *IEEE Transactions on Energy Conversion*, Vol. 18, No. 2, pp. 306-314, Jun. 2003.

[13] M. B. de R. Corrêa, C. B. Jacobina, E. R. C. da Silva, and A. M. N. Lima, "An induction motor drive system with improved fault tolerance," *IEEE Transactions on Industry Applications*, Vol. 37, No. 3, pp. 873-879, May/Jun. 2001.

[14] C. B. Jacobina, R. L. de A. Ribeiro, A. M. N. Lima, and E. R. C. da Silva, "Fault-tolerant reversible AC motor drive system," *IEEE Transactions on Industry Applications*, Vol. 39, No. 4, pp. 1077-1084, Jul./Aug. 2003.

[15] R. L. de A. Ribeiro, C. B. Jacobina, E. R. C. da Silva, and A. M. N. Lima, "Fault-tolerant voltage-fed PWM inverter AC motor drive systems," *IEEE Transactions on Industrial Electronics*, Vol. 51, No. 2, pp. 439-446, Apr. 2004.

[16] T. Elch-Heb and J. P. Hautier, "Remedial strategies for inverter ac motor system at the occurrence of a transistor drive fault," *Conference Proceedings in EPE*, pp. 4-286 – 4-291, 1991.

[17] D. Kastha and B. K. Bose, "Fault mode single-phase operation of a variable frequency induction motor drive and improvement of pulsating torque characteristics," *IEEE Transactions on Industrial Electronics*, Vol. 41, No. 4, pp. 426-433, Aug. 1994.

[18] D. Kastha and B. K. Bose, "On-line search based pulsating torque compensation of a fault mode single-phase variable frequency induction motor drive," *IEEE Transactions on Industry Applications*, Vol. 31, No. 4, pp. 802-811, Jul./Aug. 1995.

[19] D. Kastha and A. K. Majumdar, "An improved starting strategy for voltage-source inverter fed three phase induction motor drives under inverter fault conditions," *IEEE Transactions on Power Electronics*, Vol. 15, No. 4, pp. 726-732, Jul. 2000.

[20] T. H. Liu, J. R. Fu, and T. A. Lipo, "A strategy for improving reliability of field-oriented controlled induction motor drives," *IEEE Transactions on Industry Applications*, Vol. 29, No. 5, pp. 910-918, Sept./Oct. 1993.

[21] T. Elch-Heb and J. P. Hautier, "Remedial strategy for inverter-induction machine system faults using two-phase operation," *Conference Proceedings in European Conference on Power Electronics and Applications*, Vol. 5, pp. 151-156, Sep. 1993.

[22] J. R. Fu and T. A. Lipo, "A strategy to isolate the switching device fault of a current regulated motor drive," *Conference Proceedings in IEEE Industry Applications Society Annual Meeting*, Vol. 2, pp. 1015-1020, Oct. 1993.

[23] H. W. Van Der Broeck and J. D. Van Wyk, "A comparative investigation of a three-phase induction machine drive with a component minimized voltage-fed inverter under different control options," *IEEE Transactions on Industry Applications*, Vol. IA-20, No. 2, pp. 309-320, Mar./Apr. 1984.

[24] G. A. Covic and G. L., "DC link imbalance compensation in four-switch inverter AC motor drives," *Electronics Letters*, Vol. 33, No. 13, pp. 1101-1102, Jun. 1997.

[25] G. L. Peters, G. A. Covic, and J. T. Boys, "Eliminating output distortion in four-switch inverters with three-phase loads," *IEE Proceedings in Electric Power Applications*, Vol.145, No. 4, pp. 326-332, Jul. 1998.

[26] F. Blaabjerg, S. Freysson, H.-H. Hansen, and S. Hansen, "A new optimized space-vector modulation strategy for a component-minimized voltage source inverter," *IEEE Transactions on Power Electronics*, Vol. 12, No. 4, pp. 704-714, Jul. 1997.

[27] F. Blaabjerg, D. O. Neacsu, and J. K. Pedersen, "Adaptive SVM to compensate dc-link voltage ripple for four-switch three-phase voltage-source inverters," *IEEE Transactions on Power Electronics*, Vol. 14, No. 4, pp. 743-752, Jul. 1999.

[28] M. B. de R. Corrêa, C. B. Jacobina, E. R. C. da Silva, and A. M. N. Lima, "A general PWM strategy for four-switch three-phase inverters," *IEEE Transactions on Power Electronics*, Vol. 21, No. 6, pp. 1618-1627, Nov. 2006.

[29] A. M. S. Mendes and A. J. M. Cardoso, "Fault-tolerant operating strategies applied to three-phase induction-motor drives," *IEEE Transactions on Industrial Electronics*, Vol. 53, No. 6, pp. 1807-1817, Dec. 2006.

[30] A. M. S. Mendes, X. M. Lopez-Fernandez, and A. J. M. Cardoso, "Thermal behavior of a three-phase induction motor fed by a fault-tolerant voltage source inverter," *IEEE Transactions on Industry Applications*, Vol. 43, No. 3, pp. 724-730, May/Jun. 2007.

[31] P. N. Enjeti and A.Rahman, "A new single-phase to three-phase converter with active input current shaping for low cost ac motor drives," *IEEE Transactions on Industry Applications*, Vol. 29, No. 4, pp. 806-813, Jul./Aug. 1993.

[32] Chingchi Chen, D. M. Divan, D.M., and D. W. Novotny, "A hybrid inverter/ cycloconverter-based variable-speed three-phase induction motor drive for single-phase inputs," *IEEE Transactions on Industry Applications*, Vol. 31, No.3, pp. 630-635, May/Jun. 1995.

[33] Gi-Taek Kim and T. A. Lipo, T.A, "VSI-PWM rectifier/inverter system with a reduced switch count," *IEEE Transactions on Industry Applications*, Vol. 32, No. 6, pp. 1331-1337, Nov./Dec. 1996.

[34] C. B. Jacobina, C.B.; M. B. d. R. Correa, E. R. C. da Silva, and A. M. N. Lima, "Induction motor drive system for low-power applications," *IEEE Transactions on Industry Applications*, Vol. 35, No. 1, pp. 52-61, Jan./Feb. 1999.

[35] B. K. Lee, B. Fahimi, and M. Ehsani, "Overview of reduced parts converter topologies for AC motor drives," *Conference Proceedings in 32nd Annual Power Electronics Specialists Conference*, Vol. 4, pp. 2019-2024, 17-21 Jun. 2001.

[36] B. A. Welchko, and T. A. Lipo, "A novel variable-frequency three-phase induction motor drive system using only three controlled switches," *IEEE Transactions on Industry Applications*, Vol. 37, No. 6, pp. 1739-1745, Nov./Dec. 2001.

[37] C. B. Jacobina, M. B. d. R. Correa, A. M. N. Lima, and E. R. C. da Silva, "AC motor drive systems with a reduced-switch-count converter," *IEEE Transactions on Industry Applications*, Vol. 39, No. 5, pp. 1333-1342, Sep./Oct. 2003.

[38] C. B. Jacobina, I. S. De Freitas, E. R. C. da Silva, A. M. N. Lima, and R. L. A. Ribeiro, "Reduced switch count dc-link ac–ac five-leg converter," *IEEE Transactions on Power Electronics*, Vol. 21, No. 5, pp. 1301-1310, Sep. 2006.

[39] Dong-Choon Lee and Young-Sin Kim, "Control of single-phase-to-three-phase AC/DC/AC PWM converters for induction motor drives," *IEEE Transactions on Industrial Electronics*, Vol. 54, No. 2, pp. 797-804, Apr. 2007.

[40] C. B. Jacobina, I. S. de Freitas, and A. M. N. Lima, "DC-link three-phase-to-three-phase four-leg converters," *IEEE Transactions on Industrial Electronics*, Vol. 54, No. 4, pp. 1953–1961, Aug. 2007.

[41] C. B. Jacobina, E. C. dos Santos, E. R. C. da Silva, M. B. d. R. Correa, and A. M. N. Lima, and T. M. Oliveira, "Reduced switch count multiple three-phase ac machine drive Systems," *IEEE Transactions on Power Electronics*, Vol. 23, No. 2, pp. 966-976, Mar. 2008.

[42] S. Kwak and H. A. Toliyat, "Fault-tolerant topologies and switching function algorithms for three-phase matrix converter based ac motor drives against open and short phase failures," *Conference Proceedings in IEEE International Electric Machines & Drives Conference*, Vol. 1, pp. 886-891, May 2007.

[43] S. Kwak, H. A. Toliyat, "An approach to fault-tolerant three-phase matrix converter drives," *IEEE Transaction on Energy Conversion*, Vol. 22, No. 4, pp. 855-863, Dec. 2007.

[44] S. Kwak and H. A. Toliyat, "Remedial switching function approach to improve reliability for ac–ac converters," *IEEE Transaction on Energy Conversion*, Vol. 22, No. 2, pp. 541-543, Jun. 2007.

[45] S. Li and L. Xu, "Strategies of fault tolerant operation for three-level PWM inverters," *IEEE Transactions on Power Electronics*, Vol. 21, No. 4, pp. 933-940, Jul. 2006.

[46] S. Khomfoi and L. M. Tolbert, "Fault diagnosis and reconfiguration for multilevel inverter drive using AI-based techniques," *IEEE Transactions on Industrial Electronics*, Vol. 54, No. 6, pp. 2954-2968, Dec. 2007.

[47] K. S. Smith, L. Ran, and J. Penman, "Real-time detection of intermittent misfiring in a voltage-fed PWM inverter induction-motor drive," *IEEE Transactions on Industry Applications*, Vol. 44, pp. 468-476, Jul./Aug. 1997.

[48] R. Peuget, S. Courtine, and J. P. Rognon, "Fault detection and isolation on a PWM inverter by knowledge-based model," *IEEE Transactions on Industry Applications*, Vol. 34, pp. 1318-1326, Nov./Dec. 1998.

[49] R. L. de A. Ribeiro, C. B. Jacobina, E. R. C. da Silva, and A. M. N. Lima, "Fault detection of open-switch damage in voltage-fed PWM motor drive systems," *IEEE Transactions on Power Electronics*, Vol. 18, No. 2, pp. 587-593, Mar. 2003.

[50] L. Zhang, I. B. Aris, and L. N. Hulley, "A knowledge-based system for on-line fault diagnosis of power inverter circuits for ac machines," *European Power Electronics Conference*, pp. 3.334-3.339, 1995.

[51] A. M. S. Mendes and A. J. Marques Cardoso, "Fault diagnosis in a rectifier-inverter system used in variable speed ac drives by the average current park's vector approach," *European Power Electronics Conference*, pp. 1-9, 1999.

[52] K. Debebe, V. Rajagopalan, and T. S. Sankar, "Expert systems for fault diagnosis of VSI fed drives," *Proceedings of IEEE Conference on Industry Applications*, pp. 368-373, 1991.

[53] P. J. Chrzan and R. Szczesny, "Fault diagnosis of voltage fed inverter for induction motor drive," *IEEE International Symposium in Industrial Electronics*, pp. 1011-1016, 1996.

[54] D. Kastha and B. K. Bose, "Investigation of fault modes of voltage-fed inverter system for induction motor drive," *IEEE Transactions on Industry Applications*, Vol. 30, No. 4, pp.1028- 038, Jul./Aug. 1994.

[55] N. Mohan, T. M. Undeland, and W. P. Robbins, *Power electronics-converters, applications, and design*, John Wiley & Sons, Inc., 2nd Edition, 1995.

[56] A. Lahyani, P. Venet, G. Grellet, and P.-J. Viverge, "Failure prediction of electrolytic capacitors during operation of a switchmode power supply," *IEEE Transactions on Power Electronics*, Vol. 13, No. 6, pp. 1199-1207, Nov. 1998.

[57] B. A. Welchko, J. Wai, T. M. Jahns, and T. A. Lipo, "Magnet-flux-nulling control of interior PM machine drives for improved steady-state response to short-circuit faults," *IEEE Transactions on Industry Applications*, Vol. 42, No. 1, pp. 113-120, Jan./Feb. 2006.

[58] Rammohan Rao Errabelli, and Peter Mutschler, "Fault-tolerant voltage source inverter for permanent magnet drives," *IEEE Transactions on Power Electronics*, Vol. 27, No. 2, pp. 500-508, Jan./Feb. 2012.

[59] B. Tabbache, M. Benbouzid, A. Kheloui, J. M. Bourgeot, and A. Mamoune, "An improved fault-tolerant control scheme for PWM inverter-fed induction motor-based EVs," *ISA Trans.*, vol. 52, no. 6, pp. 862–869, 2013.

[60] M. Jannati *et al.*, "Vector control of star-connected 3-phase induction motor drives under open-phase fault based on rotor flux field-oriented control," *Electr. Power Components Syst.*, vol. 44, no. 20, pp. 2323–2337, 2016.

[61] P. Sobanski and T. Orlowska-Kowalska, "Faults diagnosis and control in a low-cost fault-tolerant induction motor drive system," *Math. Comput. Simul.*, vol. 131, pp. 217–233, 2017.

[62] D. Zhou, Y. Li, J. Zhao, F. Wu, and H. Luo, "An embedded closed-loop fault-tolerant control scheme for nonredundant VSI-fed induction motor drives," *IEEE Trans. Power Electron.*, vol. 32, no. 5, pp. 3731–3740, 2017.

[63] M. Jannati, A. Monadi, N. Rumzi, N. Idris, and M. J. Abdul, “Experimental evaluation of FOC of 3-phase IM under open-phase fault,” *Int. J. Electron.*, vol. 104,no. 10, pp. 1675–1688, 2017.

[64] R. Maamouri, M. Trabelsi, M. Boussak, F. M. Sahli, and R. Maamouri, “Fault diagnosis and fault tolerant control of a three-phase VSI supplying sensorless speed controlled induction motor drive,” *Electr. Power Components Syst.*, vol. 0, no. 0, pp. 1–15, 2018.

[65] K. D. Hoang, Z. Q. Zhu, and M. P. Foster, “Influence and compensation of inverter voltage drop in direct torque-controlled four-switch three-phase PM brushless AC drives,” *IEEE Trans. Power Electron.*, vol. 26, no. 8, pp. 2343–2357, 2011.

[66] A. M. Bassem El Badsi, Badii Bouzidi, “DTC scheme for a four-switch inverter-fed induction motor emulating the six-switch inverter operation,” *IEEE Trans. Power Electron.*, vol. 28, no. 7, pp. 3528–3538, 2013.

[67] M. K. Metwally and H. Z. Azazi, “Four-switch three-phase inverter performance fed sensorless speed control induction motor drives using model reference adaptive system,” *Electr. Power Components Syst.*, vol. 42, no. 7, pp. 727–736, 2014.

[68] Dehong Zhou, Jin Zhao, and Yang Liu, “Predictive torque control scheme for three-phase four-switch inverter-fed induction motor drive with DC-link voltages offset suppression,” *IEEE Trans. Power Electron.*, vol. 30, no. 6, pp. 3309–3318, 2015.

[69] C. Zhu, Z. Zeng, and R. Zhao, “Comprehensive analysis and reduction of torque ripples in three-phase four-switch inverter-fed PMSM drives using space vector pulse-width modulation,” *IEEE Trans. Power Electron.*, vol. 32, no. 7, pp. 5411–5424, 2017.

[70] M. Farhadi, M. T. Fard, M. Abapour, and M. T. Hagh, “DC-AC converter-fed induction motor drive with fault-tolerant capability under open- and short-circuit switch failures,” *IEEE Trans. Power Electron.*, vol. 33, no. 2, pp. 1609–1621, 2018.

[71] M. Tousizadeh, H. S. Che, J. Selvaraj, and N. Abd, “Fault-tolerant field oriented control of three-phase induction motor based on unified feed-forward method,” *IEEE Trans. Power Electron.*, vol. 0, no. 0, pp. 1–1, 2018.

[72] M. Tousizadeh, H. S. Che, and J. Selvaraj, “Performance comparison of fault-tolerant three-phase induction motor drives considering current and voltage limits,” *IEEE Trans. Ind. Electron.*, vol. 66, no. 4, pp. 2639–2648, 2019.

[73] S. Yang, A. Bryant, P. Mawby, D. Xiang, L. Ran, and P. Tavner, “An industry-based survey of reliability in power electronic converters,” *IEEE Trans. Ind. Appl.*, vol. 47, no. 3, pp. 1441–1451, 2011.

[74] S. Yantao, and B. Wang, “Survey on reliability of power electronic systems,” *IEEE Trans. Power Electronics.*, vol. 28, no. 1, pp. 591–604, 2013.

[75] B. Mirafzal, “Survey of fault-tolerance techniques for three-phase voltage source inverters,” *IEEE Trans. Ind. Electron.*, vol. 61, no. 10, pp. 5192–5202, 2014.

[76] W. Zhang, D. Xu, P. N. Enjeti, H. Li, J. T. Hawke, and H. S. Krishnamoorthy, “Survey on fault-tolerant techniques for power electronic converters,” *IEEE Trans. Power Electron.*, vol. 29, no. 12, pp. 6319–6331, 2014.

[77] A. Sayed-Ahmed, B. Mirafzal, and N. A. O. Demerdash, “Fault-tolerant technique for Δ-connected AC-motor drives,” *IEEE Trans. Energy Convers.*, vol. 26, no. 2, pp. 646–653, 2011.

[78] E. Levi, “Advances in converter control and innovative exploitation of additional degrees of freedom for multiphase machines,” *IEEE Trans. Ind. Electron.*, vol. 63, no. 1, pp. 433–448, 2016.

[79] W. N. W. A. Munim, M. J. Duran, H. S. Che, M. Bermudez, I. Gonzalez-Prieto, and N. A. Rahim, “A unified analysis of the fault tolerance capability in six-phase induction motor drives,” *IEEE Trans. Power Electron.*, vol. 32, no. 10, pp. 7824–7836, 2017.

[80] A. M. Massoud, S. Ahmed, A. S. Abdel-Khalik, and M. S. Hamad, “Postfault operation of a nine-phase six-terminal induction machine under single open-line fault,” *IEEE Trans. Ind. Electron.*, vol. 65, no. 2, pp. 1084–1096, 2018.

[81] Sampong Srilad, Satean Tunyasrirut, and Tianchai Susri, “Implementation of a sclar controlled induction motor drives,” in *Proceedings of the 2006 SICE-ICASE International Joint Conference of the IEEE*, 2007, pp. 3605–3610.

[82] F. Blaschke, “The principle of field-orientation applied to transvector closed-loop control system for rotating field machines,” *Siemens Rev.*, vol. XXXIX, no. 5, pp. 217–220, 1972.

[83] P. Vas, *Sensorless vector and direct torque control*. Oxford University Press, USA, 1998.

[84] D. Casadei, F. Profumo, G. Serra, and A. Tani, “FOC and DTC : Two viable schemes for induction motors torque control,” *IEEE Trans. Power Electron.* , vol. 17, no. 5, pp. 779–787, Sep. 2002.

[85] J. Rodriguez and P. Cortes, *Predictive control of power converters and electrical drives*, 1st ed. John Wiley and Sons, 2012.

[86] I. Takahashi and T. Noguchi, “A new quick-response and high-efficiency control strategy of an induction motor,” *IEEE Trans. Ind. Appl.*, vol. IA-22, no. 5, pp. 820–827, Sep. 1986.

[87] G. S. Buja and M. P. Kazmier kowski, “Direct torque control of PWM inverter-fed AC motors — A survey,” *IEEE Trans. Ind. Electron.*, vol. 51, no. 4, pp. 744–757, Aug. 2004.

[88] B. Bose, *Modern power electronics and AC drives*, 1st ed. Prentice-Hall, 2002.

[89] Y. Lai and J. Chen, “A new approach to direct torque control of induction motor drives for constant inverter switching frequency and torque ripple reduction,” *IEEE Trans. Energy Convers.*, vol. 16, no. 3, pp. 220–227, Sep. 2001.

[90] S. K. Lin and C. H. Fang, “Sliding-Mode direct torque control of an induction motor,” in *27th Annual Conference of the IEEE Industrial Electronics Society*, 2001, pp. 2171–2177.

[91] Z. Zhang, R. Tang, B. Bai, and D. Xie, “Novel direct torque control based on space vector modulation with adaptive stator flux observer for induction motors,” *IEEE Trans. Magn.*, vol. 46, no. 8, pp. 3133–3136, Aug. 2010.

[92] M. N. Uddin and M. Hafeez, “FLC-based DTC scheme to improve the dynamic performance of an IM drive,” *IEEE Trans. Ind. Appl.*, vol. 48, no. 2, pp. 823–831, 2012.

[93] S. Gdaim, A. Mtibaa, and M. F. Mimouni, “Design and experimental implementation of DTC of an induction machine based on fuzzy logic control on FPGA,” *IEEE Trans. Fuzzy Syst.*, vol. 23, no. 3, pp. 644–655, Jun. 2015.

[94] N. Venkataramana Naik and S. P. Singh, “A comparative analytical performance of F2DTC and PIDTC of induction motor using DSPACE-1104,” *IEEE Trans. Ind. Electron.*, vol. 62, no. 12, pp. 7350–7359, Dec. 2015.

[95] P. Z. Grabowski and F. Blaabjerg, “Direct torque neuro-fuzzy control of induction motor drive. DSP implementation. ,” in *Proceedings of the 24th Annual Conference of the IEEE IECON ’98.*, 1998, pp. 657–661.

[96] J. Maes and J. A. Melkebeek, “Speed-Sensorless direct torque control of induction motors using an adaptive flux observer,” *IEEE Trans. Ind. Appl.*, vol. 36, no. 3, pp. 778–785, May 2000.

[97] P. Z. Grabowski, M. P. Kazmierkowski, B. K. Bose, and F. Blaabjerg, “A simple direct torque neuro-fuzzy control of PWM-inverter-fed induction motor drive,” *IEEE Trans. Ind. Electron.*, vol. 47, no. 4, pp. 863–870, Aug. 2000.

[98] R. Kennel and A. Linder, “Predictive control of inverter supplied electrical drives,” in *IEEE 31st Annual Power Electronics Specialists Conference, 2000.*, 2000, pp. 761–766.

[99] S. J. Henriksen, “Digital predictive current control of induction machines,” 2001.

[100] R. Kennel, A. Linder, and M. Linke, “Generalized predictive control (GPC) - ready for use in drive applications,” in *Power Electronics Specialists Conference, PESC*, 2001, pp. 1839–1844.

[101] C. Lascu, I. Boldea, and F. Blaabjerg, “Direct torque control of sensorless induction motor drives: A sliding-mode approach,” *IEEE Trans. Ind. Appl.*, vol. 40, no. 2, pp. 582–590, 2004.

[102] E. E. EL-Kholy, S. Mahmoud, R. Kennel, A. EL-Refaei, and F. Elkady, “Torque ripple minimization for induction motor drives with direct torque control,” *Electr. Power Components Syst.*, vol. 33, no. 8, pp. 845–859, 2005.

[103] A. Linder and R. Kennel, “Direct model predictive control - A new direct predictive control strategy for electrical drives,” in *European Conference on Power Electronics and Applications*, 2005, pp. P1–P10.

[104] P. Correa, M. Pacas, and J. Rodriguez, “Predictive torque control for inverter-fed induction machines,” *IEEE Trans. Ind. Electron.*, vol. 54, no. 2, pp. 1073–1079, Apr. 2007.

[105] P. Cortés, M. P. Kazmierkowski, R. M. Kennel, D. E. Quevedo, and J. Rodríguez, “Predictive control in power electronics and drives,” *IEEE Trans. Ind. Electron.*, vol. 55, no. 12, pp.4312–4324, Dec. 2008.

[106] K. B. Lee and F. Blaabjerg, “Sensorless DTC-SVM for induction motor driven by a matrix converter using a parameter estimation strategy,” *IEEE Trans. Ind. Electron.*, vol. 55, no. 2, pp. 512–521, 2008.

[107] K. Shyu, J. Lin, and V. Pham, “Global minimum torque ripple design for direct torque control of induction motor drives,” *IEEE Trans. Ind. Electron.*, vol. 57, no. 9, pp. 3148–3156, Sep. 2010.

[108] J. Beerten, J. Verveckken, and J. Driesen, “Predictive direct torque control for flux and torque ripple reduction,” *IEEE Trans. Ind. Electron.*, vol. 57, no. 1, pp. 404–412, Jan. 2010.

[109] T. Abdalla, H. Hairik, and A. Dakhil, “Direct torque control system for a three phase induction motor with fuzzy logic based speed controller,” in *Energy, Power and Control*, 2010, no. 2, pp. 131–138.

[110] T. Geyer, “Computationally efficient model predictive direct torque control,” *IEEE Trans.POWER Electron.*, vol. 26, no. 10, pp. 2804–2816, Oct. 2011.

[111] S. Kouro, P. Cortés, R. Vargas, U. Ammann, and J. Rodríguez, “Model predictive control —a simple and powerful method to control power converters,” *IEEE Trans. Ind. Electron.*, vol. 56, no. 6, pp. 1826–1838, Jun. 2009.

[112] O. Aissa, S. Moulahoum, I. Colak, N. Kabache, and B. Babes, “Improved performance and power quality of direct torque control of asynchronous motor by using intelligent controllers,” *Electr. Power Components Syst.*, vol. 44, no. 4, pp. 343–358, 2016.

[113] T. Geyer, G. Papafotiou, and M. Morari, “Model predictive control in power electronics : a hybrid systems approach,” in *44th IEEE Conference on Decision and Control, and the European Control Conference*, 2005, pp. 5606–5611.

[114] D. Bao-Cang, *Modern predictive control*. CRC Press, 2009.

[115] J. Richalet, A. Rault, J. L. Testud, and J. Papon, “Model predictive heuristic control: application to industrial processes,” *Automatica*, vol. 14, no. 5, pp. 413–428, Sep. 1978.

[116] J. M. Maciejowski, *Predictive control with constraints*. Prentice Hall, 2002.

[117] J. Holtz and S. Stadtfeld, “A predictive controller for the stator current vector of AC machines fed from a switched voltage source,” in *Proceedings of IEEE International Power Electronics Conference*, 1983, pp. 1665–1675.

[118] R. Kennel and D. Schroder, “Predictive control strategy for converters,” in *Proceedings of the third IFAC Symposium*, 1983, pp. 415–422.

[119] J. Rodriguez, M. P. Kazmier kowski, J. R. Espinoza, P. Zanchetta, H. Abu-rub, H. A. Young, and C. A. Rojas, “State of the art of finite control set model predictive control in power electronics,” *IEEE Trans. Ind. Informatics*, vol. 9, no. 2, pp. 1003–1016, May 2013.

[120] F. Wang, S. Li, X. Mei, W. Xie, J. Rodriguez, and R. M. Kennel, “Model based predictive direct control strategies for electrical drives: an experimental evaluation of PTC and PCCmethods,” *IEEE Trans. Ind. Informatics*, vol. 11, no. 3, pp. 671–681, Jun. 2015.

[121] J. Rodríguez, R. M. Kennel, J. R. Espinoza, M. Trincado, C. A. Silva, and C. A. Rojas, “High performance control strategies for electrical drives: an experimental assessment,”

[122] S. A. Davari, D. A. Khaburi, and R. Kennel, “An improved FCS – MPC algorithm for an induction motor with an imposed optimized weighting factor,” *IEEE Trans. Power Electron.*, vol. 27, no. 3, pp. 1540–1551, Mar. 2012.

[123] P. Karamanakos, P. Stolze, R. M. Kennel, S. Manias, and H. du T. Mouton, “Variable switching point predictive torque control of induction machines,” *IEEE J. Emerg. Sel. Top. Power Electron.*, vol. 2, no. 2, pp. 285–295, Jun. 2014.

[124] Y. Zhang and H. Yang, “Generalized two-vector-based model-predictive torque control of induction motor drives,” *IEEE Trans. Power Electron.*, vol. 30, no. 7, pp. 3818–3829, Jul. 2015.

[125] C. A. Rojas, J. Rodríguez, F. Villarroel, J. R. Espinoza, C. A. Silva, and M. Trincado, “Predictive torque and flux control without weighting factors,” *IEEE Trans. Ind. Electron.*, vol. 60, no. 2, pp. 681–690, Feb. 2013.

[126] D. Zhou, J. Zhao, and Y. Liu, “Predictive torque control scheme for three-phase four switch inverter-fed induction motor drives with dc-link voltages offset suppression,” *IEEE Trans. Power Electron.*, vol. 30, no. 6, pp. 3309–3318, Jun. 2015.

[127] Y. Zhang and H. Yang, “Model-predictive flux control of induction motor drives with switching instant optimization,” *IEEE Trans. Energy Convers.*, vol. 30, no. 3, pp. 1113–1122, Sep. 2015.

[128] F. Wang, Z. Zhang, R. Kennel, and J. Rodríguez, “Model predictive torque control with an extended prediction horizon for electrical drive systems,” *Int. J. Control*, vol. 88, no. 7, pp. 1379–1388, 2015.

[129] T. Geyer, G. Papafotiou, and M. Morari, “Model predictive direct torque control — Part I: concept, algorithm, and analysis,” *IEEE Trans. Ind. Electron.*, vol. 56, no. 6, pp. 1894–1905, Jun. 2009.

[130] G. Papafotiou, J. Kley, K. G. Papadopoulos, P. Bohren, and M. Morari, “model predictive direct torque control — Part II : implementation and experimental evaluation,” *IEEE Trans. Ind. Electron.*, vol. 56, no. 6, pp. 1906–1915, Jun. 2009.

[131] V. I. Meleshin, D. V. Zhiklenkov, and A. A. Ganshin, “Efficient three-level boost converter for various applications,” in *15th International Power Electronics and Motion Control Conference and Exposition, EPE-PEMC 2012 ECCE Europe*, 2012, pp. 1–8.

[132] C. Balakishan, N. Sandeep, M. V. Aware, and P. Bauer, “Design and implementation of three-level DC-DC converter with golden section search based MPPT for the photovoltaic applications,” *Adv. Power Electron.*, vol. 2015, p. 9, 2015.

[133] R. Krishna, D. Soman, S. Kottayil, and M. Leijon, “Pulse delay control for capacitor voltage balancing in a three-level boost neutral point clamped inverter,” *IET Power Electron.*, vol. 8, no. 2, pp. 268–277, 2015.

[134] B. Wu, *High- Power converters and AC drives*. John Wiley and Sons, 2006.

[135] J. Holtz, “The dynamic representation of AC drive systems by complex signal flow graphs,” in *IEEE International Symposium on Industrial Electronics ISIE’94*, 1994, pp. 1–6.

[136] L. Zakaria and K. Barra, “Predictive direct torque and flux control of an induction motor drive fed by a direct matrix converter with reactive power minimization,” in *10th IEEE International Conference on Networking, Sensing and Control (ICNSC)*, 2013, pp. 34–39.

[137] G. C. Goodwin, J. C. Agüero, E. Mauricio, C. Garrido, M. E. Salgado, and J. I. Yuz, “Sampling and sampled-data models: the interface between the continuous world and digital algorithms,” *IEEE Control Systems Magazine*, no. 5, pp. 34–53, Oct-2013.

[138] C. A. Rojas, J. I. Yuz, M. Aguirre, and J. Rodriguez, “A comparison of discrete-time models for model predictive control of induction motor drives,” in *2015 IEEE International Conference on Industrial Technology (ICIT)*, 2015, pp. 568–573.

Publications

Publications

Journals: (Accepted)

- Y Bhaskar S S Gupta & S Srinivasa Rao (2019) *"Experimental evaluation of direct torque-controlled 3-phase induction motor under inverter faults",* ***International Journal of Electronics (Taylor & Francis),*** **Vol: 107: Issue:5, 719-739.**

- Y Bhaskar S S Gupta & S Srinivasa Rao (2020): *"A Modified Inverter Topology for Fault-Tolerant DTC Induction Motor Drive",* ***International Journal of Electronics (Taylor & Francis),*** **Vol: 107: Issue: 12, 1985-2005.**

- Y Bhaskar S S Gupta & S Srinivasa Rao: *"Predictive Torque Control of Three-Phase Induction Motor Drive with Inverter Switch Fault-Tolerance Capabilities"* ***IEEE-Journal of Emerging and Selected Topics in Power Electronics,*** **DOI: 10.1109/JESTPE.2020.3020328**

Journals: (Under Review)

- Y Bhaskar S S Gupta & S Srinivasa Rao: *"Experimental Evaluation of Three-Phase Induction Motor Drive during Pre-fault and Post-fault Operation"* is communicated to ***International Transactions on Electrical Energy Systems (John Wiley & Sons)*.**

Conferences:

- Bhaskar. S. S. Gupta Yelamarthi and Srinivasa Rao Sandepudi, *"Fault-Tolerant Converter Topology for Speed Control of Induction Motor Drive,"* ***2020 IEEE International Conference on Emerging Frontiers in Electrical and Electronic Technologies (IEEE-ICEFEET 2020).***

- Bhaskar. S. S. Gupta Yelamarthi and Srinivasa Rao Sandepudi, *"Scalar Control of Induction Motor Drive with Inverter Fault-Tolerance Capability,"* ***2020 IEEE International Conference on Emerging Frontiers in Electrical and Electronic Technologies (IEEE-ICEFEET 2020).***

- Bhaskar. S. S. Gupta Yelamarthi and Srinivasa Rao Sandepudi, *"An Improved Fault Tolerant Converter Topology for Filed Oriented Controlled Induction Motor Drive,"* ***2019 IEEE International Conference on Power Electronics, Control and Automation (IEEE-ICPECA), 2019.***

- Bhaskar. S. S. Gupta Yelamarthi and Srinivasa Rao Sandepudi, *"Reconfiguration of Voltage Source Inverter for Field-Oriented Controlled Induction Motor Drive during Open-Circuit and Short-Circuit Faults,"* ***2019 IEEE International Conference on Power Electronics, Control and Automation (IEEE-ICPECA), 2019****.*

- Bhaskar. S. S. Gupta Yelamarthi and Srinivasa Rao Sandepudi, *"A novel fault-tolerant converter topology for induction motor drive,"* ***2018 IEEE International Conference on Power Electronics Drives and Energy Systems (IEEE-PEDES), 2018****.*